UNDERSTANDING THE PHASE TRANSFORMATION MECHANISM OF METASTABLE AMORPHOUS BORON NITRIDE

by

METİN ÖRNEK

A Dissertation submitted to the

School of Graduate Studies

Rutgers, The State University of New Jersey

in partial fulfillment of the requirements

For the degree of

Doctor of Philosophy

Graduate Program in Materials Science and Engineering

written under the direction of

Richard A. Haber

and approved by

_____

_____

_____

_____

_____

New Brunswick, New Jersey

October, 2018

ABSTRACT OF THE DISSERTATION

Understanding the Phase Transformation Mechanism of Metastable Amorphous Boron Nitride

by METİN ÖRNEK

Dissertation Director:
Richard A. Haber

Boron nitride (BN) is an attractive ceramic material existing in various polymorphic structures such as low-density amorphous, turbostratic, explosive, hexagonal, rhombohedral phases, and high-density wurtzite and cubic phases. Among these, hexagonal (h-BN) and cubic (c-BN) forms of BN have been widely used for various industrial applications thanks to their superior properties. For instance, h-BN possesses high thermal conductivity, high oxidation resistance, and low friction coefficient in air. On the other hand, c-BN is a super hard structural ceramic with a hardness value of ~ 45-70 GPa, second only to diamond. Its superior chemical stability and oxidation resistance, as compared to diamond, makes it the material of choice in cutting and grinding tools, where diamond fails.

The chemical and structural characteristics of h-BN or c-BN strongly depend on the starting material used for their synthesis. Among the starting materials, BCNO compounds are the most common and widely used precursors for h-BN and c-BN synthesis. However, there is lack of understanding on how the chemical and

microstructural characteristics of the BCNO precursors impact the formation of BNs and the chemical and microstructural characteristics of the BN formed.

To this end, first BCNO compounds with various chemical/structural characteristics have been synthesized by systematically varying starting composition (boric acid (H_3BO_3) - melamine ($C_3H_6N_6$) ratio) and synthesis temperature. Synthesized BCNOs were then subjected to post heat or heat-pressure treatments under equilibrium or non-equilibrium environments to study the relationship between the chemical and microstructural characteristics of the BCNO compounds and their impacts on the formation and structural ordering of h-BN and c-BN. It was found that higher H_3BO_3 content in the starting composition promotes h-BN formation and its structural ordering. In addition, post heat and heat-pressure treatments also confirmed the above phenomena. The possible mechanisms leading to these phenomena are discussed within the framework of thermodynamic and kinetic principles.

It was also found that plasma spraying metastable BCNO compounds results in c-BN formation without applying external pressure, which, typically higher than 6 GPa, is essential for c-BN formation. Moreover, formation of metastable explosive (e-BN) and wurtzite (w-BN) phases of BN was achieved, for the first time, by emulsion detonation synthesis (EDS) method at the pressures of 5 and 7 GPa, respectively. The results suggest that EDS method has a potential to synthesis metastable and high-density phases of BN.

Keywords: Amorphous; Metastable; BCNO; Synthesis; Crystallization; Phase evolution; Reaction mechanism; Crystalline; Structural ordering; High density; Low density; Cubic boron nitride; Hexagonal boron nitride; Ceramic; High pressure; High temperature; Plasma spraying; Emulsion detonation synthesis; Densification; Sintering.

ACKNOWLEDGMENTS

Getting a Ph.D. degree, especially when you are abroad and thousand miles away from your roots is a very challenging task with lots of ups-and-downs as in every part of the life. Therefore, I would like to thank everyone who helped me through my time at Rutgers. First, I would like to express my deep and sincere gratitude my advisor, Dr. Richard A. Haber for his help, guidance and patience throughout not only my studies and research, but also throughout the life perspective. Thank you, Dr. Haber, for believing in me and pushing me to explore my limits! And special thanks to Dr. Chawon Hwang. It is my honor to work with you through our times at Rutgers. I have learnt a lot from you about science, research, and life. This thesis, our research, and studies would not have been possible without your endless help, effort and patience with me. Thank you for mentoring me throughout my Ph.D. and being an elder brother to me!

Special thanks to Michelle M. Sole, who is a super hero for Haber's group. The words are not enough to explain how grateful I am for you being here at Rutgers. I would like to thank Dr. Lisa Klein for her support and help making the integration period easier for international students, and I would like to thank my dissertation committee: Dr. John M. Matthewson, Dr. Steven L. Miller, and Dr. Richard Lehman. And special thanks to Dr. Vladislav Domnich for his endless help and patience when I was bothering him every day to get the reviews of the manuscripts, and for our long talks about life and politics. Thanks to my collaborators, Dr. Kevin J. Hemker, Dr. Kelvin Y. Xie, Dr. K. Madhav Reddy, and Dr. E. Koray Akdogan for their help, effort, advices and collaboration throughout my research. And I'd like to thank the former and current administrative and technical staff in the materials science department for their help during my time at Rutgers. I'd like to thank

Jennifer Weir, Jun Won, Avie Shah, Austin J. Cruz, Knyckolas Sutherland, and Kaitlin Wang for their help, assistance and friendship.

I am also grateful for graduate scholarship provided by the Ministry of National Education, the Republic of Turkey, and thanks to Defense Advanced Research Projects Agency (DARPA), Office of Naval Research (ONR), and National Science Foundation (NSF) for their research grants, which enabled me to do research and complete this dissertation.

To all former and current members of Happy Valley: Kanak A. Kwelkar, Nick Ku, Vince DeLucca, Tyler Munhollan, Dr. Fabio Nicodemi, Dr. Sukanya Murali, Bruce Wang, Mustafa Al Azzawi, Ian Maher, Antony Etzold, Mark Shaffer, Dr. Atta Ulah Khan and Mike G. Thank you all for your help and friendship. It was very fun to work with you. And the Turks: Fatih, Abdullah, Mert, Ender, Zeynep, Hulya, Berra, Ilyas, Muharrem, and Orsan. Thank you all for invaluable times, friendship and most importantly for making me feel that I am a part of a huge family.

Even though I cannot thank enough, I'd like to express my gratitude to my parents, my brother, and my sister. Thank you for your endless support and encouragement, and, of course, love. Thank you for always being there for me and motivating me to achieve my goals and for everything else. I am very proud of you. I have tried my best to make you proud and I hope that I have made it.

And my lovely wife, Neslihan. Thank you for being my soul mate, your love and patience. I would not have made it without you, your endless support and encouragement. I love you!

DEDICATION

Sometimes, you need to steal time from yourself, and from your beloved ones to achieve your goals. I wish that it would just be possible to turn the clock back…

I dedicate this thesis to my niece, Inci Serra, and to my nephew, Kenan. I am so sorry that I could not be there for you while you grow up, and I have missed a lot of things. I hope you forgive me. I love you so much!

TABLE OF CONTENTS

Preface

This thesis is comprised of a series of publications that represent the major accomplishments and serve as separate chapters, in addition to chapters of introduction, conclusion and future work. The series of publications that show the major accomplishments are comprised of five individual papers that are published in peer-reviewed material science or ceramic journals and one paper that is submitted to a peer-reviewed material science journal. The list of the papers, which correspond to Chapters 2-7, is as follows:

1. M. Örnek, C. Hwang, K.M. Reddy, V. Domnich, S.L. Miller, E.K. Akdoğan, K.J. Hemker, R.A. Haber, *Formation of BN from BCNO and the development of ordered BN structure: I. Synthesis of BCNO with various chemistries and degrees of crystallinity and reaction mechanism on BN formation*, Ceram. Int. 44 [13] (2018) 14980-14989. DOI: 10.1016/j.ceramint.2018.05.126

2. C. Hwang, M. Örnek, K.M. Reddy, V. Domnich, S.L. Miller, K. Hemker, R.A. Haber, *Effect of synthesis conditions of BCNO on the formation and structural ordering of BN at 1200 °C and 1 GPa,* Diam. Relat. Mater. 87 (2018) 156–162. DOI: 10.1016/j.diamond.2018.06.002

3. M. Örnek, C. Hwang, S. Xiang, K.Y. Xie, A. Etzold, B. Yang, R. A. Haber, *Effect of synthesis conditions of BCNO on the formation and structural ordering of boron nitride at high temperatures*, submitted.

4. K. Madhav Reddy, C. Hwang, M. Örnek, S.L. Miller, W.E. Mayo, A. Burgess, R.A. Haber, K.J. Hemker, *Observations of nanocrystalline cubic boron nitride formed with plasma spraying*, Acta Mater. 116 (2016) 155–165. DOI: 10.1016/j.actamat.2016.06.038

5. M. Örnek, K.M. Reddy, C. Hwang, V. Domnich, A. Burgess, S. Pratas, J. Calado, K.Y. Xie, S.L. Miller, K.J. Hemker, R.A. Haber, *Observations of explosion phase boron nitride formed by emulsion detonation synthesis*, Scr. Mater. 145 (2018) 126–130. DOI: 10.1016/j.scriptamat.2017.10.026

6. M. Örnek, C. Hwang, K.Y. Xie, S. Pratas, J. Calado, A. Burgess, V. Domnich, K.J. Hemker, R.A. Haber, *Formation of metastable wurtzite phase boron nitride by emulsion detonation synthesis*, J. Am. Ceram. Soc., 101 (2018) 3276-3281. DOI: 10.1111/jace.15560

Chapter 1.

Introduction

When talking about ceramics, for many people products that come to his/her mind are pottery, sculpture, wares and tiles, which are classified as traditional ceramics. However, developments in material science have paved a way to produce a new class of ceramics, i.e. advanced ceramics that are currently being used to overcome difficult tasks in vast real-life applications. One of the prominent examples of this is diamond, a solid form of carbon crystallized in a cubic structure. Diamond is a well-known and commonly used structural ceramic with extreme Vickers hardness (Hv) of ~ 50-70 GPa [1, 2]. Cutting and grinding tools, wear components, coatings, and semiconductors are only a fraction of the application areas of diamond. However, diamond suffers from low chemical and thermal stability at high temperatures and deteriorates when used to machine ferrous metals or their alloys [3].

Boron nitride (BN) is a widely used ceramic material that has similar crystallographic structure to that of carbon. In recent years, cubic (c-BN) and hexagonal (h-BN) forms of BN have received considerable interest due to their unique properties. In addition to being the hardest structural ceramic and commercial material, sp^3 bonded c-BN exhibits high compressive strength and stiffness, high thermal conductivity, and high electrical resistivity [4-6]. Moreover, c-BN also shows higher thermal stability as well as higher chemical inertness in comparison to diamond [6, 7]. These properties make c-BN the material of choice for applications in abrasives, cutting tools, armor materials, and

electronic devices [8]. Cubic BN (c-BN) can be synthesized through high pressure-high temperature (HPHT) processes e.g. detonation, dynamic shock or static high-pressure methods at pressures of 5-50 GPa and at temperatures of 1200-2000°C [4, 8, 9]. However, the requirement of the HPHT conditions to synthesize c-BN makes it a challenging task due to limitations on the equipment side. Moreover, the HPHT nature of the processes only allows the formation of small-scale powders; this also limits the application of the material itself. Therefore, there has been an ongoing interest to synthesize high density and super hard c-BN at reduced pressure and temperature. Several approaches including precursor optimization (smaller particle size of the used precursors, less developed crystallographic structures such as amorphous and turbostratic phases), catalysts solvent, supercritical fluid and etc. have been performed to overcome these challenges on the synthesis of super hard BNs [10-14].

On the other hand, h-BN form is the most stable BN polymorph and has B and N atoms arranged in an sp^2 bonded honeycomb layered structure, which is analogous to graphite [6]. Its chemical inertness, high thermal conductivity and higher thermal stability (compared to graphite) make it a potential candidate for hydrogen storage and nanoelectronic devices, where carbon nanotubes and nanosheets are employed [15-18]. Moreover, h-BN is widely used in metallurgy, cosmetics, and paints.

For the synthesis of BN ceramics, BCNO compounds have been used as starting materials, which are typically prepared by a boron bearing (boric acid and boron oxide) and nitrogen bearing compounds (melamine, urea) [16, 18-20]. Previous investigators have reported that the synthesis conditions and properties of the resultant h-BN or c-BN are strongly dependent on the characteristics of the starting BCNO compounds [21-24].

However, detailed information on the starting BCNO compounds or their effect on phases and microstructures that develop during the synthesis of c-BN or h-BN is not available. In addition, the types of BCNO compounds reported are limited in terms of characteristics such as structural development level and chemical composition. Therefore, understanding the microstructural development of the various types of BCNO compounds that differ in structural disorder, atomic bonding structure, and chemical composition, is required to develop advanced strategies to synthesize crystalline BNs at further-reduced transition temperature, threshold pressure, or both.

This thesis will focus on the synthesis of metastable BN and BCNO compounds and will investigate how the synthesis conditions of BCNO such as boric acid (H_3BO_3) to melamine ($C_3H_6N_6$) molar ratio in the starting composition and heat treatment temperature impact the BCNO formation, their chemistry, and degree of crystallinity. Moreover, this thesis will also focus on how the above correlation will impact BN formation from BCNO and its structural ordering under equilibrium conditions (conventional high pressure and high temperature treatments) and non-equilibrium conditions (ultra-fast heating and cooling along with the high pressures).

Summary of Contents

In this thesis, the chapters 2, 3, 5, 6, and 7 represent five individual articles that are published in peer-reviewed material science and ceramic journals. In addition, chapter 4 represents a manuscript that has been submitted to a peer-reviewed material science journal. Chapters 2-5 investigate and focus on the synthesis of BCNO, and formation and structural ordering of BN from BCNO at various temperatures and pressures under

equilibrium and non-equilibrium conditions. Chapters 6-7 focus on metastable BN formation under non-equilibrium conditions – emulsion detonation synthesis. Chapter 8 provides major conclusions that were obtained through the studies that structured this thesis. Chapter 9 paves the way for possible future works that arise from the interpretation of the data obtained through the studies as discussed in earlier chapters. Brief summaries of each chapter are as follows.

Chapter 2 represents the results of the investigation on the formation of BCNO compounds that have been synthesized from various H_3BO_3:$C_3H_6N_6$ mixtures and at low temperature range (400-1000°C). The effect of H_3BO_3 content in the starting composition and heat treatment temperature on the BCNO synthesis and BN formation from BCNO were comprehensively investigated. The results indicate that BN forms from BCNO compounds. The temperature for BN formation decreases as the BA content in the starting composition increases. In addition, the structural ordering of BN formed from BCNO compounds increases, as determined by shorter interlayer distances and larger crystallite sizes along the a- and c- axes. In light of the findings of this study, a reaction mechanism that governs BN formation from BCNO compounds is suggested and the thermodynamic and kinetic aspects of the above phenomena is discussed.

Chapter 3 represents the results of the investigation on the formation and structural ordering of BN from BCNO at 1 GPa and 1200°C, utilizing BCNO compounds that were prepared earlier as discussed in Chapter 2. Results indicate that BN formation and its structural ordering is promoted as the H_3BO_3 content in the starting material and temperature increases during the synthesis of BCNO, which well agrees and confirms the findings in Chapter 2.

Chapter 4 represents the results of the investigation on the formation and structural ordering of BN from BCNO at 1400-1800°C (involving the 3-dimensional structural ordering in addition to interlayer distances and crystallite sizes), again utilizing BCNO compounds that were prepared earlier as discussed in Chapter 2. Results show that highly structurally ordered h-BN that have similar crystallographic features to that of commercial h-BN can be synthesized at lower temperatures (1600°C) than the industrially applied temperatures (~ 2000°C) by increasing the H_3BO_3 content in the starting composition. The findings in this chapter well agree and complement Chapters 2 and 3.

Chapter 5 represents the results of the investigation on BN formation from BCNO compounds under extreme temperatures along with fast cooling environments (non-equilibrium conditions) by subjecting BCNO compounds to plasma spray. Results provide direct observation on the formation of super hard cubic phase BN ~ 10-20 nm in size in hexagonal matrix by plasma spray without applying any external pressure. Moreover, the addition of H_3BO_3 into BCNO compound increased the yield of the formed c-BN.

Chapter 6 represents the results of the investigation on metastable BN formation commercial h-BN under extreme temperatures and pressures along with fast cooling environments (non-equilibrium conditions) by subjecting BCNO compounds to the newly developed emulsion detonation synthesis (EDS) method. Results show that metastable explosion phase of BN (e-BN) ~10-20 nm in size is successfully synthesized in h-BN matrix at 5 GPa, which indicates that EDS can be a promising pathway to synthesize metastable BN phases.

Chapter 7 represents the continuation of the work on metastable BN synthesis from commercial h-BN using emulsion detonation synthesis. Results show that metastable

wurtzite phase of BN (w-BN), that is either embedded or grown from h-BN matrix, from nanoscale to ~1 micrometer in size is successfully synthesized at 7 GPa. This indicates that EDS can be a promising pathway to synthesize high density and super hard phases of BN.

Chapter 8 provides major conclusions of the findings obtained through previous chapters. Chapter 9 offers some direction on the basis of the findings discussed in earlier chapters and, thus could be considered as future work.

References

[1] N. Dubrovinskaia, V.L. Solozhenko, N. Miyajima, V. Dmitriev, O.O. Kurakevych, L. Dubrovinsky, Superhard nanocomposite of dense polymorphs of boron nitride: Noncarbon material has reached diamond hardness, Applied Physics Letters, 90 (2007) 101912.

[2] H. Sumiya, T. Irifune, Indentation hardness of nano-polycrystalline diamond prepared from graphite by direct conversion, Diamond and Related Materials, 13 (2004) 1771-1776.

[3] Q. Huang, D. Yu, B. Xu, W. Hu, Y. Ma, Y. Wang, Z. Zhao, B. Wen, J. He, Z. Liu, Nanotwinned diamond with unprecedented hardness and stability, Nature, 510 (2014) 250.

[4] Y. Tian, B. Xu, D. Yu, Y. Ma, Y. Wang, Y. Jiang, W. Hu, C. Tang, Y. Gao, K. Luo, Z. Zhao, L.M. Wang, B. Wen, J. He, Z. Liu, Ultrahard nanotwinned cubic boron nitride, Nature, 493 (2013) 385-388.

[5] R.H. Wentorf, Synthesis of the Cubic Form of Boron Nitride, The Journal of Chemical Physics, 34 (1961) 809-812.

[6] R. Haubner, M. Wilhelm, R. Weissenbacher, B. Lux, Boron nitrides—properties, synthesis and applications, Springer (2002).

[7] G. Demazeau, High pressure diamond and cubic boron nitride synthesis, Diamond and Related Materials, 4 (1995) 284-287.

[8] L. Vel, G. Demazeau, J. Etourneau, Cubic boron nitride: synthesis, physicochemical properties and applications, Materials Science and Engineering: B, 10 (1991) 149-164.

[9] S.M. Gavrilkin, S.S. Batsanov, Y.A. Gordopolov, A.S. Smirnov, Effective Detonation Synthesis of Cubic Boron Nitride, Propellants, Explosives, Pyrotechnics, (2009).

[10] B.P. Singh, V.L. Solozhenko, G. Will, On the low-pressure synthesis of cubic boron nitride, Diamond and Related Materials, 4 (1995) 1193-1195.

[11] V.L. Solozhenko, New concept of BN phase diagram: an applied aspect, Diamond and Related Materials, 4 (1994) 1-4.

[12] M.M. Bindal, S.K. Singhal, B.P. Singh, R.K. Nayar, R. Chopra, A. Dhar, Synthesis of cubic boron nitride using magnesium as the catalyst, Journal of Crystal Growth, 112 (1991) 386-401.

[13] M. Kagamida, H. Kanda, M. Akaishi, A. Nukui, T. Osawa, S. Yamaoka, Crystal growth of cubic boron nitride using Li3BN2 solvent under high temperature and pressure, Journal of Crystal Growth, 94 (1989) 261-269.

[14] H. Sumiya, T. Iseki, A. Onodera, High pressure synthesis of cubic boron nitride from amorphous state, Materials Research Bulletin, 18 (1983) 1203-1207.

[15] C. Gautam, C.S. Tiwary, S. Jose, G. Brunetto, S. Ozden, S. Vinod, P. Raghavan, S. Biradar, D.S. Galvao, P.M. Ajayan, Synthesis of Low-Density, Carbon-Doped, Porous Hexagonal Boron Nitride Solids, ACS Nano, (2015).

[16] B. Ertug, Powder Preparation, Properties and Industrial Applications of Hexagonal Boron Nitride, (2013).

[17] X. Hou, Z. Yu, K.-C. Chou, Facile synthesis of hexagonal boron nitride fibers with uniform morphology, Ceramics International, 39 (2013) 6427-6431.

[18] A. Lipp, K.A. Schwetz, K. Hunold, Hexagonal boron nitride: Fabrication, properties and applications, Journal of the European Ceramic Society, 5 (1989) 3-9.

[19] J. Thomas, N.E. Weston, T. O'connor, Turbostratic1 Boron Nitride, Thermal Transformation to Ordered-layer-lattice Boron Nitride, Journal of the American Chemical Society, 84 (1962) 4619-4622.

[20] R. Haubner, M. Wilhelm, R. Weissenbacher, B. Lux, Boron Nitrides — Properties, Synthesis and Applications, in: M. Jansen (Ed.) High Performance Non-Oxide Ceramics II, Springer Berlin Heidelberg2002, pp. 1-45.

[21] T. Hagio, K. Nonaka, T. Sato, Microstructural development with crystallization of hexagonal boron nitride, Journal of Materials Science Letters, 16 (1997) 795-798.

[22] J.Y. Choi, S.J.L. Kang, O. Fukunaga, J.K. Park, K. Eun, Effect of B2O3 and hBN crystallinity on cBN synthesis, Journal of the American Ceramic Society, 76 (1993) 2525-2528.

[23] L. Vel, G. Demazeau, Nucleation and growth of cubic BN crystals in the presence of Ca3B2N4 + xLif as flux-precursor, Solid State Communications, 79 (1991) 1-4.

[24] X. Zhang, Z. Lu, J. Lin, Y. Fan, L. Li, X. Xu, L. Hu, F. Meng, J. Zhao, C. Tang, Spectra Properties of BCNO Phosphor Prepared by a Two-Step Method at Low Sintering Temperature, ECS Journal of Solid State Science and Technology, 2 (2012) R39-R43.

Chapter 2.

Formation of BN from BCNO and the development of ordered BN structure: I. Synthesis of BCNO with various chemistries and degrees of crystallinity and reaction mechanism on BN formation

Metin Örnek[a], Chawon Hwang[a,*], K. Madhav Reddy[b+], Vladislav Domnich[a], Steven L. Miller[c], E. Koray Akdoğan[a], Kevin J. Hemker[b], Richard A. Haber[a,*]

[a] *Department of Materials Science and Engineering, Rutgers, The State University of New Jersey, Piscataway, NJ 08854*

[b] *Department of Mechanical Engineering, Johns Hopkins University, Baltimore, MD 21218*

[c] *H&M Analytical Services Inc., Cream Ridge, NJ 08514*

*Corresponding author e-mail: chawon.hwang@rutgers.edu; rich.haber@rutgers.edu, and address: 607 Taylor Road, Piscataway, NJ 08854, USA. Tel: +1(848) 445-5924, Fax: +1(732) 445-5926.

[+]Author present address: *State Key Laboratory of Metal Matrix Composites, Shanghai Jiao Tong University, Shanghai 200240, China.*

Abstract

We synthesized BCNO compounds and investigated how the synthesis conditions impact i) BCNO formation, their chemistry and degree of crystallinity, and ii) BN formation from BCNO and its structural ordering. Heating boric acid (H_3BO_3) and melamine ($C_3H_6N_6$) mixture yields intermediate amorphous BCNO compound. Increasing the synthesis temperature, and H_3BO_3 to $C_3H_6N_6$ ratio promote BN formation and its structural ordering. We propose a possible reaction mechanism for BN formation from H_3BO_3 and $C_3H_6N_6$ mixture and we explain the observations based on thermodynamic and kinetic considerations. An increase in synthesis temperature promotes BN formation since the reactions are endothermic. An increase in H_3BO_3 to $C_3H_6N_6$ ratio promotes BN formation since theoretical BN formation temperature decreases with the above ratio. Furthermore, it enhances material transfer and mobility of the BN layer by forming B_2O_3 phase. We also propose a processing-structure correlation map that can help determining experimental conditions for single-phase amorphous BCNO synthesis.

Keywords: Boron nitride; BCNO; Amorphous; Reaction mechanism; Structural ordering.

Footnotes: A part of the results in this study has been presented at the 39th International Conference and Expo on Advanced Ceramics and Composites of The American Ceramic Society, Daytona Beach, Florida.

1. Introduction

Boron Nitride (BN) is a well-known ceramic that exists in various polymorphic forms such as high-density cubic and wurtzite phases, low-density amorphous, hexagonal, rhombohedral, and explosive BN phases [1-6]. In recent years, the high-density cubic form of BN (c-BN) has received considerable interest due to its unique properties. c-BN, being the hardest commercial structural ceramic, exhibits high compressive strength and stiffness, high thermal conductivity, and high electrical resistivity, as well as superior thermal stability and chemical inertness in comparison to diamond [7]. Such unique properties make c-BN one of the most favorable candidates for applications in abrasives, cutting tools, armor materials, and electronic devices [4, 8].

The low density hexagonal form of BN (h-BN), which has been extensively used in a variety of applications, is the most stable BN polymorph under ambient conditions, in which B and N atoms are arranged in an sp^2 bonded honeycomb layered structure [9]. Its chemical inertness, high thermal stability, electrical resistance and thermal conductivity make h-BN the material of choice for applications such as high temperature solid lubricants in metallurgy and insulators in electronics industry, to name a few [10]. Moreover, the superior chemical inertness and thermal stability of h-BN as compared to graphite makes it a potential candidate for hydrogen storage and nanoelectronic devices, where carbon nanotubes and nanosheets are traditionally employed [11, 12].

The BCNO compounds have been used as precursors in the synthesis of c-BN or h-BN [13-15]. Prior works have shown that synthesis conditions and properties of the resultant c-BN or h-BN strongly correlate with the chemistry and degree of crystallinity of the starting materials in the BCNO system. Choi et al. showed a decrease in the threshold

pressure and temperature for c-BN formation when the crystallinity of precursor decreased [13]. Similarly, Vel et al. obtained an order of magnitude higher yield in c-BN when amorphous BN precursor was used instead of crystalline BN precursors [14]. Singh et al. showed that the chemistry of BCNO precursor governs the degree of crystallinity in the resultant h-BN [15]. Zhang et al. obtained various quantities of crystalline and amorphous BN by altering precursor chemistries in the synthesis of BCNO [16].

In these previous studies, valuable attempts were made to establish correlations between the chemistry and degree of crystallinity of BCNO precursor and the formation of BN. Nonetheless, systematic studies are lacking on i) the synthesis of BCNO compounds with various chemistries and degrees of crystallinity, and ii) the formation of BN from BCNO compounds over a wide range of compositions and temperatures. Therefore, we have undertaken a study to investigate how synthesis conditions impact (i) the formation of BCNO compounds and their chemical and microstructural characteristics, and (ii) the formation of BN from BCNO compounds and its structural ordering. Furthermore, to explain the findings obtained through the investigation, we have proposed a possible reaction mechanism within the frameworks of thermodynamics and kinetics principles. We also have proposed a processing-structure correlation map which may help synthesize single-phase amorphous BCNO compounds.

2. Experimental Procedures

2.1 Powder Synthesis

Boric acid (H_3BO_3; Optibor®, U.S. Borax, Inc., California) and melamine ($C_3N_6H_6$; MelaminebyDSM^{TM}, DSM, Netherlands) were chosen as starting materials to

synthesize BCNO compounds based on their commercial availability and cost effectiveness compared to other raw materials such as elemental boron and urea (source for N). In this study, the H_3BO_3:$C_3N_6H_6$ (hereafter referred to as BA:M) molar ratio was varied as 1:1, 1.5:1, 2:1, 3:1 and 6:1 to study its effect on BCNO chemistry, and phase/microstructure development. Molar ratios higher than 6:1 were not considered due to the excessive residual H_3BO_3 content in the resultant BCNO even if a high synthesis temperature were used [17]. Similarly, the lowest molar ratio was limited to 1:1 to avoid excessive sublimation of melamine ($C_3N_6H_6$) [17]. A solid-state two-step heating process was chosen for synthesizing BCNO because of its simplicity and the fact that it requires relatively shorter times compared to wet-chemical methods. As such, it is more suitable for the synthesis of relatively larger quantities of BCNO.

Thermal gravimetric analysis (TGA) and differential thermal analysis (DTA) were undertaken using a TA Instruments (Delaware) Q600 analyzer under N_2 atmosphere (10 °C/min heating rate) to assess the thermal reaction behavior of the starting 1:1 BA:M molar mixture. The heat and weight loss curves (Supplementary Fig. 1) show that the starting materials experience noticeable reactions up to 350°C, followed by gradual changes from 350°C to 1000°C. Based on the thermal analyses results, the temperatures for studying the BCNO formation as a function of BA:M molar ratio were chosen as 400, 500, 600, 800, 900, and 1000°C. In addition, as the heating temperature goes over 1000°C, the formation of BN becomes more prominent than the formation of BCNO [10]. Since this study focuses more on the synthesis of BCNO compounds and the intitial stage of BN formation than the synthesis of BN, we limited the temperature to a lower range, up to 1000°C.

Initial heat treatments were conducted at 200°C in atmospheric air for 2 hours using a muffle furnace to remove moisture. Powders thus obtained were crushed and sieved through a #200 sieve to enhance particle size uniformity. Final heat treatments were conducted while maintaining nitrogen gas flow rate at 2 L/min in a tubular furnace. A heating rate of 240 °C/hour was used. The isothermal dwell time was set to 3 hours in each experiment. Next, the tubular furnace was cooled down naturally to room temperature from the heat treatment temperature. The average cooling rate of the samples ranged from 70 °C/hour to 53 °C/hour when cooled from 1000°C and 400°C, respectively. The average cooling rate of the samples was in between these limits for intermediate processing temperatures.

2.2 Characterization

Synthesized BCNO compounds were crushed and sieved through a #200 sieve and held in a drying furnace at 110°C for 24 hours before ensuing analytical analyses. X-ray diffraction (XRD) was used for qualitative phase analysis, assessment of crystallinity and the size of the crystallites using a PANalytical (Netherlands) X'Pert Diffractometer at 45kV and 40 mA with Cu Kα (λ=1.540598 Å) radiation at a scanning rate of $0.04°min^{-1}$. Crystallite sizes (L) for BN were calculated from the Scherrer equation [18]. $L = (K \times \lambda)/(\beta \times \cos\theta)$, where K is a dimensionless shape factor (0.9 for (002) plane), λ is the wavelength of X-ray beam (Cu Kα, 1.540598 Å), β is the full width half maximum (FWHM) of diffraction peak (radian), and θ is Bragg angle (degree).

Fourier Transform infrared (FTIR) spectroscopy was used to assess the chemical bonding characteristics in BCNO using a Mattson Instruments (Wisconsin) Galaxy 5000 Series spectrometer (KBr pellet technique). Field-emission scanning electron microscopy

(FE-SEM) was used to observe powder morphologies using a Zeiss-Sigma (Germany) FE-SEM. Energy dispersive X-Ray spectroscopy (EDX) was used to analyze chemical compositions using an Oxford-XMaX80 (United Kingdom) EDX detector that was coupled to FE-SEM with an operating voltage at 5 keV. Combustion analysis (CA) was used to determine the carbon content of synthesized powders using LECO Corp. (Michigan) CS-230 carbon analyzer. High-resolution transmission electron microscopy (HRTEM) investigations were carried out to study the morphology, crystal structure, and interlayer distance using a Philips (Netherlands) FEI CM-300 microscope with incident electron beam energy of 300 keV. Chemical bonding characteristic of synthesized BCNO was also investigated by means of electron energy loss spectroscopy (EELS) using Gatan 200 EELS system coupled to the HRTEM.

3. Results

Figure 1 shows the chemical compositions of synthesized compounds based on EDX analyses. All synthesized compounds show the elemental signals of boron, carbon, nitrogen, and oxygen on their EDX spectra, confirming they are BCNO compounds. For all BA:M ratios, boron and oxygen contents increased and carbon and nitrogen contents decreased as synthesis temperature increased up to certain intermediate temperatures: 800°C for BA:M=1:1 and 3:1; 600°C for BA:M=6:1. We attribute this trend to the higher degree of decomposition of melamine with increasing temperature in comparison to boric acid. As the temperature further increased over the certain intermediate temperatures boron and nitrogen contents further increased while oxygen content dramatically decreased. This can be attributed to either increased evaporation of boric acid at high temperature or

enhanced release of oxygen accompanied by advances in reactions. The trend in carbon content was further confirmed using combustion analysis since the EDX technique may have also detected carbon from the carbon tape used as a sample holder. Table 1 shows the carbon content of the synthesized BCNOs as a function of BA:M ratio and synthesis temperature. For all ratios, carbon content decreased with increasing synthesis temperature, and only little amounts of carbon were detected as the synthesis temperature increased to 1000°C: e.g. 3.2 wt. % for BA:M=1:1 and around 0.2 and 0.3 wt. % for BA:M=3:1 and 6:1, respectively. The carbon content results by combustion analysis as well as the yield data as shown in Supplementary Fig. 2 support enhanced release of carbon and oxygen accompanied by advances in reactions. Actual numbers of all the elemental analyses data can be found in the Supplementary Table 1.

To identify the effects of synthesis temperatures on long-range crystallographic order of BCNO compounds, we employed XRD analyses. Fig. 2 shows XRD patterns of BCNO compounds, including those of the products after initial heat treatment at 200˚C. Melamine diborate ($C_3H_6N_6{\cdot}2H_3BO_3$) was observed in all the initial heat treatment products. As BA:M ratio increased, residual boric acid was also observed, showing increase in peak intensities with increasing BA:M ratio. BCNO compounds synthesized between 400 and 800°C exhibit broad humps at low diffraction angles (2θ=20~30° and 40~45°) for all ratios, indicating that they have amorphous structure. Increasing the synthesis temperature to 900°C for BA:M=3:1 and 6:1 revealed Bragg peaks around $2\theta \approx 26.3$ that are consistent with the (002) reflection of BN with a hexagonal unit cell [19, 20]. This indicated that a crystalline BN phase with hexagonal unit cell formed (nucleated) within the amorphous BCNO matrix. Further increasing the synthesis temperature to

1000°C resulted in higher intensities of BN (002) peaks, suggesting that an increase in synthesis temperature promoted the formation of BN. On the other hand, BA:M=2:1 showed BN (002) peak only in the 1000°C sample, while BA:M=1:1 showed no crystalline peak up to 1000˚C. We also observed a decrease in the widths of the amorphous hump around 2θ=25-30° as BA:M ratio increases. These observations suggest that increase in BA:M ratio promotes the formation of BN as well. Taken together, it seems that the effect of BA:M ratio on the BN formation becomes less prominent with an increase in the synthesis temperature, and vice versa. But the data in this study is limited to unambigiuosly claim the above pheonomena. A more detailed discussion will be provided in the continuing paper.

FE-SEM imaging was conducted to observe the morphologies. BCNO compounds showed irregular shapes and did not show notable change depending on BA:M ratio and synthesis temperature. Representative SEM micrographs of BCNO compounds are provided in the Supplementary Fig. 3.

Based on the position of the BN (002) peak, interplanar distance (d_{002}) was calculated, which corresponds to the distance between (002) planes along c-axis in hexagonal unit cell. Figure 3 shows the variation of d_{002} as a function of BA:M ratio and synthesis temperature, including classification guidelines for BNs with hexagonal unit cell. Thomas and O'Connor classified BNs with hexagonal unit cell into three sub-polytypes, based on the values of d_{002} and crystallite sizes: turbostratic (t-BN), mesographitic (m-BN) and highly ordered (h-BN) [20]. Among these, t-BN and m-BN are the intermediate structures that form prior to the formation of highly ordered h-BN [20, 21]. They exhibit a lack of three-dimensional order compared to highly ordered h-BN. The stacking layers at

(002) planes are disordered, resulting in shorter coherence lengths and larger interplanar distances (d_{002}) along the c-axis [2, 19, 20]. In terms of d_{002} values Thomas and O'Connor approximately classifies t-BN and m-BN as having d_{002}>~0.350 nm and 0.333<d_{002}<~0.350 nm, respectively, as compared to highly ordered h-BN, d_{002}=0.333 nm [20, 22]. Based on the criteria and calculated values for d_{002} the BNs formed can be classified to m-BN. As BA:M ratio increases, the observed d_{002} values decreased, getting close to the value of highly ordered h-BN. This indicates that increasing the BA:M ratio promotes BN to advance its structural ordering.

We employed FTIR spectroscopy to complement the XRD analysis by probing the changes in the local structure and the chemical bonding characteristics. Figure 4 shows the FTIR spectra of BCNO compounds synthesized at 400, 500, 600 and 800°C. The spectra for 900 and 1000°C were not included as BN dominates the vibration spectra and do not add anything further to the present discussion. One common vibrational mode that was observed in all spectra is the absorption band appearing from 3200 to 3700 cm^{-1}, which is attributed to hydroxyl or water groups [23]. The band at around 2400 cm^{-1} is due to the presence of atmospheric CO_2 and can be disregarded [24]. The broad band observed from 1100 to 1800 cm^{-1} is attributed to the asymmetric stretching of B-O-B rings in BO_3 and BO_4 units, and B–O stretching vibrations in metaborate chains and orthoborates [25, 26]. The broader features around 800 and 1350 cm^{-1} are attributed to amorphous sp^2-bonding in BN [27]. Additionally, absorption bands were observed near 1300, 1600 and 2170 cm^{-1}, which were attributed to C-N bonding [28, 29]. The absorption spectrum of highly ordered crystalline h-BN is characterized by two narrow bands at 800 cm^{-1} and 1367 cm^{-1}, representing the B-N-B bending and B-N stretching vibration modes, respectively [30].

The vibrational spectra of t-BN and m-BN are very similar to that of h-BN [23]. The characteristic bands of crystalline BN at 800 cm^{-1} and 1367 cm^{-1} were not discernible on the FTIR spectra of BCNO compounds synthesized at T≤600°C and for BA:M≤2:1, of which spectra are dominated by vibrational modes associated with structural units of meta- and orthoborates (1100~1800 cm^{-1}) [25, 26]. On the other hand, the characteristic bands of crystalline BN (800 cm^{-1} and 1367 cm^{-1}) are discernible for BCNO compounds synthesized at temperatures as low as 600°C for BA:M=3:1 and 500°C for BA:M=6:1. BCNO compounds synthesized at 800°C exhibited pronounced absorption bands of crystalline BN at 800 and 1367 cm^{-1} for all BA:M ratios. FTIR analysis supports the observations made based on XRD analysis, i.e., increases in synthesis temperature and BA:M ratio promotes crystalline BN formation. In terms of synthesis temperature where BN formation observed, the two analysis methods show a difference: for BA:M=6:1, XRD (800-900°C) and FTIR (400-500°C). The difference originates from the detection limits of the techniques, XRD analysis being less sensitive to the detection of small crystallites in the presence of a pronounced amorphous phase (cf. Fig. 2).

To obtain more direct evidence of BN formation from amorphous BCNO compounds we employed HRTEM and EELS for BA:M=6:1, as shown in Fig. 5. Here, Fig. 5a corresponds to the microstructure of the 400°C sample, showing an amorphous structure, i.e., no ordered lattice formation. On the other hand, 500°C sample (Fig. 5b) showed localized regions displaying ordered lattice formation. The lattice spacing measured from the ordered structure is ~0.37 +/- .02 nm, indicating that these nanocrystalline regions are t-BN. The images for the 600°C sample (Fig. 5c) shows nanocrystalline regions with increased sizes and decreased lattice spacing (~0.34 nm),

which lies in the m-BN range. The HRTEM images for BA:M=3:1 can be found in Supplementary Fig. 4, among which only 600°C sample showed nanocrystalline regions. The plots next to TEM images in Fig. 5 show EELS spectra for each sample. We monitored the sigma (σ) and pi (π) bonding of boron, carbon, nitrogen, and oxygen by probing the K-edges of each element. Specifically, the K-edges associated with sigma (σ) and pi (π) bonds in B at 191.6 and 198.7 eV, C at 285.0 and 296.0 eV, N at 398.0 and 407.0 eV, and O at 531.0 and 538.0 eV, respectively [31-33]. The 400°C sample (Fig. 5a) showed no clear distinction between the σ and π bonds, suggesting that there is no crystalline ordering within the BCNO amorphous matrix. On the other hand, the 500°C and 600°C samples showed clear distinction between σ and π bonds, indicating the presence of sp^2 bonded BN layers. These HRTEM/EELS analyses support the results obtained from the XRD and FTIR analyses.

Based on these characterizations results, we propose a processing-structure correlation map that can help in the synthesis of single-phase amorphous BCNO compounds as shown in Fig. 6. The points represent the temperatures where the formation of crystalline BN (structural ordering) was observed either indirectly by FTIR analysis (for BA:M=1:1 and 2:1) or directly by HRTEM analysis (for BA:M=3:1 and 6:1). We also included the experimental result by Gautam et al. who showed the formation of 2D h-BN layers for BA:M=9:1 at 300°C [34]. The plot shows a clear trend, i.e., an increase in the BA:M ratio promotes the formation of BN at lower temperatures. Moreover, the plot indicates that it is possible to obtain fully amorphous BCNO by the judicious choice of processing temperature and BA:M ratio over wide ranges, which span 400-600°C for temperature and 1:1-6:1 for BA:M ratio.

4. Discussion

Through the foregoing analyses we observed that i) heating boric acid and melamine (BA+M) yields amorphous BCNO as intermediate compound, ii) higher heating temperatures promote formation of crystalline BN with varying degree of structural ordering from amorphous BCNO, and iii) increasing the BA:M ratio promotes formation of crystalline BN at lower temperatures and advances its structural ordering at certain temperatures. To explain these observations, we propose a possible reaction mechanism including both thermodynamic and kinetic considerations.

4.1 Reaction mechanism

Several groups suggested reaction mechanisms for the formation of BN using different starting materials systems. Hubáček et. al. provided a comprehensive review for the starting systems of H_3BO_3/B_2O_3+NH3 and $H_3BO_3/B_2O_3+CO(NH_2)_2$, which contain no or lower contents of carbon compared to the system ($H_3BO_3+C_3H_6N_6$) investigated in this study [35]. They proposed a reaction mechanism involving the formation of an intermediate compound, $HO(BN)_xH$ (where x is proportional to the size of a BN monolayer), which has hexagonal symmetry. With an increase in heating temperature, planar boron nitride network forms and grows by linking the surrounding HOBNH monomers and at T>1000°C the intermediate compound yields BN and B_2O_3, with volatile gases (N_2 and H_2) and H_2O evolving as reaction byproducts. The degree of structural ordering was postulated to depend on the number of the linked layers, i.e. 26 layers of BN for t-BN and 188 layers for highly ordered h-BN. For B_2O_3+C system, Aydogdu et. al. proposed a carbothermic formation of BN through the reaction of gaseous B_2O_3 with solid C in N_2 gas flow [36]. For the $H_3BO_3+CO(NH_2)_2+Na_2CO_3$ system, Çamurlu et. al.

proposed the so-called ionic mechanism, through which BN forms by the reaction between borate ions and dissolved nitrogen in borate melt [37]. Considering the low solubility of the nitrogen in the B_2O_3 melt (0.1% at 1200˚C) [38], this mechanism is unlikely to be the major mechanism in the formation of BN in BCNO matrix in this study.

However, we have found no study on the reaction mechanism for BN formation from H_3BO_3+$C_3H_6N_6$ system. Thus, here we propose a reaction mechanism for BN formation from H_3BO_3+$C_3H_6N_6$ system, based on literature reports, assumptions, and the experimental observations reported herein. Because of the similarity in the starting systems, we assumed the reaction mechanism for H_3BO_3+$C_3H_6N_6$ is similar to that for the H_3BO_3+$CO(NH_2)_2$ system suggested by Hubáček et al., except that $C_3H_6N_6$ contains a higher amount of carbon than $CO(NH_2)_2$. For BA:M=2:1, a possible overall reaction can be expressed as follows.

$$2H_3BO_{3(s)} + C_3H_6N_{6(s)} \rightarrow BN_{(s)} + \frac{1}{2}B_2O_3 + 3NH_{3(g)} + 3CO_{(g)} + N_{2(g)} + \frac{3}{2}H_2O_{(g)} \quad (1)$$

Our choise of BN and B_2O_3 as solid reaction products in Eq. 1 are based on the study reported by Hagio et al. and our own observations. Hagio et al. studied the formation and structural ordering of h-BN by heating melamine diborate ($C_3H_6N_6 \cdot 2H_3BO_3$) and showed that BN and B_2O_3 formed as reaction products [39]. We also observed BN formation along with formation of B_2O_3 after post heat-pressure treatment of BCNO compounds, as shown in the accompanying article. For the overall reaction (Eq. 1), we propose two intermediate reactions (see Eqs. 2 and 3 below) based on the formation of

BCNO as intermediate compound and the TGA curve of BA+M mixture (BA:M=2:1, see Fig. 7). The TGA curve shows stepwise weight losses, i.e., one big/sharp weight loss up to around 350°C, including H_2O evolution around 100°C, and another small/gradual weight loss above that temperature. Accordingly, we divided the overall reaction (Eq. 1) into two steps. For the first step (up to 350°C), the possible reactions are as follows. Boric acid (H_3BO_3) loses its absorbed and structural water over the RT-200°C range, and forms metaboric acid (HBO_2) [40]. The HBO_2 thus formed then reacts with melamine ($C_3H_6N_6$) to form melamine diborate ($C_3H_6N_6 \cdot 2H_3BO_3$), which was confirmed by XRD (see Fig. 2). As temperature increases further, NH_3 and additional H_2O are expelled over the 200-350°C range, resulting in the formation of BCNO as an intermediate compound (Eq. 2) [41, 42].

$$2H_3BO_{3(s)} + C_3H_6N_{6(s)} \rightarrow B_2C_3N_3O_{4.5(s)} + 3NH_{3(g)} + \frac{3}{2}H_2O_{(g)} \quad (2)$$

For the second step, gases such as CO and N_2 evolve from the BCNO as the temperature is further increased, which results in the formation of BN and B_2O_3 as shown below.

$$B_2C_3N_3O_{4.5(s)} \rightarrow BN_{(s)} + \frac{1}{2}B_2O_{3_{(g)}} + 3CO_{(g)} + N_{2(g)} \quad (3)$$

Here, the composition of a BCNO compound is variable and depends on the species and amounts of gases assumed to evolve. In Eq. 3, we matched that the composition and amounts of evolving gases to match the weight loss estimated through TGA curve and the product yield as shown in Supplementary Fig. 2 as close as possible.

The intermediate compound (BCNO) that is suggested in this study is similar to those suggested by Hubáček et al. (HOBNH or $HO(BN)_xH$) for the H_3BO_3+$CO(NH_2)_2$ system. However, the intermediate compound in this study contained carbon and no hydrogen. The existence of carbon in the intermediate compound in this study is supported by the chemical analyses data (EDX and combustion methods) and seems logical considering the larger amount of carbon in melamine ($C_3H_6N_6$) compared to that in urea ($CO(NH_2)_2$). Regarding hydrogen, it is possible that the intermediate compound contains hydrogen as a form of -OH group as suggested by Hubáček et al., though we assumed that hydrogen is expelled as H_2O in the first reaction step (see Eq. 2). However, it is difficult to solely attribute the observed –OH vibrational modes to –OH groups based on FTIR analysis alone. That is so because such –OH modes may originate from absorbed H_2O as well.

For higher BA:M ratio, e.g. BA:M=6:1, we modified the reaction equations as follows.

$$6H_3BO_{3(s)} + C_3H_6N_{6(s)} \rightarrow 2BN_{(s)} + 2B_2O_{3(s)} + 2NH_{3(g)} + 3CO_{(g)} + N_{2(g)} + 9H_2O_{(g)} \quad (4)$$

The overall reaction for BA:M=6:1 (Eq. 4) can be divided into 2 intermediate reactions in a similar manner to BA:M=2:1, and the intermediate reactions can be expressed as shown in Eqs. 5 and 6.

$$6H_3BO_{3(s)} + C_3H_6N_{6(s)} \rightarrow B_6C_3N_4O_{9_{(s)}} + 2NH_{3(g)} + 9H_2O_{(g)} \quad (5)$$

$$B_6C_3N_4O_{9_{(s)}} \rightarrow 2BN_{(s)} + 2B_2O_{3(s)} + 3CO_{(g)} + N_{2(g)} \quad (6)$$

4.2 Thermodynamic considerations

Based on the proposed reactions, we calculated the corresponding changes in enthalpies and Gibbs free energies to gain thermodynamic insight to the reactions under consideration. The standard enthalpy of formation (ΔH_f°) of the overall reaction was calculated as ΔH_f°=321 kJ/mol for Eq. 1 (BA:M=2) and as ΔH_f°=612 kJ/mole for Eq. 4 (BA:M=6:1), by using NIST-JANAF thermochemical database [43, 44]. As the calculated ΔH_f° data show, the formation of BN through the intermediate BCNO phase is strongly endothermic for all BA:M ratios considered in this study. Hence, an increase in temperature should shift the reactions (Eqs. 1 and 4) to the right as per the Van't Hoff relation,

$$\frac{\partial ln(K)}{\partial ln\left({}^{1}/_{T}\right)} = -\frac{\Delta H_f^\circ}{R} \tag{7}$$

where K is the equilibrium constant, R is the universal gas constant and T is the absolute temperature [45]. As shown above, the consideration of enthalpies of formation can explain the effect of temperature on the formation of BN from BA+M mixtures, i.e., an increase in synthesis temperature promotes BN formation since the reactions involved are endothermic. However, such consideration does not explain the effect of BA:M ratio on the formation of BN –i.e., an increase in BA:M ratio promotes BN to form at a lower temperature and enhances its structural ordering at certain temperatures.

Consequently, we calculated and compared the temperature dependences of Gibbs free energies (ΔG_f) for BA:M=2:1 (Eq. 1) and BA:M=6:1 (Eq. 4) to understand the effect of BA:M ratio on the formation of BN. Figure 8 shows the Gibbs free energies calculated

for the ratios as a function of temperature. Temperature dependence of Gibbs free energy is negative for both ratios, indicating that the BN formation entropies of the reactions are positive. A more important and interesting point to note is that the temperature dependence of Gibbs free energy (the slope of ΔG_f vs temperature) for BA:M=6:1 is more negative than that of BA:M=2:1. This, in turn, leads to lower theoretical BN formation temperature for BA:M=6:1 than BA:M=2:1, which can clearly explain the observation we made, i.e., an increase in BA:M ratio promotes BN formation at lower temperature.

We point out that we passed a high-volume rate nitrogen flow (2 L/min) over reactions studied herein to ascertain that gas phase equilibria was never reached, which would otherwise choke the reactions. The nitrogen flow passed over the "system" was at ambient pressure (~1 atm) and of high flow rate with high enough escape velocity on the exit side (the exit gas was bubbled through a flask). For any chemical reaction under isothermal and isobaric conditions such as the ones considered in this study, $\Delta G_{Rx}=RTln(Q/K)$, which is $\Delta G_{Rx} <0$ for $Q<K$ (G_{Rx} is Gibbs free energy of the reaction, Q is the activity quotient, and K is the equilibrium constant). We have ensured $Q<K$ in the study presented herein by flowing a high-volume rate nitrogen gas.

We note that the theoretical temperature for BN formation (~460°C) is close to the observed temperature (between 400 and 500°C) for BA:M=6:1, but for BA:M=2:1 there is a considerable difference between theoretical temperature (~1200°C) and observed one (between 900 and 1000°C). The discrepancy may be related possible differences between proposed reactions and reactions that actually occur, for example, in terms of the components and amounts of evolving gases and possible evaporation of B_2O_3 with increasing temperature. The discrepancy could be reduced by observing the actual gases

evolving during reactions in-situ with the help of mass spectroscopy, which is beyond the scope of this study. We also note no study is available attempting to explain the governing reactions for BN formation from BA+M mixture or other similar systems by using thermodynamic analyses such as the ones presented herein. Hence, the analyses presented in this study constitute a foundation for further thermodynamic modeling of formation reactions in ensuing future studies.

4.3 Kinetic considerations

In the foregoing discussion, which we based on derived formation reactions and related thermodynamic considerations, we were able to explain why an increase in BA:M ratio reduced the theoretical BN formation temperature. Moreover, the associated advance in structural ordering of the formed BN can be further explained by kinetic considerations. As shown in the foregoing chemical equations, the BN formation from BA+M mixture (or BA+Urea mixture) is accompanied by B_2O_3 formation and an increase in BA:M ratio leads to the formation of additional B_2O_3, which melts around 450˚C [46]. Once liquid B_2O_3 forms, it would enhance material transfer and layer mobility for the formed BN and thus enhance its structural ordering as suggested and evidenced by several groups. For instance, Thomas et al. showed that the presence of B_2O_3 promoted the ordering from t-BN to h-BN [20]. Hagio et al. revealed that removal of excess B_2O_3 from the starting BN specimen suppressed the advance of structural ordering upon heat treatment [39]. In another study, Çamurlu et al. showed that additions of sodium carbonate to amorphous BN, which forms sodium borate melt when heated, improved h-BN crystal growth as well as yield [37]. These findings indicated that formation of B_2O_3, as a byproduct, plays an important role in

enhancing the kinetics of structural ordering of the formed BN. In summary, increasing BA:M ratio produces two-fold effect: i) it promotes BN formation at lower temperatures by reducing the theoretical BN formation temperature, and ii) it promotes structural ordering of formed BN by enhancing material transfer and mobility of individual BN layers.

5. Concluding Remarks

We synthesized BCNO compounds with various chemistries and degrees of crystallinity by systematically varying the H_3BO_3 to $C_3H_6N_6$ ratio in the starting composition and the synthesis temperature. We investigated how the synthesis conditions impacted i) the formation of BCNO compounds and their chemistries and degrees of crystallinity and ii) the formation of BN from BCNO compounds and its structural ordering.

Through XRD, FTIR, HRTEM, and EELS analyses we observed that: i) heating the H_3BO_3 and $C_3H_6N_6$ mixture yields amorphous BCNO as intermediate compounds, ii) increase in synthesis temperature promotes crystalline BN formation from amorphous BCNO compounds, and iii) increasing the H_3BO_3 to $C_3H_6N_6$ ratio promotes BN formation at lower temperatures and advances its structural ordering at certain temperatures. We proposed a reaction mechanism for the BN formation from H_3BO_3 and $C_3H_6N_6$ mixture and explained the observations based on thermodynamic and kinetic considerations. An increase in the synthesis temperature promotes BN formation since the reactions are endothermic. Increase in H_3BO_3:$C_3H_6N_6$ ratio promotes BN formation since the theoretical temperature for BN formation decreases with the increase in H_3BO_3:$C_3H_6N_6$ molar ratio.

Furthermore, an increase in the H_3BO_3:$C_3H_6N_6$ molar ratio promotes the structural ordering of the formed BN because it enhances material transfer and mobility of individual BN layers by forming additional amounts of the B_2O_3 phase. We also proposed a processing-structure correlation map that can help synthesize single-phase amorphous BCNO compounds.

Acknowledgments

This research was sponsored by and was accomplished under the Office of Naval Research Grant No: N00014-17-1-2532 and Defense Advanced Research Projects Grant No: W31P4Q-13-1-0001. Additional support was received from the National Science Foundation I/UCRC Award No: 1540027. The authors would like to thank Dr. Daniel Kopp for his help with thermal analysis, and Jennifer Weir and Jun Won for their valuable assistance in the laboratory. Metin Örnek acknowledges graduate scholarship from the Ministry of National Education, the Republic of Turkey.

References

[1] R.H. Wentorf, Cubic Form of Boron Nitride, J. Chem. Phys., 26 (1957) 956.

[2] E.J.M. Hamilton, S.E. Dolan, C.M. Mann, H.O. Colijn, C.A. McDonald, S.G. Shore, Preparation of Amorphous Boron Nitride and Its Conversion to a Turbostratic, Tubular Form, Science, 260 (1993) 659-661.

[3] C. Ji, V.I. Levitas, H. Zhu, J. Chaudhuri, A. Marathe, Y. Ma, Shear-induced phase transition of nanocrystalline hexagonal boron nitride to wurtzitic structure at room temperature and lower pressure, Proc. Natl. Acad. Sci. U.S.A., 109 (2012) 19108-19112.

[4] R. Haubner, M. Wilhelm, R. Weissenbacher, B. Lux, Boron Nitrides — Properties, Synthesis and Applications, in: M. Jansen (Ed.) High Performance Non-Oxide Ceramics II, Springer Berlin Heidelberg (2002), pp. 1-45.

[5] S. Batsanov, L. Kopaneva, E. Lazareva, I. Kulikova, R. Barinsky, On the Nature of Boron Nitride E-Phase, PEP., 18 (1993) 352-355.

[6] M. Örnek, K.M. Reddy, C. Hwang, V. Domnich, A. Burgess, S. Pratas, J. Calado, K.Y. Xie, S.L. Miller, K.J. Hemker, R.A. Haber, Observations of explosion phase boron nitride formed by emulsion detonation synthesis, Scripta Mater., 145 (2018) 126-130.

[7] Y. Tian, B. Xu, D. Yu, Y. Ma, Y. Wang, Y. Jiang, W. Hu, C. Tang, Y. Gao, K. Luo, Z. Zhao, L.M. Wang, B. Wen, J. He, Z. Liu, Ultrahard nanotwinned cubic boron nitride, Nature, 493 (2013) 385-388.

[8] X. Zhang, H.-G. Boyen, N. Deyneka, P. Ziemann, F. Banhart, M. Schreck, Epitaxy of cubic boron nitride on (001)-oriented diamond, Nat. Mater., 2 (2003) 312.

[9] L. Song, L. Ci, H. Lu, P.B. Sorokin, C. Jin, J. Ni, A.G. Kvashnin, D.G. Kvashnin, J. Lou, B.I. Yakobson, P.M. Ajayan, Large Scale Growth and Characterization of Atomic Hexagonal Boron Nitride Layers, Nano Lett., 10 (2010) 3209-3215.

[10] A. Lipp, K.A. Schwetz, K. Hunold, Hexagonal boron nitride: Fabrication, properties and applications, J. Eur. Ceram. Soc., 5 (1989) 3-9.

[11] D. Golberg, Y. Bando, Y. Huang, T. Terao, M. Mitome, C. Tang, C. Zhi, Boron Nitride Nanotubes and Nanosheets, ACS Nano, 4 (2010) 2979-2993.

[12] W.-Q. Han, L. Wu, Y. Zhu, K. Watanabe, T. Taniguchi, Structure of chemically derived mono- and few-atomic-layer boron nitride sheets, Appl. Phys. Lett., 93 (2008) 223103.

[13] J.Y. Choi, S.J.L. Kang, O. Fukunaga, J.K. Park, K. Eun, Effect of B2O3 and hBN crystallinity on cBN synthesis, J. Am. Ceram. Soc., 76 (1993) 2525-2528.

[14] L. Vel, G. Demazeau, Nucleation and growth of cubic BN crystals in the presence of $Ca_3B_2N_4$ + xLiF as flux-precursor, Solid State Commun., 79 (1991) 1-4.

[15] L. Singh, V. Chopra, Effect of preparation conditions on the crystallinity of chemically synthesized BCNO nanophosphor, J. Mater. Res. Technol., 27 (2011) 967-972.

[16] X. Zhang, Z. Lu, J. Lin, Y. Fan, L. Li, X. Xu, L. Hu, F. Meng, J. Zhao, C. Tang, Spectra Properties of BCNO Phosphor Prepared by a Two-Step Method at Low Sintering Temperature, ECS J. Solid State Sci. Technol., 2 (2012) R39-R43.

[17] T. Kawasaki, Y. Kuroda, H. Nishikawa, H. Hara, Hexagonal system boron nitride powder, US Patent (US5854155 A)(1998).

[18] B.E. Warren, X-Ray Diffraction in Random Layer Lattices, Phys. Rev., 59 (1941) 693-698.

[19] S. Alkoy, C. Toy, T. Gönül, A. Tekin, Crystallization behavior and characterization of turbostratic boron nitride, J. Eur. Ceram. Soc., 17 (1997) 1415-1422.

[20] J. Thomas, N.E. Weston, T.E. O'Connor, Turbostratic Boron Nitride, Thermal Transformation to Ordered-layer-lattice Boron Nitride, J. Am. Chem. Soc., 84 (1962) 4619-4622.

[21] M. Hubáček, M. Ueki, T. Sato, V. Brožek, High-temperature behaviour of hexagonal boron nitride, Thermochimica Acta, 282 (1996) 359-367.

[22] O. Hod, Graphite and Hexagonal Boron-Nitride have the Same Interlayer Distance. Why?, J. Chem. Theory Comput., 8 (2012) 1360-1369.

[23] M. Baraton, T. Merle, P. Quintard, V. Lorenzelli, Surface activity of a boron nitride powder: a vibrational study, Langmuir, 9 (1993) 1486-1491.

[24] D. Portehault, C. Giordano, C. Gervais, I. Senkovska, S. Kaskel, C. Sanchez, M. Antonietti, High-Surface-Area Nanoporous Boron Carbon Nitrides for Hydrogen Storage, Adv. Funct. Mater., 20 (2010) 1827-1833.

[25] C. Gautam, A.K. Yadav, A.K. Singh, A Review on Infrared Spectroscopy of Borate Glasses with Effects of Different Additives, ISRN Ceramics, 2012 (2012) 1-17.

[26] Y. Cheng, H. Xiao, W. Guo, W. Guo, Structure and crystallization kinetics of PbO–B_2O_3 glasses, Ceram. Int., 33 (2007) 1341-1347.

[27] S.I. Hirano, T. Yogo, S. Asada, S. Naka, Synthesis of amorphous boron nitride by pressure pyrolysis of borazine, J. Am. Ceram. Soc., 72 (1989) 66-70.

[28] A.Y. Liu, R.M. Wentzcovitch, M.L. Cohen, Atomic arrangement and electronic structure of BC_2N, Phys. Rev. B, 39 (1989) 1760-1765.

[29] T. Hasegawa, K. Yamamoto, Y. Kakudate, Influence of raw gases on B–C–N films prepared by electron beam excited plasma CVD, Diam. Relat. Mater., 12 (2003) 1045-1048.

[30] R. Geick, C.H. Perry, G. Rupprecht, Normal Modes in Hexagonal Boron Nitride, Phys. Rev., 146 (1966) 543-547.

[31] C.C. Ahn, O.L. Krivanek, EELS Atlas: A Reference Collection of Electron Energy Loss Spectra Covering All Stable Elements, Gatan (1983).

[32] Y. Meng, H.K. Mao, P.J. Eng, T.P. Trainor, M. Newville, M.Y. Hu, C. Kao, J. Shu, D. Hausermann, R.J. Hemley, The formation of sp3 bonding in compressed BN, Nat. Mater., 3 (2004) 111-114.

[33] K.M. Reddy, C. Hwang, M. Ornek, S.L. Miller, W.E. Mayo, A. Burgess, R.A. Haber, K.J. Hemker, Observations of nanocrystalline cubic boron nitride formed with plasma spraying, Acta Mater., 116 (2016) 155-165.

[34] C. Gautam, C.S. Tiwary, S. Jose, G. Brunetto, S. Ozden, S. Vinod, P. Raghavan, S. Biradar, D.S. Galvao, P.M. Ajayan, Synthesis of Low-Density, Carbon-Doped, Porous Hexagonal Boron Nitride Solids, ACS Nano, (2015).

[35] M. Hubáček, M. Ueki, Chemical reactions in hexagonal boron nitride system, J. Solid State Chem., 123 (1996) 215-222.

[36] A. Aydoğdu, N. Sevinç, Carbothermic formation of boron nitride, J. Eur. Ceram. Soc., 23 (2003) 3153-3161.

[37] H.E. Çamurlu, Effect of Na_2CO_3 on hexagonal boron nitride prepared from urea and boric acid, Ceram. Int., 37 (2011) 1993-1999.

[38] T. Wakasugi, F. Tsukihashi, N. Sano, Thermodynamics of Nitrogen in B_2O_3, B_2O_3-SiO_2, and B_2O_3-CaO Systems, J. Am. Ceram. Soc., 74 (1991) 1650-1653.

[39] T. Hagio, K. Nonaka, T. Sato, Microstructural development with crystallization of hexagonal boron nitride, J. Mater. Sci. Lett., 16 (1997) 795-798.

[40] J. Parsons, Vibrational spectra of orthorhombic metaboric acid, J. Chem. Phys., 33 (1960) 1860-1866.

[41] L. Costa, G. Camino, Thermal behaviour of melamine, J. Therm. Anal. Calorim., 34 (1988) 423-429.

[42] J. Zhong, Y. Feng, H. Wang, D. Hu, Fabrication and characterization of hexagonal boron nitride powder by a precursor conversion method, J. Ceram. Process. Res., 14 (2013) 269-273.

[43] P. Linstrom, W. Mallard, NIST chemistry webbook, NIST standard reference database number 69, National Institute of Standards and Technology, Gaithersburg MD, 20899, (2010).

[44] M.W. Chase, National Institute of Standards and Technology (US), NIST-JANAF thermochemical tables, J. Phys. Chem. Ref. Data, Monograph, (1998).

[45] C. Lupis, Chemical thermodynamics of materials. New York, Amsterdam: North-Holland, Elsevier (1983).

[46] W.S. Coblenz, D. Lewis, In Situ Reaction of B_2O_3 with AlN and/or Si_3N_4 to Form BN-Toughened Composites, J. Am. Ceram. Soc., 71 (1988) 1080-1085.

Tables

Table 1. Representative carbon content (wt. %) of BCNOs prepared using BA:M ratios of 1:1, 3:1, and 6:1 with synthesis temperatures of 400°C≤T≤1000°C based on combustion analysis.

Starting BA:M Ratio	**Synthesis Temperature**			
	400°C	600°C	800°C	1000°C
1:1	26.0	24.1	6.5	3.2
3:1	11.6	10.5	3.6	0.2
6:1	5.6	4.3	1.2	0.3

Figures

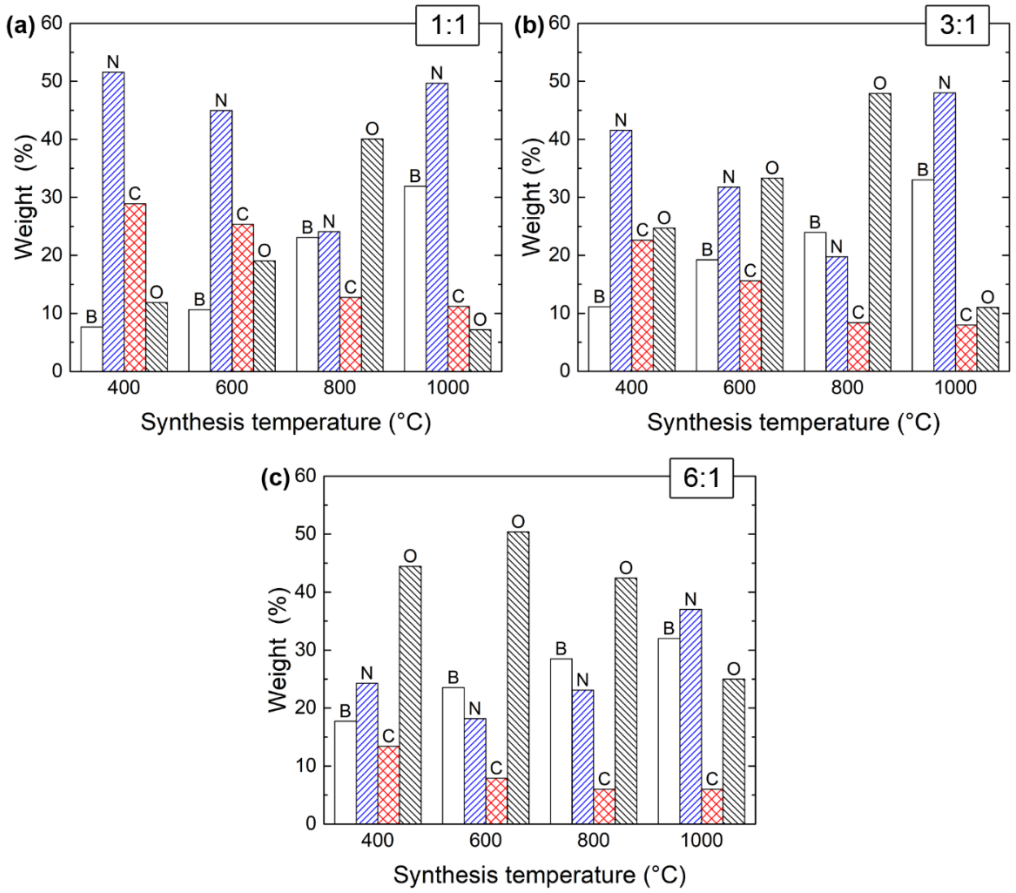

Figure 1. Representative variations of BCNO chemical composition as a function of BA:M ratio and temperature in the range 400-1000°C.

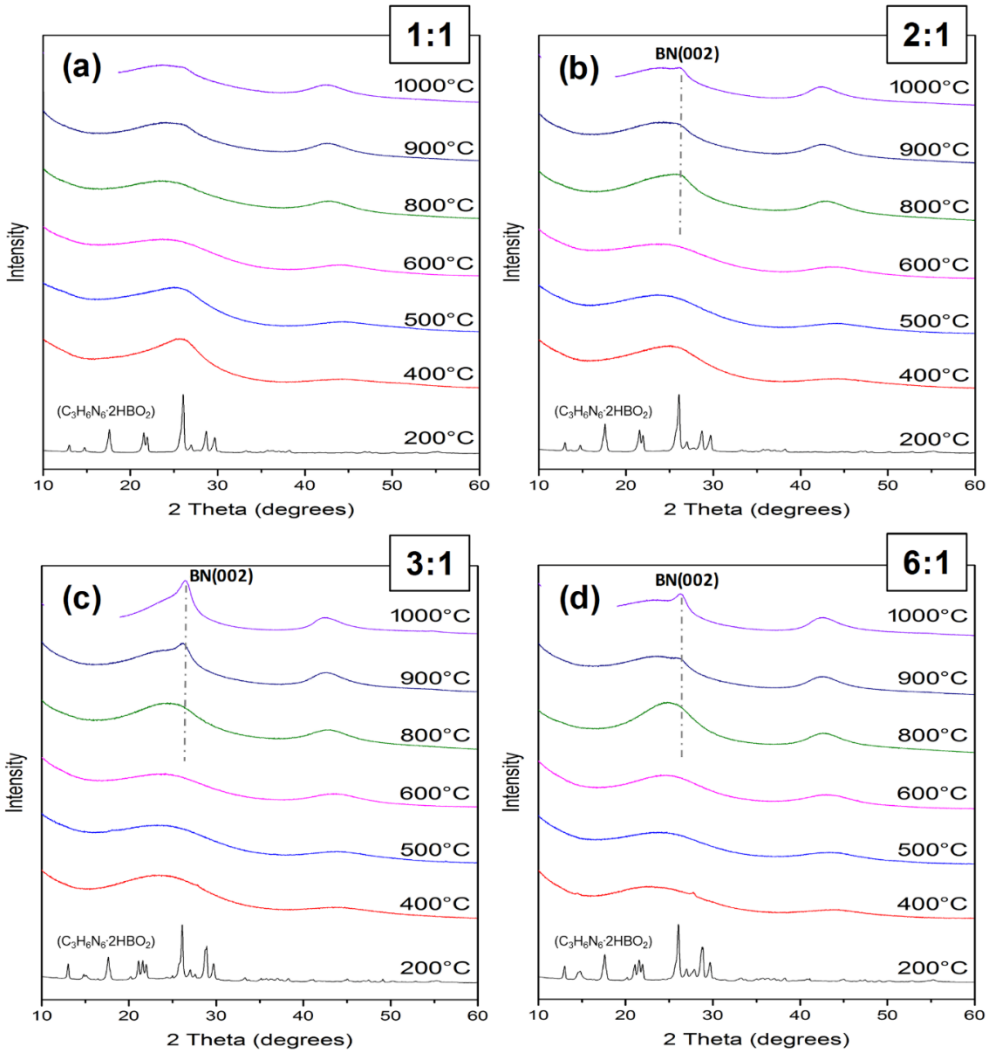

Figure 2. X-ray spectra showing phase and long-range crystallographic structure evolution in BCNO as a function of temperature in the range 400-1000°C for various BA:M ratios.

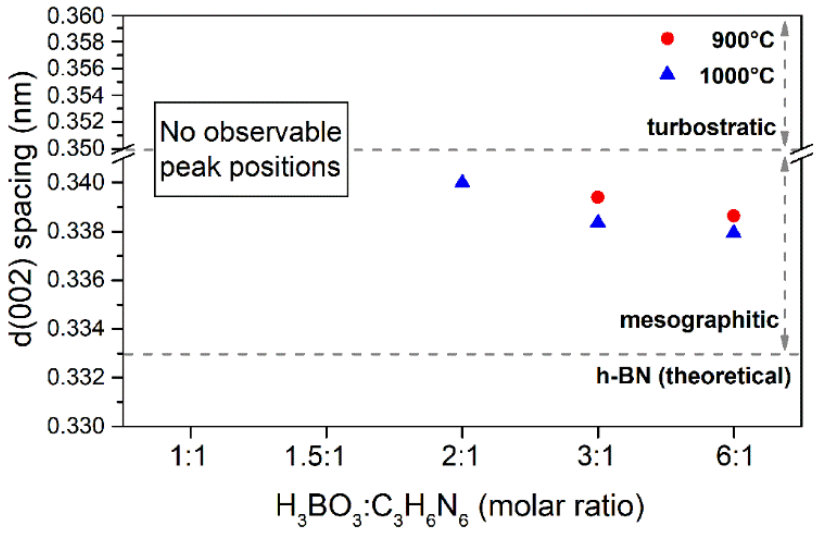

Figure 3. The variation of d_{002} spacing as a function of BA:M ratio in the isothermal synthesis of BCNO over the range 900-1000°C.

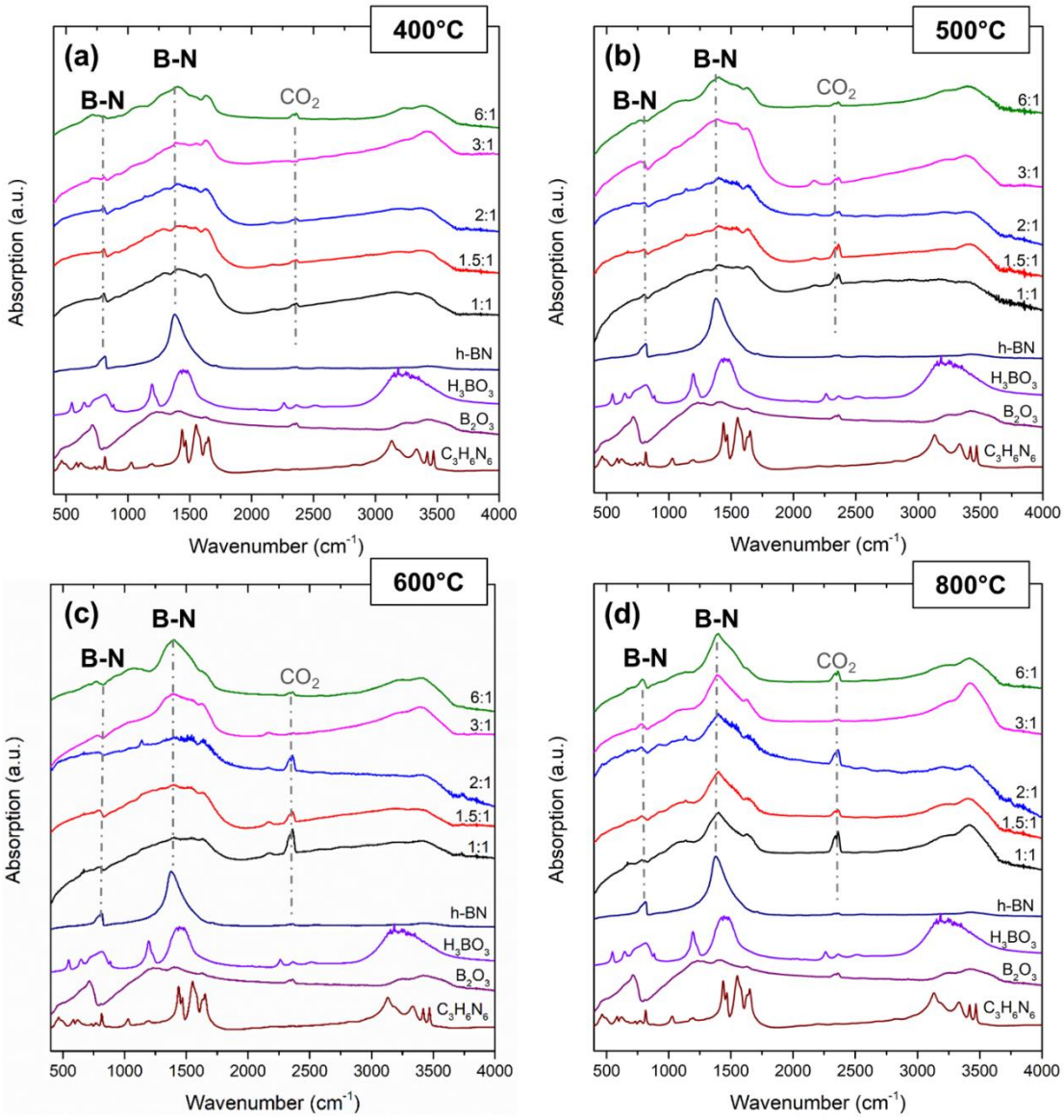

Figure 4. Representative variations in the vibrational spectra of BCNO as a function of BA:M ratio and temperature in the range 400-800°C: **a)** 400°C, **b)** 500°C, **c)** 600°C and **d)** 800°C. Included in the plots are the vibration spectra of reference materials (h-BN, H_3BO_3, $C_3H_6N_6$, and B_2O_3). At temperatures as low as 500°C, B-N bending and stretching vibrations become discernable in the FTIR spectra for BA:M=6:1 ratio.

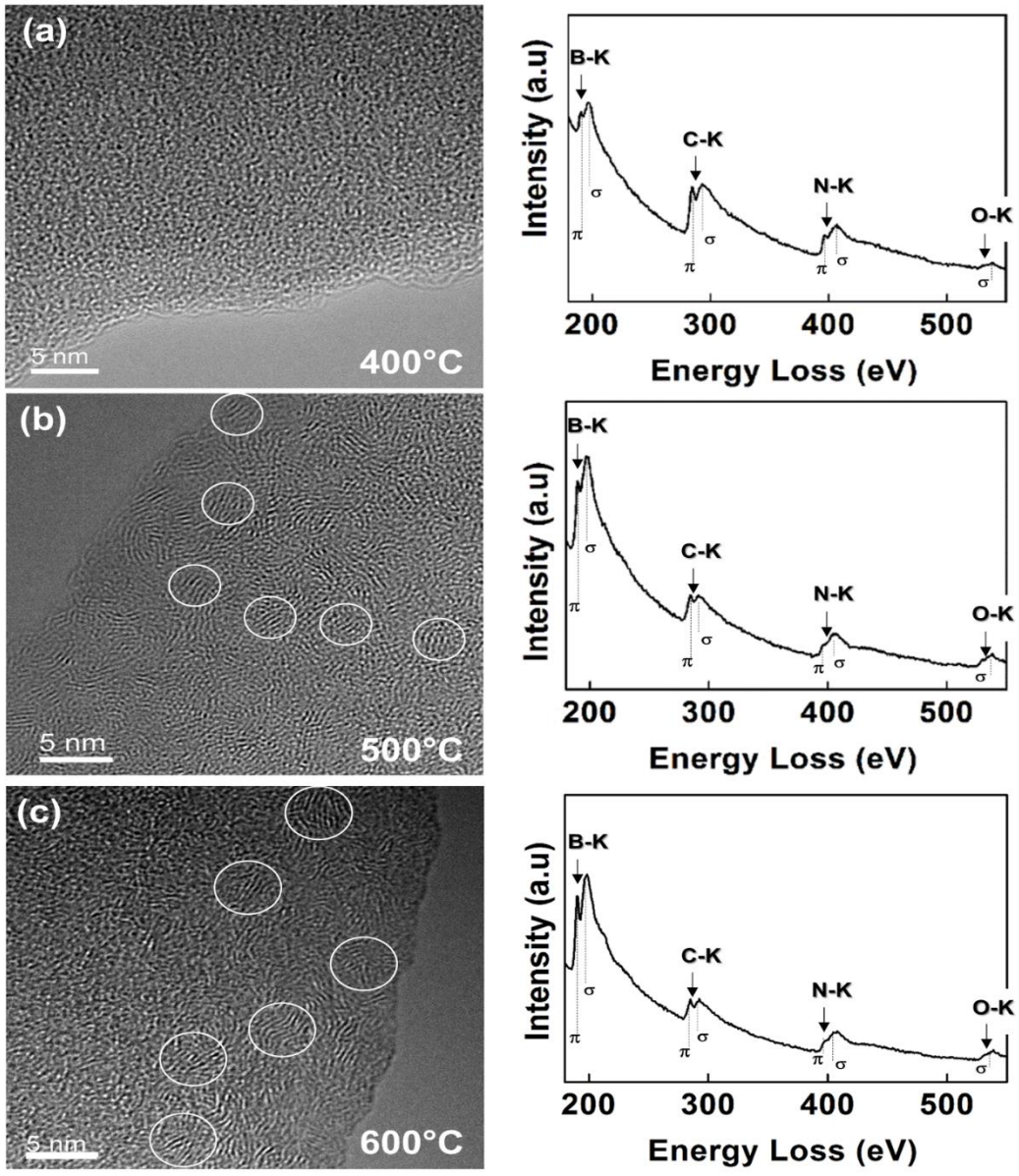

Figure 5. Representative TEM micrographs and associated EELS spectra of BCNO for BA:M=6:1 ratio and synthesis temperature **a)** 400°C, **b)** 500°C, and **c)** 600°C.

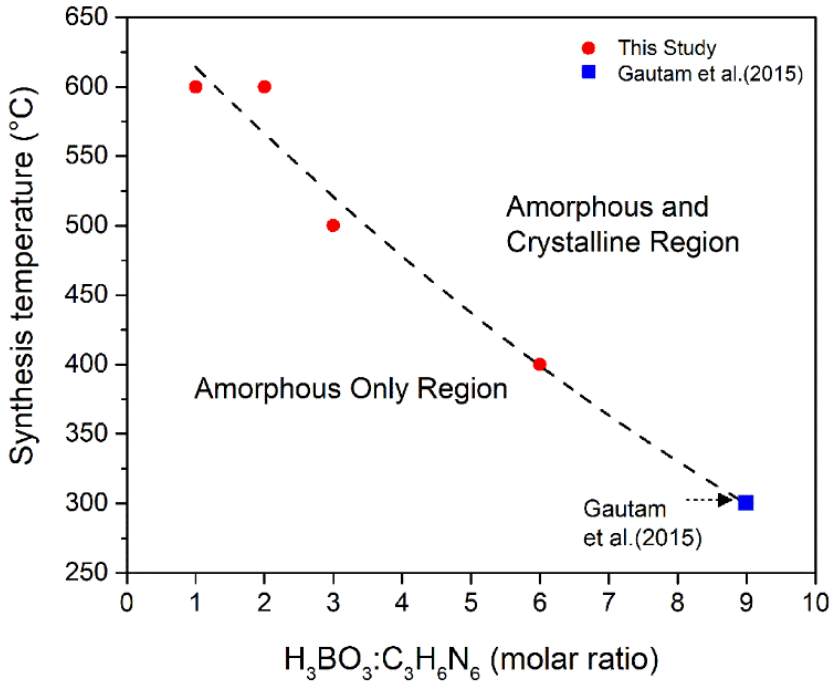

Figure 6. Processing-structure correlation map for synthesizing single phase amorphous BCNO. The temperature for the nucleation of crystalline BN, as determined from FTIR and HRTEM/EELS analyses, decreases quasi-linearly with increasing H_3BO_3:$C_3H_6N_6$ molar ratio. Combinations of temperature and H_3BO_3:$C_3H_6N_6$ molar ratio that fall below the dashed line result in the formation of single phase amorphous BCNO compounds, while the combinations above the line result in the formation of nanocrystalline BN in the amorphous matrix.

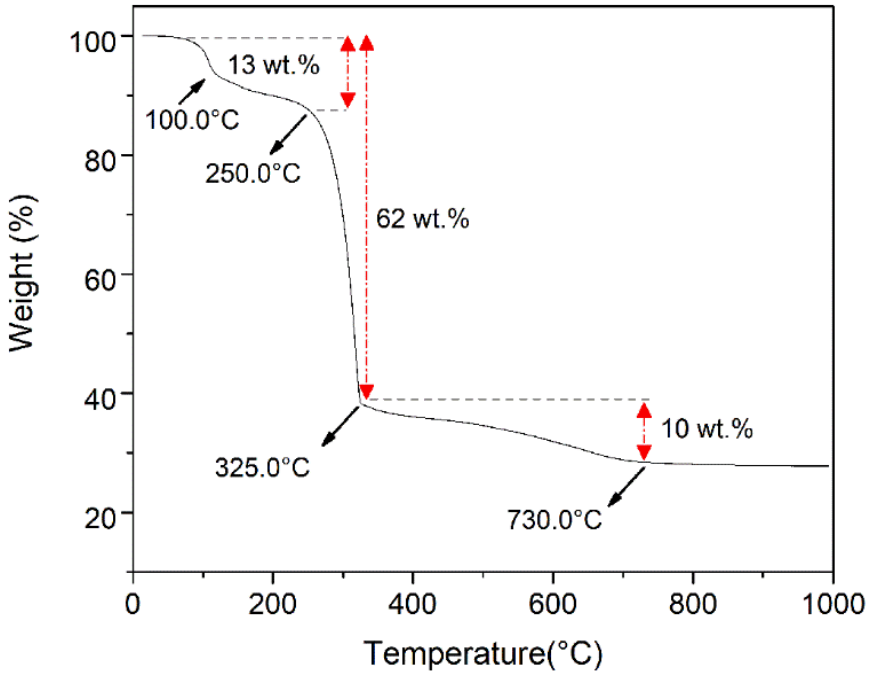

Figure 7. TGA curve for the mixture of BA:M=2:1, showing weight changes and prominent temperatures during the heating from room temperature to 1000°C.

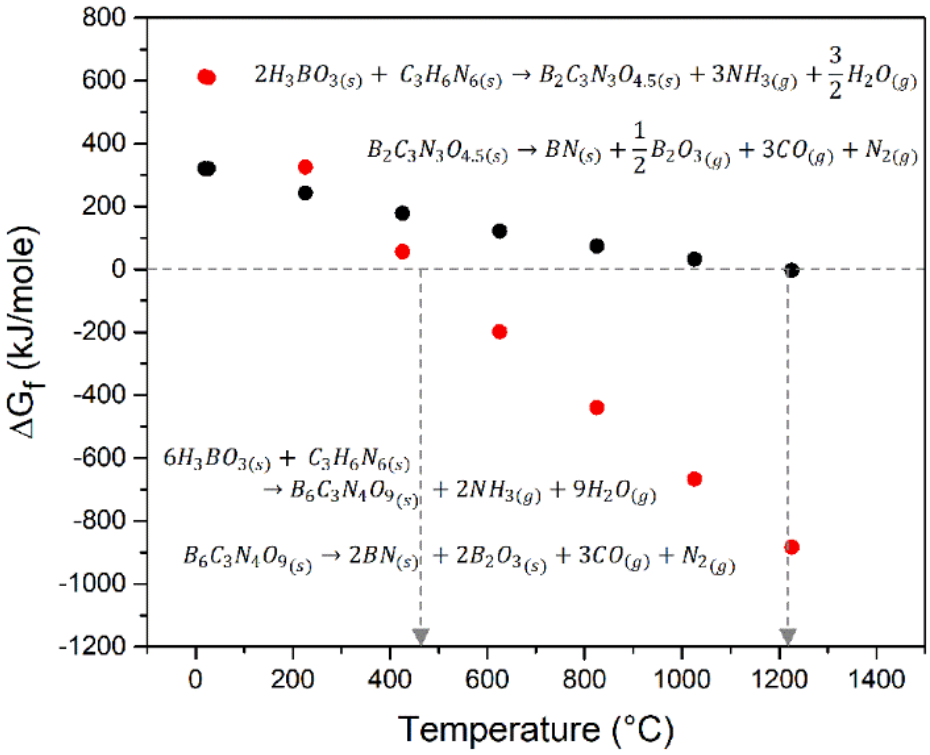

Figure 8. Comparison of temperature dependence of formation Gibbs free energy for BN formation from H_3BO_3 and $C_3H_6N_6$ mixture for BA:M=2:1 (black dots) and 6:1 (red dots), showing a drastic decrease in the theoretical temperature of BN formation by 700°C.

Supplementary Figures

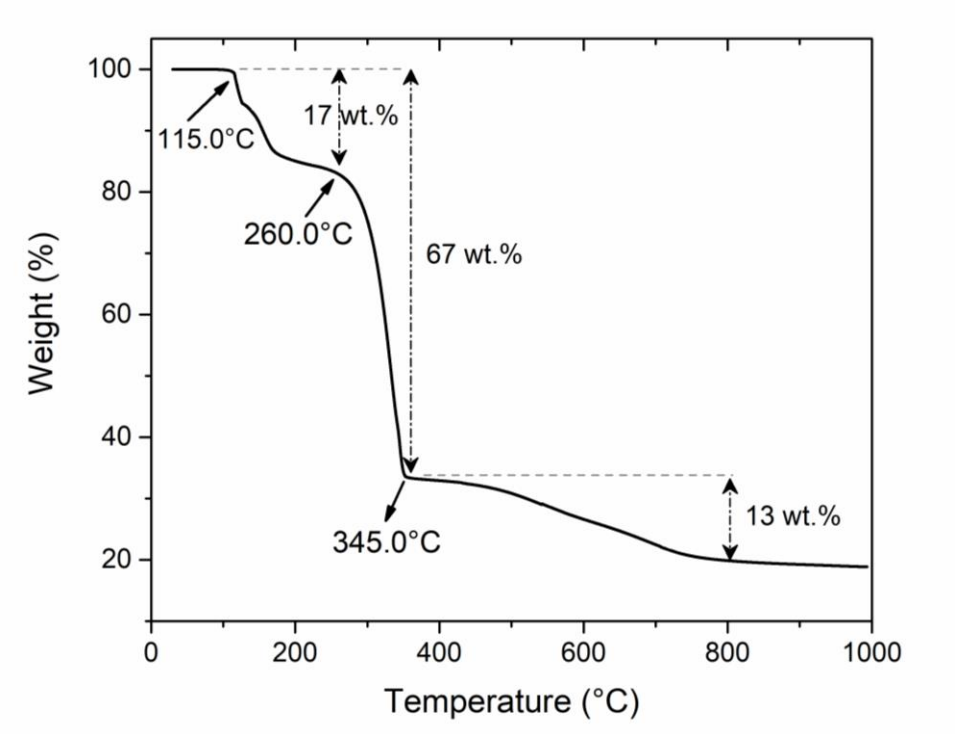

Supplementary Figure 1. TGA curve for the mixture of BA:M=1:1.

Supplementary Fig. 1 depicts that the starting mixture of BA:M=1:1 experience noticeable weight loss up to 350°C, resulting in approximately 67 wt % loss. The TGA curve shows gradual changes, e.g.13 wt % loss. from 350°C to 800°C.

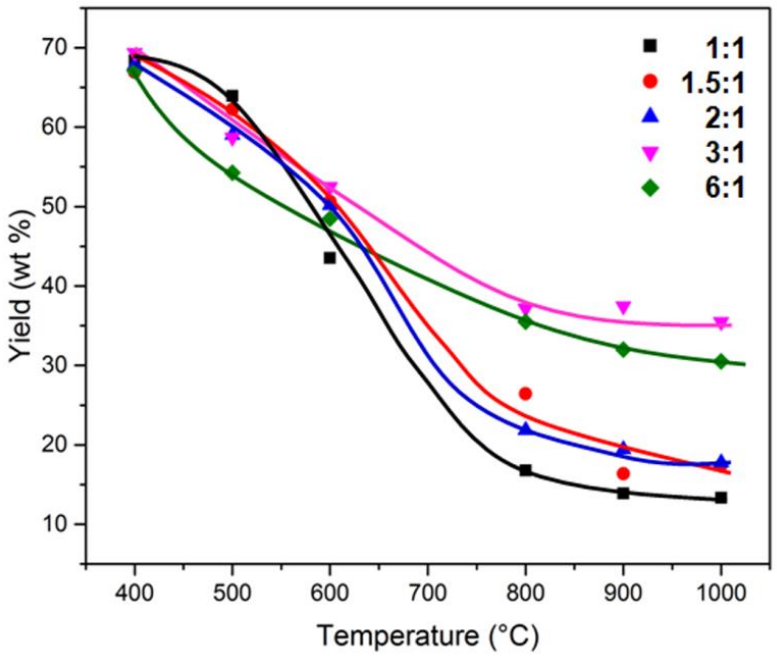

Supplementary Figure 2. The variation of BCNO yields as a function of BA:M ratio in the temperature range 400-1000°C, calculated from the measured weights of the starting mixture (BA+M) and the final BCNO compounds.

Heat treatments at 400°C yielded approximately 32 wt.% loss on average for all ratios. BA:M=1:1 ratio, which has the highest melamine content in the starting composition, resulted in a large weight loss when the synthesis temperature increased to 1000°C (13.4 wt.%). This is attributed to the higher degree of decomposition of melamine with increasing synthesis temperature as compared to boric acid. Increasing BA:M ratio up to 3:1 resulted in higher yields. The highest yield for 1000°C samples was obtained for BA:M=3:1 ratio (35.5 wt.%). Further increase in BA:M ratio to 6:1 resulted in relatively lower yield than that for 3:1, which can be due to either increased evaporation of boric acid or more releases of carbon and oxygen during heating. The results of EDX analysis (Fig. 1c) support the release of carbon and oxygen during heating.

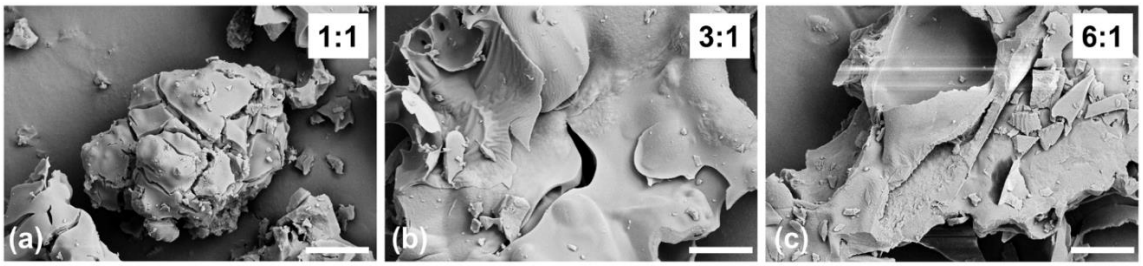

Supplementary Figure 3. Representative FE-SEM micrographs of BCNO compounds synthesized at 1000°C using a**)** 1:1, **b)** 3:1, and **c)** 6:1 of BA:M ratios. Scale bars in micrographs correspond to 10 μm.

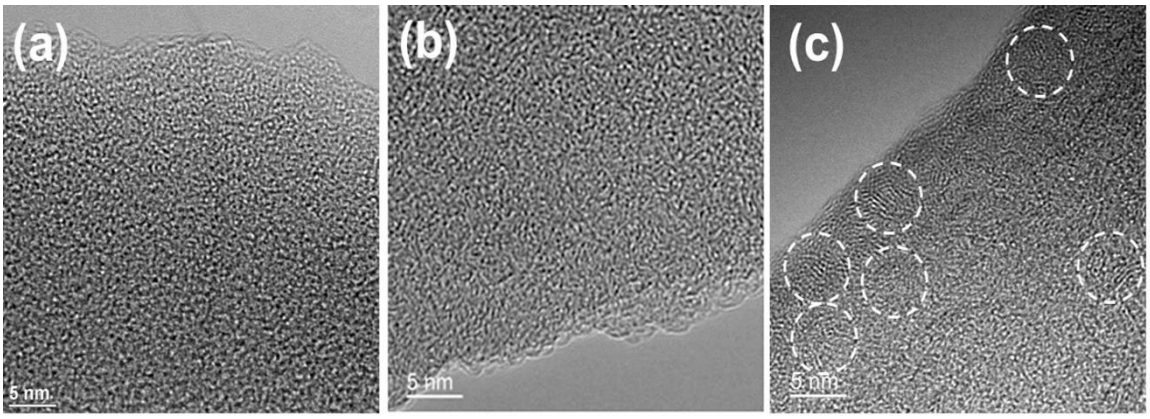

Supplementary Figure 4. Representative TEM micrographs of BCNO for BA:M= 3:1 and synthesis temperature **a)** 400°C, **b)** 500°C, and **c)** 600°C.

Supplementary Fig. 4 shows the representative TEM micrographs of BCNO compounds prepared using 3:1 molar ratio of BA:M. Suppl. Fig.3a and 3b corresponds to the microstructure of sample heat treated at 400°C and 500°C, both showing amorphous structure, i.e., no ordered lattice formation. On the other hand, the 600°C sample (Suppl. Fig.4c) had localized regions that displayed ordered lattice formation. The lattice spacing measured from the ordered structure is ~0.365 nm, indicating that these nanocrystalline regions are t-BN.

Supplementary Table

Supplementary Table 1. Representative elemental analysis results of BCNOs prepared using BA:M ratios of 1:1, 3:1, and 6:1 with synthesis temperatures of 400°C ≤ T ≤ 1000°C based on EDX analyses.

Synthesis Conditions		**Elemental Analysis (wt. %)**			
Starting BA:M Ratio	Synthesis Temperature (°C)	Boron	Nitrogen	Carbon	Oxygen
1:1	400	7.6	51.6	28.9	11.9
	600	10.7	44.9	25.4	19.0
	8000	23.1	24.1	12.8	40.0
	1000	31.9	49.7	11.2	7.2
3:1	400	11.1	41.6	22.6	24.7
	600	19.3	31.8	15.6	33.3
	800	23.9	19.8	8.4	47.9
	1000	33.0	47.4	8.1	11.5
6:1	400	17.7	24.3	13.4	44.6
	600	23.5	18.2	7.9	50.4
	800	28.5	23.1	6.0	42.4
	1000	32.1	37.3	6.2	24.4

Chapter 3.

Effect of synthesis conditions of BCNO on the formation and structural ordering of BN at 1200°C and 1 GPa

Chawon Hwang[1,*], Metin Örnek[1], Kolan Madhav Reddy[2†], Vladislav Domnich[1], Steve L. Miller[3], Kevin Hemker[2], and Richard A. Haber[1,*]

[1]*Department of Materials Science and Engineering, Rutgers, The State University of New Jersey, Piscataway, NJ 08854, USA.*

[2]*Department of Mechanical Engineering, Johns Hopkins University, Baltimore, MD 21218, USA.*

[3]*H&M Analytic Services Inc., Cream Ridge, NJ 08514, USA.*

*Corresponding author e-mail: chawon.hwang@rutgers.edu; rich.haber@rutgers.edu, and address: 607 Taylor Road, Piscataway, NJ 08854, USA (Tel: +1(848)445-5924)

† Author's present address: *State Key Laboratory of Metal Matrix Composites, School of Materials Science and Engineering, Shanghai Jiao Tong University, Shanghai 200240, China.*

Abstract

We investigated the correlation between the synthesis conditions of BCNO compounds and the formation and structure ordering of BN by subjecting BCNO compounds to a post heat-pressure treatment at 1200˚C and 1 GPa. We made a direct observation that BN grains form from BCNO matrix. We found that the formation and structural ordering of BN strongly depend on the synthesis conditions of BCNO compounds. An increase in synthesis temperature promotes the formation of BN since the reaction process involved is endothermic. An increase in boric acid to melamine ratio promotes the formation and structural ordering of BN since i) it reduces the theoretical temperature for BN formation and ii) it enhances mass transfer and mobility of BN layers by forming additional amount of B_2O_3 phase. Further, loading pressure of 1 GPa resulted in a more compressed layered structure of the resultant BN.

Keywords: BCNO compound; Boron nitride; Structure ordering; Post treatment; Heat; Pressure.

1. Introduction

Boron nitride (BN) is known to exist in various polymorphic forms such as hexagonal (h-BN), turbostratic (t-BN), amorphous (a-BN), rhombohedral (r-BN), wurtzite (w-BN), cubic (c-BN), orthorhombic (o-BN), and explosive (e-BN) [1-4]. Among these, thermodynamically stable phases are h-BN (low density phase) and c-BN (high density phase), both of which have found applications in various fields because of their unique properties. h-BN has been used as a high-temperature lubricant because of its high thermal stability in air (up to 1000°C) and low friction coefficient (0.24 in dry air), as a refractory material because of its non-wettability to high-temperature melts, and as an additive to cosmetic products because of its chemical inertness [5-7]. c-BN has been used as an abrasive for grinding and tooling because of its extremely high hardness (~45 or 70 GPa, second only to diamond) and high temperature oxidation resistance (up to 1000°C). For engineering hardened or alloyed steels, c-BN is superior to diamond because of its chemical stability to ferrous metals and their alloys [8-12].

For the synthesis of BN, BCNO compounds are one of the typical and important starting materials. Their chemical or structural characteristics have strong impacts on the synthesis conditions and properties of the resultant BN phases [2, 13-15]. For example, in our previous study we showed that the starting composition of BCNO compounds strongly impacts the temperature at which hexagonal BN phase forms from BCNO compounds [15]. In the synthesis of c-BN, the degree of crystallinity and particle size of the starting BN phase play an important role in reducing pressure and temperature for c-BN transformation from h-BN, which typically occurs above 8 GPa and 2100°C [16, 17]. By using h-BN with low crystallinity and small particle size, it is possible to reduce the pressure and

temperature for c-BN formation down to 6 GPa and 1200°C [18]. When amorphous BN is used, the typical conditions can be reduced to 7 GPa at 800°C [19]. Nonetheless, it is not well understood how the chemical and structural characteristics of BCNO compounds impact the structure ordering of BN during a post treatment, especially under high temperature and pressure.

In our previous study we investigated the correlation between the synthesis conditions of BCNO compounds and the formation and structural ordering of BN during a heat treatment up to 1000˚C [15]. In this study we investigated the above correlation by subjecting BCNO compounds to a post heat-pressure treatment at 1200˚C and 1 GPa. Our focus was to identify i) whether the reaction mechanism proposed in our previous study still plays a role during a post heat-pressure treatment and ii) whether a loading pressure of 1 GPa at 1200˚C has any impact on the structure ordering of BN forms.

2. Experimental Details

2.1 Synthesis of BCNO compounds

BCNO compounds were prepared by heating mixtures of boric acid (H_3BO_3, Borax, Optibor®) and melamine ($C_3H_6N_6$, DSM, MelaminebyDSM^{TM}) with different ratios (1:1, 3:1, and 6:1 mole ratio). A two-step heating process was employed: first heating at 200°C in air for 2 hours and second heating at 400°C, 600°C, and 800°C for 3 hours in N_2 gas atmosphere (2 L/min). Details of synthesis procedure can be found in our previous study [15]. BCNO compounds thus obtained were pulverized (alumina mortar and pestle) and sieved through a #200 sieve to make the particle size consistent and washed with methanol (10 wt% solid content for 30 min) to remove possible residual boric acid.

2.2 Heat-pressure treatment

Powders thus obtained were dried at 100°C for 2 hours and loaded into titanium (Ti) capsules (3 mm OD, 0.5 mm wall thickness, and 8~10 mm length; lids with 0.3 mm thickness), which were hermetically sealed using arc-welding. The sample capsule prepared was loaded into a piston-cylinder type high pressure-high temperature (HPHT) equipment (QUICKPress, Depth of the Earth Co., AZ, USA). Pressure was generated using a hydraulic ram inside the cylinder containing the sample capsule surrounded by a graphite furnace assembly. Heat was generated through a graphite furnace surrounding the sample capsule. Detailed configuration of HPHT experiment can be found in elsewhere [20]. Pressure was calibrated by detecting melting of NaCl at 1004°C and 1 GPa [21]. Temperature was monitored using a Pt-Pt10%Rh thermocouple inserted into the furnace assembly. The pressure was increased to 1 GPa at room temperature, and then the temperature was isobarically increased to 1200°C (± 15°C) and held for 15 min. After heating, samples were isobarically quenched to room temperature.

2.3 Characterization

BCNO compounds as-prepared and post treated were characterized using XRD (PANalytical, PW3040/60), FE-SEM (ZEISS, SIGMA) equipped with energy dispersive X-ray spectroscopy (EDX) detector (OXFORD, X-MAX 80), carbon analyzer (LECO, CS230), and TEM (Philips, FEI CM-300) equipped with electron energy loss spectroscopy (EELS, Gatan 200). XRD was employed to identify phases formed and calculate d-spacing value and parallel layer group parameter (which typically corresponds to average crystallite size, hereafter noted as layer parameter) [2, 22]. *D*-spacing value and layer parameter along *c*-axis for hexagonal unit cell were calculated using the full width at half maximum

(FWHM) and position of (002) reflection according to the Scherrer equation, see below, and the Bragg equation, respectively [2].

$$L_c = (K \times \lambda)/(\beta \times cos\theta),$$

where L_c is layer parameter along c-axis, K is a dimensionless shape factor (0.9 for (002) plane), λ is the wavelength of the X-ray beam (Cu Kα, 1.54187 Å), β is the full width at half maximum (FWHM) of diffraction peak (radian), and θ is the Bragg angle (degree) [2, 22]. SEM and TEM were employed to observe morphology and microstructure. EDX and carbon analyzer were employed to analyze chemical composition. EELS was employed to analyze chemical elements and the bonding type between elements.

3. Results

3.1 Characteristics of BCNO compounds prepared

Fig. 1a shows XRD patterns of representative BCNO compounds prepared at 800°C. The XRD patterns showed no distinct peak but two broad maxima around 2θ values of 24° and 42°. Regarding the structure of BCNO compounds with this feature, previous reports classified it to either amorphous or turbostratic [13, 23]. In our previous study, we reported that the BCNO compounds prepared with the same technique show either amorphous structure only or an amorphous matrix containing local structural ordering depending on the synthesis conditions: i.e., BCNO compounds prepared at 400°C, amorphous structure only; compounds prepared at 800°C (Fig. 1a), amorphous matrix containing local structural ordering [15]. As the boric acid to melamine ratio (hereafter noted as BA:M ratio) increased, the two broad maxima became more distinct and sharp. Fig. 1b shows chemical compositions of BCNO compounds prepared at different

temperatures, of which BA:M=1:1. As the synthesis temperature increased, the nitrogen and carbon contents decreased while the boron and oxygen contents increased. We attribute this trend to the decomposition of melamine, of which the decomposition temperature is around 350°C. The trend of carbon content was confirmed using combustion analysis: carbon content decreased as synthesis temperature increased.

3.2 Post heat-pressure treatment – Effect of variation in synthesis temperature

Synthesized BCNO compounds were subjected to post heat-pressure treatment at 1200°C and 1 GPa. Fig. 2 shows XRD patterns of post heat-pressure treated (hereafter noted as post treated) BCNO compounds, of which BA:M=1:1 and synthesis temperatures were 400°C, 600°C, and 800°C. Commercial h-BN (ZYP Coatings, Inc., Grade ZG) was also included as a comparison sample. Post treated 400°C (synthesis temperature) sample showed two distinct peaks around 26° and 43°. As the synthesis temperature increased to 800°C, the peak around 26° became sharp and shifted to a larger angle, where (002) reflection of h-BN displays. The peak around 43° resolved into two peaks around 42° and 43°, where (100) and (101) reflections of h-BN show. In addition, peaks of boron oxide (JCPDS card No. 06-0297) were also observed in the post treated 800°C (synthesis temperature) sample.

Figure 3 shows SEM and TEM micrographs of BCNO compounds after heat-pressure treatments. Post treated 400°C (synthesis temperature) sample did not show distinct grains, although local structural ordering is evident from TEM observation (Fig. 3a and d). When the synthesis temperature increased to 600°C (Fig. 3b and e) and 800°C (Fig. 3c and f), the samples showed nearly spherical grains with diameters of 10-20 nm for the 600°C sample and 50-60 nm for the 800°C sample.

3.3 Post heat-pressure treatment – Effect of variation in starting composition

BCNO compounds with variations in starting composition (BA:M=1:1, 3:1, and 6:1 with a synthesis temperature of 400°C) were subjected to heat-pressure treatment at 1200°C and 1 GPa. Fig. 4 shows XRD patterns of the post treated BCNO compounds. Post treated sample with BA:M=1:1 showed two distinct peaks around 26° and 43°. As the BA:M ratio increased to BA:M=6:1, the peak at 26° sharpened and shifted towards a higher angles and the peak around 43° resolved into two peaks around 42° and 43°. This trend is similar to what was observed with the variation in synthesis temperature (Fig. 2). In addition, post treated samples of BA:M=3:1 and 6:1 showed peaks of boron oxide.

Figure 5 shows microstructures of the post treated BCNO compounds with variations in BA:M ratio (1:1, 3:1, and 6:1) and synthesis temperature (400°C and 800°C). Post treated sample of 1:1 (BA:M) and 400°C (synthesis temperature) did not show a distinct shape. On the other hand, post treated sample of 6:1 and 800°C showed grains with plate shape, which is a characteristic morphology of h-BN grains. These observations clearly show that increase in BA:M ratio promotes the structure ordering of BN.

3.4 Microstructure and chemical elements of grains formed

Post treated samples of 3:1 (BA:M) and 400°C (synthesis temperature) showed evidence of the initial stage of grain formation in SEM observations (Fig. 5b). For more detailed observations on the structure development of grains, particularly on the initiation of grain formation, we employed high resolution TEM coupled with EELS as shown in Fig. 6. We observed formation of crystalline grains with elongated shape and layered structure (about 10 nm in thickness) from a matrix phase (Fig. 6a). The grain has a layered structure with thickness of about 10 nm (Fig. 6b). We employed EELS to identify the

chemical elements of the grain (P2) and the matrix (P1). EELS spectrum of matrix (P1) showed energy loss peaks corresponding to B-K, C-K, and N-K edges, indicating the matrix is composed of boron, carbon, and nitrogen [14]. On the other hand, EELS spectrum of the grain (P2) showed only B-K and N-K edges, indicating that the grain is BN. Furthermore, the fact that all elemental peaks show π and σ bonds indicates that the BN grain consists of sp^2 bonding, which is the characteristic bonding type of hexagonal BN [14]. Taken together with XRD and SEM analyses, these results show that BN grains with hexagonal unit cell form from amorphous BCNO matrix.

4. Discussion

Among different polymorphic forms of BN, h-BN is the most thermodynamically stable phase at ambient conditions. Structural ordering of h-BN is well established by Thomas et al. on the basis of XRD analysis on BNs formed by heating boric acid-urea mixtures [22]. First, a BN phase with less-ordered hexagonal structure forms, which is termed turbostratic BN (t-BN), and the t-BN develops into a fully ordered hexagonal structure (h-BN) upon heating at higher temperatures. The term t-BN is used to define a BN phase that exhibits the lack of three-dimensional order. Characteristic XRD pattern of t-BN shows two broad diffraction peaks around 25°and 42.4°. As structural ordering proceeds, the peak around 25° becomes strong and sharp and shifts to a larger angle (approximately 26.7°), where (002) reflection of ordered h-BN displays. Following the peak around 42.4° resolves into two peaks around 41.6° and 43.8°, where (100) and (101) reflections of ordered h-BN show, accompanied by the appearance of (004) reflection. The

samples in this study showed the characteristic XRD patterns of both t-BN (i.e., 400°C in Fig. 2) and h-BN (i.e., 800°C in Fig 2).

Since ordered h-BN consists of alternating layers, in the sequence of ABAB…, *d*-spacing values and layer parameters of BN with hexagonal unit cell provide useful information to understand the structure ordering [22]. *D*-spacing value for (002) peak, *d*(002), corresponds to the distance between layers along the *c*-axis. Layer parameter for (002) peak, L_c, corresponds to the average thickness of layer group along *c*-axis. As structural ordering advances from t-BN to h-BN, *d*(002) decreases to 3.33 Å (theoretical value for h-BN) and L_c increases [22, 24]. Based on the values of *d*(002) and L_c, Thomas et al. approximately classified h-BN and t-BN as follows [2, 22]. For h-BN, *d*(002)=3.33 Å, L_c>15 nm and for t-BN, *d*(002)>3.50 Å, L_c<2 nm. Structures having intermediate values between those for h-BN and t-BN were termed mesographitic BN (m-BN). Thus, comparing *d*(002) and L_c values provides a measure of how much the structural ordering advanced to ordered h-BN. Fig. 7 shows *d*(002) and L_c values calculated for BCNO samples post treated at 1GPa and 1200°C. As synthesis temperature and BA:M ratio increased, *d*(002) decreased from 3.43(4) Å for 400°C and BA:M=1:1 to 3.32(2) Å for 800°C and BA:M=6:1, and L_c increased from 2.5 nm for 400°C and BA:M=1:1 to 19.8 nm for 800°C and BA:M=6:1. According to Thomas et al.'s criteria, BNs formed in this study can be classified as either m-BN or h-BN. Layer parameter for (100) peak, L_a, as well provides useful information on structure ordering, since L_a corresponds to average layer diameter of stacked layers along the *a* direction [22]. But, unfortunately, only a few samples in this study showed clear evolution of (10) peak to (100) and (101) peaks, thus comparing L_a was not possible.

The effect of synthesis temperature on the structure ordering of BN can be explained based on ΔH (enthalpy), in the same way as discussed in our previous study [15]. The reaction from boric acid-melamine mixture to h-BN is endothermic, thus increase in the synthesis temperature promotes formation of BN and its structural ordering. Another factor to consider is the increase in boron and oxygen contents in BCNO compounds as the synthesis temperature increases (Fig. 1b), which likely leads to the formation of boron oxide (B_2O_3) during the post treatment process. Indeed, post treated sample of 800°C (synthesis temperature) and 1:1 (BA:M) showed peaks of boron oxide (Fig. 2b). Several groups reported on the effect of B_2O_3 on the structural ordering of BN [22, 23, 25]. Thomas et al. reported that the presence of B_2O_3 promotes the ordering process from t-BN to h-BN, due to enhanced material transfer and layer mobility [22]. Choi et al. showed that presence of B_2O_3 also promotes the formation of c-BN during a high pressure high temperature process [25]. In addition to enhanced material transfer and layer mobility with the presence of B_2O_3, Çamurlu suggested another mechanism that also promotes BN formation: B_2O_3 melt dissolves nitrogen (or BN) and BN precipitates from the melt [23]. Thus, increase in the synthesis temperature has two-fold effect on the structural ordering of BN: i) it promotes the reaction towards the formation of BN and ii) it increases boron and oxygen contents in BCNO compounds, thus providing diffusion friendly environment for BN to advance its structural ordering.

Formation of B_2O_3 during post treatment can also explain the effect of BA:M ratio on the structural ordering of BN. Increase in BA:M ratio leads to the formation of additional B_2O_3 during the process, as supported by boron oxide detection from the post treated samples with high BA:M ratios (3:1 and 6:1 in Fig. 4), thus promoting the structural

ordering of BN based on the two mechanisms suggested above. In our previous study we proposed another mechanism based on thermodynamic consideration [15]. As BA:M ratio increases, the slope of ΔG (Gibbs free energy) vs temperature becomes more negative, leading to lower theoretical temperatures for BN formation. This mechanism can also explain the more advanced structural ordering of BN with increasing BA:M ratio. The impact of BA:M ratio on the structural ordering of BN becomes less prominent with increase in the synthesis temperature, and vice versa. Still, the observed trends prove that the mechanisms suggested above still takes effect during post heat-pressure treatment at 1200°C and 1 GPa.

D(002) values, which correspond to the distance between layers along the *c*-axis, reflect compression of the layered structure by applied pressure. Solozhenko compressed h-BN at RT and showed that lattice constant *c*, which is about twice *d*(002), reduced from 6.660 Å to 6.440 Å at 1 GPa, while lattice constant *a* showing little change [26]. Corrigan (1975) showed that *d*(002) of h-BN decreases to (3.08-) 3.13 Å after compression at 5.5-6.5 GPa and 1950°C [17]. Several samples in this study showed *d*(002) values less than that (3.33 Å) for h-BN and the smallest *d*(002) observed was 3.32(2) Å for the post treated sample of 800°C and BA:M=6:1. Thus, the results demonstrate that loading pressure of 1 GPa at 1200°C results in a more compressed layered structure of h-BN.

5. Conclusions

In this study we subjected BCNO compounds with various chemical and structural characteristics to a post heat-pressure treatment at 1200˚C and 1 GPa to investigate the correlation between the synthesis conditions of BCNO compounds and the formation and

structural ordering of BN during a post treatment process. Based on direct TEM observation and EELS analysis, we established that crystalline BN grains form from BCNO matrix. Based on the XRD analysis, BNs formed in this study can be classified as either m-BN or h-BN following Thomas et al.'s criteria and XRD analysis. We found that the formation and structural ordering of BN still strongly depend on the synthesis conditions of BCNO compounds and can be explained based on the reaction mechanism proposed in our previous study. An increase in temperature during post treatment as well as an increase in synthesis temperature promotes the formation of BN since the reaction process involved is endothermic. Increase in boric acid to melamine ratio promotes the formation and structural ordering of BN since i) it reduces the theoretical temperature for BN formation and ii) it enhances mass transfer and mobility of BN layer by forming additional B_2O_3 phase. Further, loading pressure of 1 GPa resulted in more compressed layered structure of BN.

Acknowledgments

This research was sponsored by the Defense Advanced Research Projects Agency under Grant No. W31P4Q-13-1-0001 and the Office of Naval Research Grant No: N00014-17-1-2532 with additional support from the Army Research Laboratory under Cooperative Agreement Number W911NF-12-2-0022 as well as support from the National Science Foundation I/UCRC Award No.1540027. The authors would like to thank Tracy Paul (Depth of the Earth) for her valuable guidance in experiments on heat-pressure treatment, and Jennifer Weir and Jun Won for their valuable assistance in the laboratory. Metin Örnek acknowledges support from the Ministry of Education, the Republic of Turkey.

References

[1] M. Petrescu, M.-G. Balint, Structure and properties modifications in boron nitride. Part I: Direct polymorphic transformations mechanisms, UPB Sci. Bull., Series B, 69 (2007) 35-42.

[2] T.E. O'connor, Process for the production of boron nitride, US Patent 3,241,919, 1966.

[3] F.H. Lin, C.K. Hsu, T.P. Tang, P.L. Kang, F.F. Yang, Thermal-heating CVD synthesis of BN nanotubes from trimethyl borate and nitrogen gas, Materials Chemistry and Physics, 107 (2008) 115-121.

[4] S. Batsanov, L. Kopaneva, E. Lazareva, I. Kulikova, R. Barinsky, On the nature of boron nitride e-phase, Propellants, explosives, pyrotechnics, 18 (1993) 352-355.

[5] R. Haubner, M. Wilhelm, R. Weissenbacher, B. Lux, Boron nitrides - properties, synthesis and applications, High Performance Non-Oxide Ceramics II, Springer2002, pp. 1-45.

[6] B. Ertug, Powder preparation, properties and industrial applications of hexagonal boron nitride, Sintering Applications, InTech2013.

[7] T. Saito, F. Honda, Chemical contribution to friction behavior of sintered hexagonal boron nitride in water, Wear, 237 (2000) 253-260.

[8] O. Kurakevych, Superhard phases of simple substances and binary compounds of the BCNO system: from diamond to the latest results (a Review), Journal of Superhard Materials, 31 (2009) 139-157.

[9] I. Konyashin, J. Bill, F. Aldinger, Plasma-assisted CVD of cubic boron nitride, Chemical Vapor Deposition, 3 (1997) 239-255.

[10] K. Teii, T. Hori, Y. Mizusako, S. Matsumoto, Origin of rectification in boron nitride heterojunctions to silicon, ACS applied materials & interfaces, 5 (2013) 2535-2539.

[11] L. Vel, G. Demazeau, J. Etourneau, Cubic boron nitride: synthesis, physicochemical properties and applications, Materials Science and Engineering: B, 10 (1991) 149-164.

[12] R. Wentorf, R.C. DeVries, F. Bundy, Sintered superhard materials, Science, 208 (1980) 873-880.

[13] T. Hagio, K. Nonaka, T. Sato, Microstructural development with crystallization of hexagonal boron nitride, Journal of materials science letters, 16 (1997) 795-798.

[14] K.M. Reddy, C. Hwang, M. Ornek, S.L. Miller, W.E. Mayo, A. Burgess, R.A. Haber, K.J. Hemker, Observations of nanocrystalline cubic boron nitride formed with plasma spraying, Acta Materialia, 116 (2016) 155-165.

[15] M. Örnek, C. Hwang, K.M. Reddy, V. Domnich, S.L. Miller, E.K. Akdoğan, K.J. Hemker, R.A. Haber, Formation of BN from BCNO and the development of ordered BN structure: I. Synthesis of BCNO with various chemistries and degrees of crystallinity and reaction mechanism on BN formation, Ceram. Int. 44 [13] 14980-14989 (2018).

[16] F. Bundy, R. Wentorf Jr, Direct transformation of hexagonal boron nitride to denser forms, The Journal of Chemical Physics, 38 (1963) 1144-1149.

[17] F. Corrigan, F. Bundy, Direct transitions among the allotropic forms of boron nitride at high pressures and temperatures, The Journal of Chemical Physics, 63 (1975) 3812-3820.

[18] M. Wakatsuki, K. Ichinose, T. Aoki, Synthesis of polycrystalline cubic BN, Materials Research Bulletin, 7 (1972) 999-1003.

[19] H. Sumiya, T. Iseki, A. Onodera, High pressure synthesis of cubic boron nitride from amorphous state, Materials research bulletin, 18 (1983) 1203-1207.

[20] C. Hwang, M. Örnek, V. Domnich, W.E. Mayo, S.L. Miller, R.A. Haber, c-BN seeding effect on the phase transition of a-BN (OC) compound, Advances in Ceramic Armor XI: A Collection of Papers Presented at the 39th International Conference on Advanced Ceramics and Composites, John Wiley & Sons, Inc., 2015, pp. 83-91.

[21] J. Akella, S. Vaidya, G.C. Kennedy, Melting of sodium chloride at pressures to 65 kbar, Physical Review, 185 (1969) 1135.

[22] J. Thomas, N.E. Weston, T.E. O'connor, Turbostratic boron nitride, thermal transformation to ordered-layer-lattice boron nitride, Journal of the American Chemical Society, 84 (1962) 4619-4622.

[23] H.E. Camurlu, Effect of Na_2CO_3 on hexagonal boron nitride prepared from urea and boric acid, Ceramics International, 37 (2011) 1993-1999.

[24] O. Hod, Graphite and hexagonal boron-nitride have the same interlayer distance. Why?, Journal of chemical theory and computation, 8 (2012) 1360-1369.

[25] J.Y. Choi, S.J.L. Kang, O. Fukunaga, J.K. Park, K. Eun, Effect of B_2O_3 and hBN crystallinity on cBN synthesis, Journal of the American Ceramic Society, 76 (1993) 2525-2528.

[26] V. Solozhenko, G. Will, F. Elf, Isothermal compression of hexagonal graphite-like boron nitride up to 12 GPa, Solid state communications, 96 (1995) 1-3.

Figures

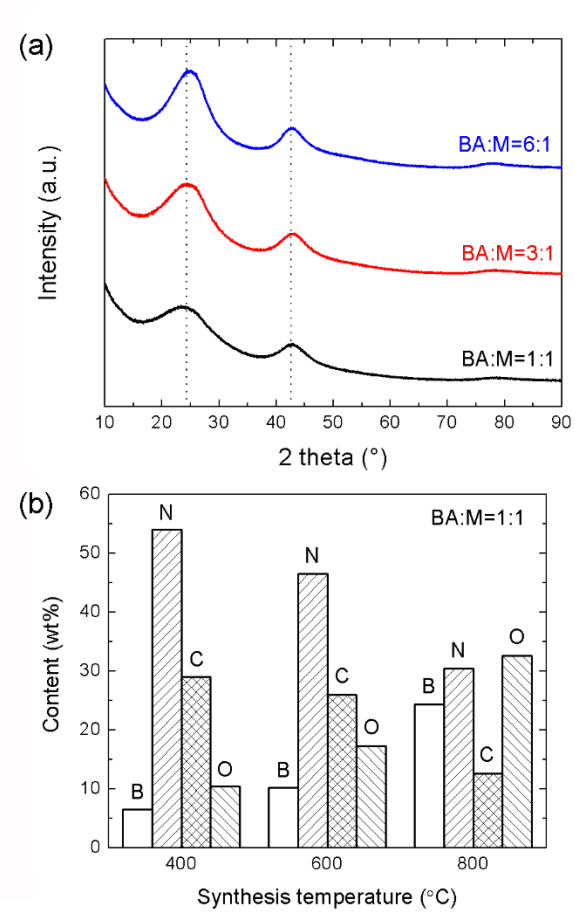

Figure 1. XRD patterns and chemical composition of BNCO compounds: (a) XRD patterns of BNCO compounds, of which synthesis temperature is 800°C and BA:M=1:1, 3:1, and 6:1 (mole); (b) chemical compositions of BNCO compounds, of which BA:M=1:1 and synthesis temperature is 400°C, 600°C, and 800°C.

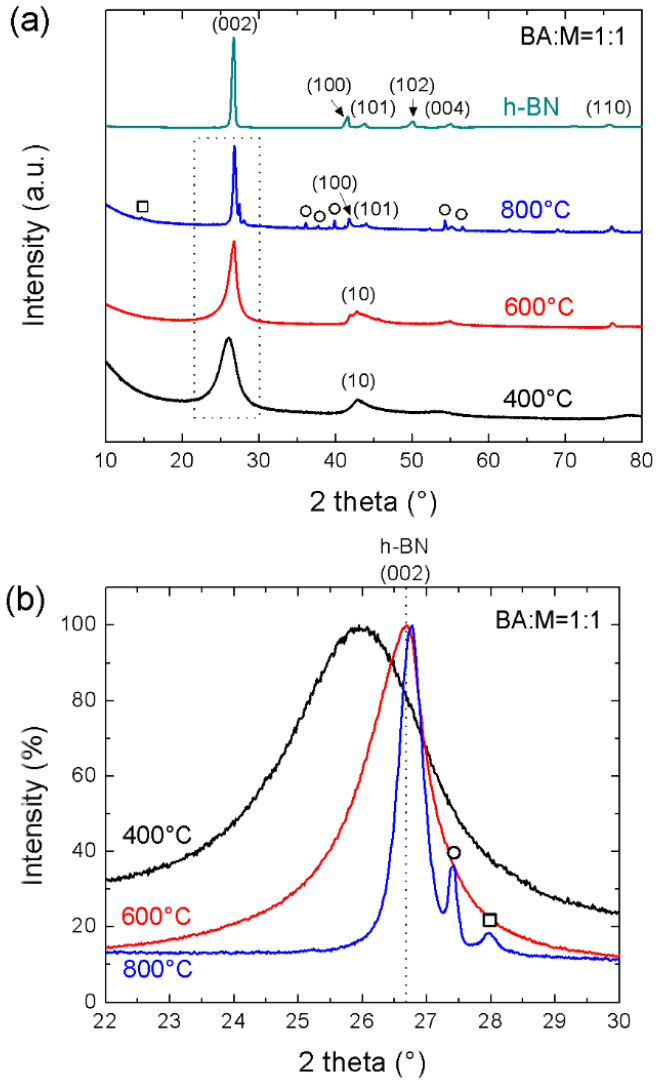

Figure 2. XRD patterns of BNCO compounds post treated at 1200°C and 1 GPa, of which BA:M=1:1 and synthesis temperatures is 400°C, 600°C, and 800°C: (a) Full XRD patterns including that of commercial h-BN for comparison, (b) Short-range patterns for the range marked in (a). Squares correspond to boron oxide (JCPDS card No. 06-0297) and circles correspond to titanium oxide, which resulted from titanium Ti capsule.

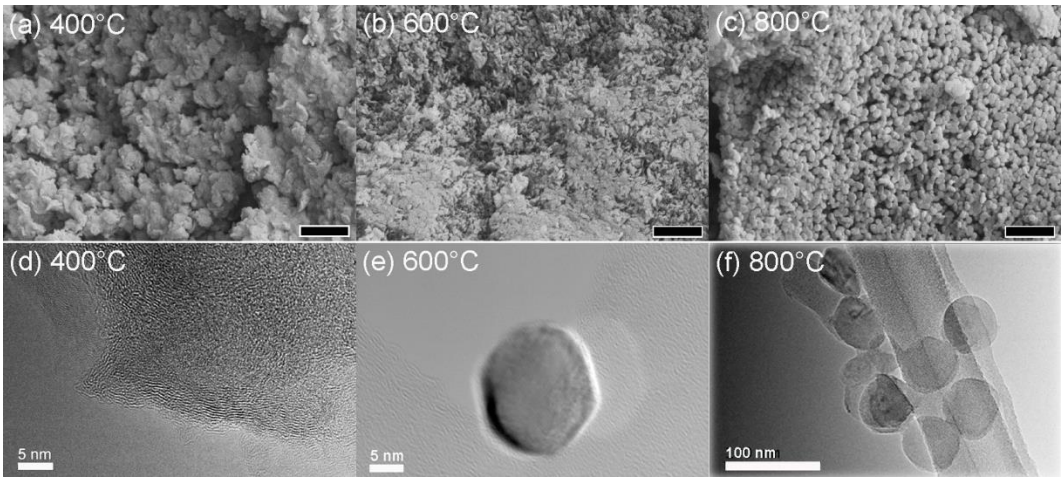

Figure 3. Microstructures of BNCO compounds post treated at 1200°C and 1 GPa, of which BA:M=1:1 and synthesis temperature is 400°C, 600°C, and 800°C: (a-c) SEM images and (d-f) TEM images. Scale bars in SEM images correspond to 400 nm.

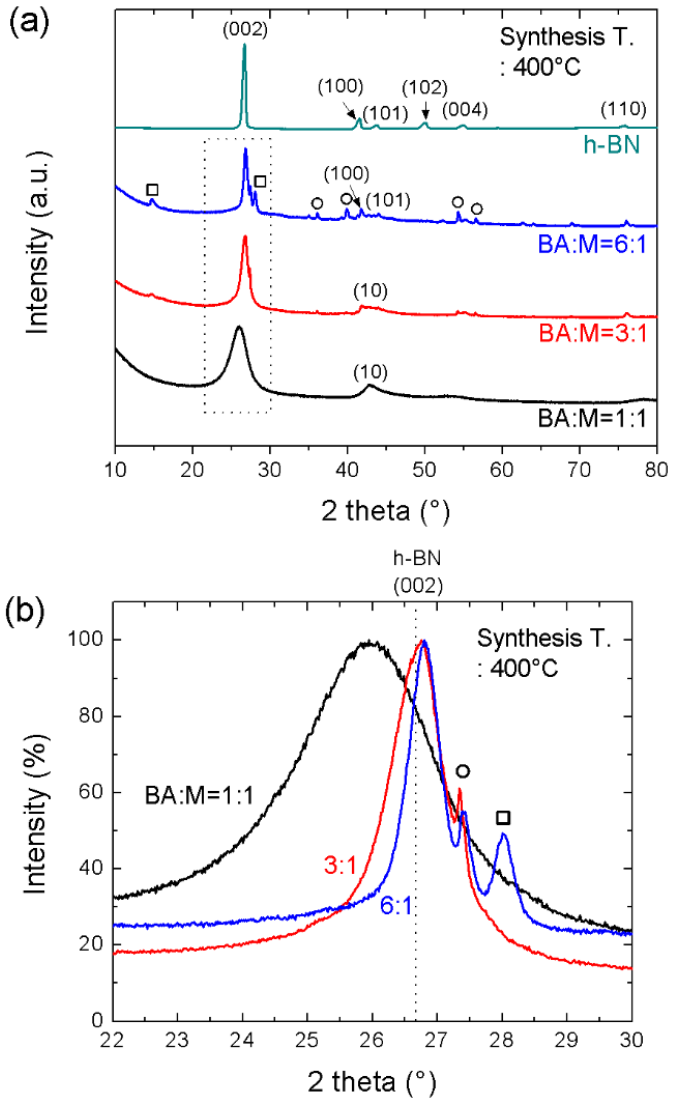

Figure 4. XRD patterns of BNCO compounds post treated at 1200°C and 1 GPa, of which synthesis temperature is 400°C and BA:M=1:1, 3:1, and 6:1: (a) Full XRD patterns including that of commercial h-BN for comparison, (b) Short-range patterns for the range marked in (a). Squares correspond to boron oxide and circles correspond to titanium oxide, which resulted from titanium Ti capsule.

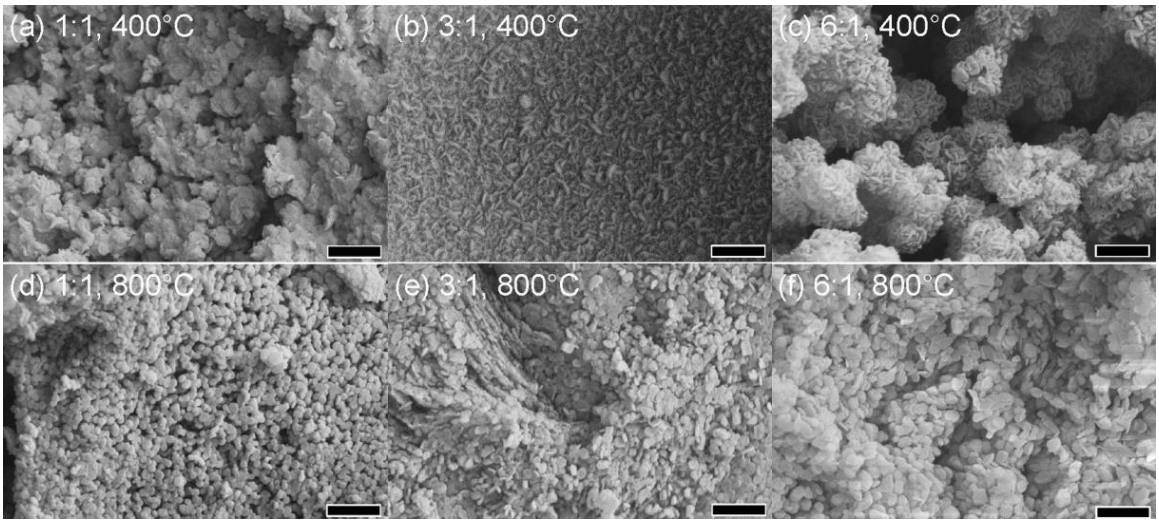

Figure 5. Microstructures of BNCO compounds post treated at 1200°C and 1 GPa, of which synthesis temperature is 400°C (a-c) and 800°C (d-f). Scale bars in images correspond to 400 nm.

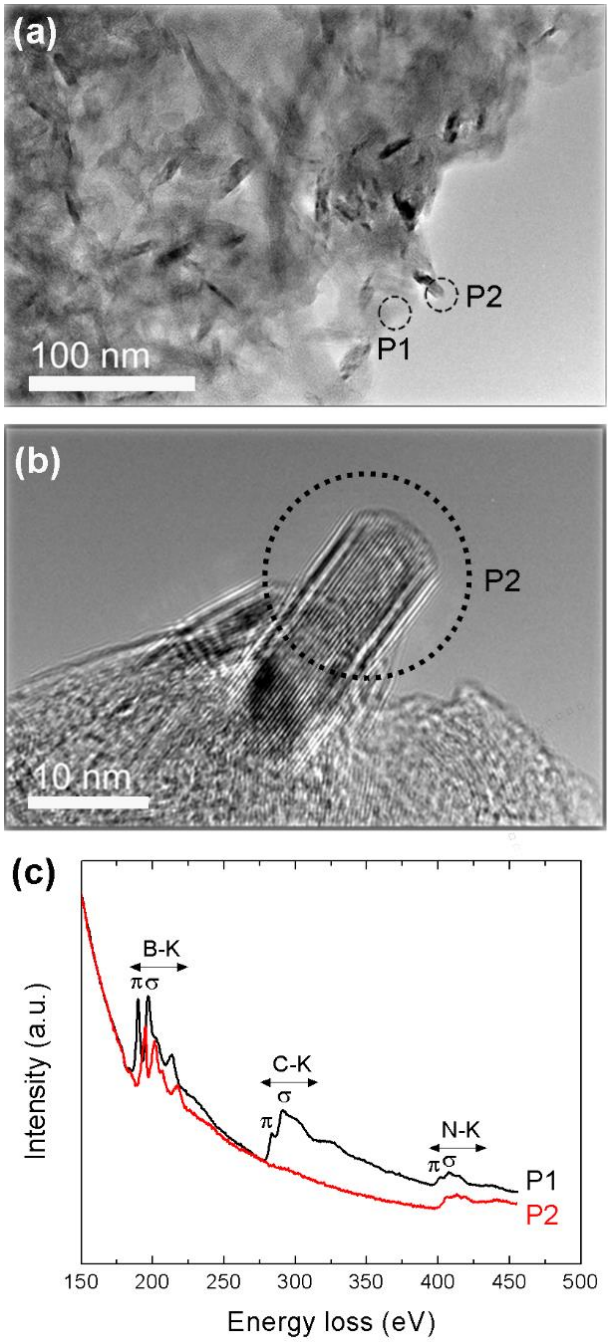

Figure 6. TEM images and EELS spectra of BNCO compounds post treated at 1200°C and 1 GPa, of which BA:M=3:1 and synthesis temperature is 400°C. Point 1 corresponds to the matrix and point 2 corresponds to the grain formed, of which magnified image is shown in (b). The scale bar in the (b) corresponds to 10 nm.

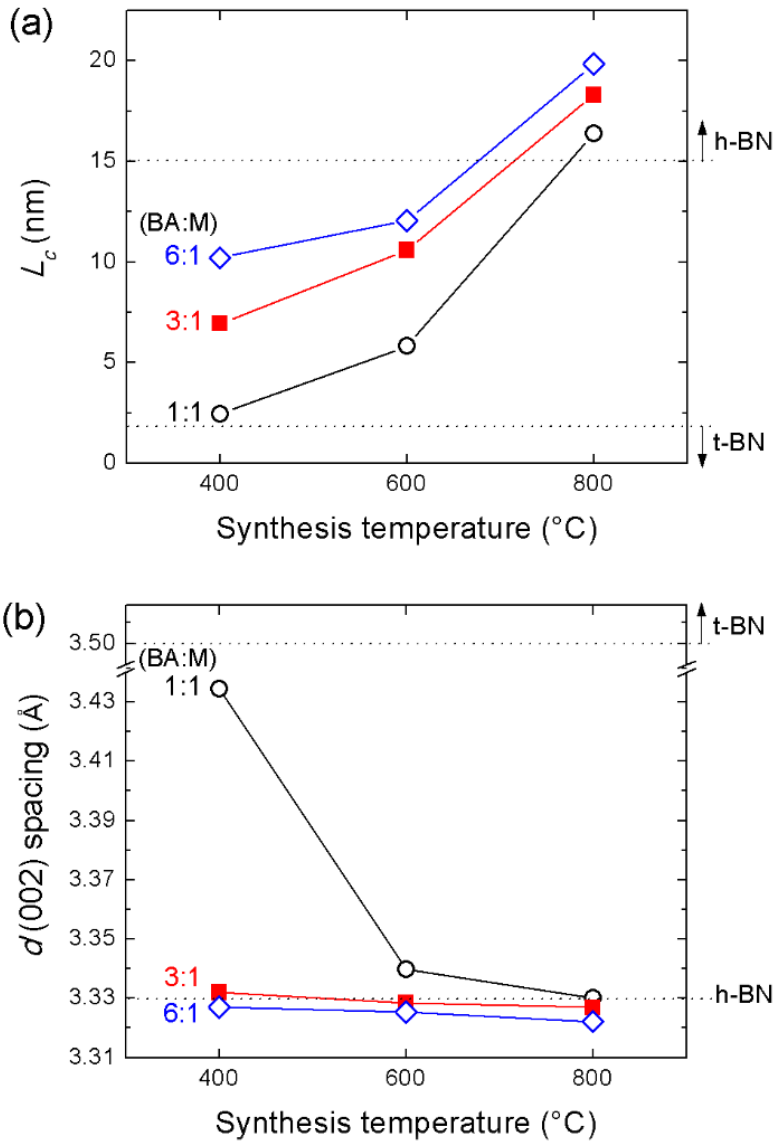

Figure 7. L_c and d(002) values for BNCO compounds post treated at 1200°C and 1 GPa. Dotted line show values correspond to t-BN and h-BN, as suggested by Thomas et al.[2,21] Lines in the figure are drawn to guide the eye.

Chapter 4.

Effect of synthesis conditions of BCNO on the formation and structural ordering of boron nitride at high temperatures

Metin Örnek[1], Chawon Hwang[1]*, Sisi Xiang[2], Kelvin Y. Xie[2], Anthony Etzold[1], Bruce Yang[1], Richard A. Haber[1]*

Department of Materials Science and Engineering, Rutgers, The State University of New Jersey, Piscataway, NJ 08854, USA

Department of Materials Science and Engineering, Texas A&M University, College Station, TX 77843, USA

*Corresponding author e-mail: (C.Hwang) chawon.hwang@rutgers.edu; (R.Haber) rich.haber@rutgers.edu and address: 607 Taylor Road, Piscataway, NJ 08854, USA. Tel: +1(848) 445-5924, Fax: +1(732) 445-5926.

Abstract

We have investigated the effect of synthesis conditions of BCNO compounds on BN formation and its structural ordering. BCNO compounds were synthesized from boric acid (H_3BO_3)-melamine ($C_3H_6N_6$) mixtures with various molar ratios (H_3BO_3:$C_3H_6N_6$ = 1:1 to 6:1) at 400°C. The BCNO compounds were then subjected to post heating between 1400°C and 1800°C under argon flow. The final products were crystalline BN with hexagonal symmetry exhibiting varying degrees of structural ordering. As the H_3BO_3 to $C_3H_6N_6$ ratio in the starting composition is increased, BN formation temperature decreases and the structural ordering of BN increases. Post heating at higher temperature also promotes BN formation and structural ordering. The findings indicate that synthesis and structural ordering of BN can be tailored by controlling starting composition and post heating temperature. These observations may provide a guideline to synthesize high or low-density polymorphs of BN at reduced pressure, temperature, or both.

Keywords: BCNO; Amorphous; Phase transformation; Boron nitride; Structural ordering; Turbostacking faults.

1. Introduction

Boron Nitride (BN) is a widely used ceramic material that has various polymorphic forms such as low density amorphous, turbostratic, hexagonal, rhombohedral, explosive phases, and high-density wurtzite and cubic phases [1–7]. Cubic (c-BN) and hexagonal (h-BN) forms of BN have received considerable interests in recent years due to their unique properties. c-BN exhibits high hardness only next to diamond due to their diamond-like covalent sp^3 bonding structure [8–11]. c-BN also shows higher thermal stability as well as higher chemical inertness in comparison to diamond, which makes c-BN favorable for applications in abrasives, cutting tools, and electronic devices [11,12]. h-BN is the most stable among BN polymorphs in ambient conditions. In this form, B and N atoms are arranged in an sp^2 bonded honeycomb layered structure that is analogous to graphite [13]. The chemical inertness, high thermal conductivity, low thermal expansion, lubricating behavior, and high thermal stability of h-BN make it applicable in vast number of industries such as chemistry, cosmetics, metallurgy, semiconductors and electronics [11,12,14,15].

For the synthesis of BN, boron-carbon-nitrogen-oxygen (BCNO) compounds have been widely used as starting materials [16–18]. It was shown that the chemistry and degree of crystallinity of the starting BCNO strongly impact the synthesis conditions (temperature and pressure), degree of phase transformation, microstructure and chemical properties of the resultant c-BN or h-BN [16–18]. For instance, Choi et al. demonstrated that the pressure for c-BN formation can be reduced by decreasing the degree of crystallinity of the starting BCNO [16]. Singh et al. showed that variations in the chemistry of starting BCNO alter the degree of crystallinity of the synthesized BNs [17]. In addition, Hagio et al. suggested that the amount of oxygen in the starting BCNO strongly affects the structural ordering of

the synthesized h-BN [18]. However, only limited variations in the starting composition or the degree of crystallinity have been tried or reported. Moreover, fewer studies that have systematically correlated the effect of synthesis conditions of BCNO with the formation and structural ordering of BN during high temperature and/or high temperature-high pressure treatments.

In our previous study we synthesized BCNO compounds with various chemistries and degrees of crystallinity and investigated how the synthesis conditions impact BN formation from BCNO and its structural ordering at low temperatures (400-1000°C) [19]. From this work, we suggested a responsible reaction mechanism. In our later study, we expanded our work to include post heat-pressure treatment to 1 GPa and 1200°C [20]. We have shown in both studies that chemistry and degree of crystallinity of BCNO have profound effects on the formation temperature and structural ordering of the BN forming, e.g. higher H_3BO_3 to $C_3H_6N_6$ molar ratio in the starting composition for BCNO synthesis promotes BN formation and its structural ordering [19,20].

In this study, we elucidate the correlation for post treatment at high temperature range (1400-1800°C) under ambient pressure. Our focuses are: (i) to explain how synthesis conditions of BCNO affect the formation of BN at elevated temperatures, (ii) to assess the structural ordering of BN formed in terms of interlayer distance, average crystallite size, and three-dimensional (3-D) ordering, and (iii) to identify the validity of the reaction mechanism that we proposed in our previous study during a high temperature post heating process.

2. Experimental Procedures

2.1 Materials and method

Synthesis of BCNO compounds was discussed entirely in our previous paper [19]. In brief, H_3BO_3 (U.S. Borax, Inc., California) and $C_3N_6H_6$ (DSM, Netherlands) were used to synthesize BCNO. To study the effect of starting compositions, H_3BO_3 to $C_3N_6H_6$ molar ratios of 1:1, 1.5, 2:1, 3:1 and 6:1 were selected. Higher or lower ratios were not considered to avoid residual H_3BO_3 or the excessive sublimation of $C_3N_6H_6$, respectively [21]. A two-step solid-state reaction was used to synthesize BCNO. H_3BO_3 and $C_3N_6H_6$ mixture undergo two heating cycles: first at 200°C in air for 2 h, and then at 400°C under nitrogen atmosphere for 3 h. BCNOs formed were crushed and sieved through a 75 μm sieve to promote particle size uniformity.

To study crystalline BN formation from BCNO and its structural ordering, high temperature post treatments were conducted in a graphite resistance furnace using graphite crucibles. The furnace chamber was vented to remove the air using a mechanical pump until the internal pressure reached $3x10^{-3}$ Torr. The chamber was then backfilled with Argon (venting/backfilling steps were repeated 3 times), and heating was started. Post treatments were conducted at 1400°C, 1600°C, and 1800°C while maintaining Ar flow of 4 L/min. The heating rate was 20 °C/min, and the dwell time at target temperature was 1 h.

2.2 Characterization

Synthesized powders were kept in a drying furnace at 110°C for 24 h prior to characterization studies. A Zeiss-Sigma (Germany) field-emission scanning electron microscopy (FE-SEM) was used to study the microstructure and powder morphologies. An

Oxford-XMaX80 Energy dispersive X-Ray spectroscopy (EDS) detector that was coupled to FE-SEM was used to analyze chemical compositions at 5 keV. Phase identification and structure ordering assessment was done using a PANalytical X'pert diffractometer at 45kV and 40 mA with Cu Kα (λ=1.540598 Å) radiation at a scanning rate of 0.04 °min^{-1}. A silicon standard (NIST SRM 640e) reference material was used to correct BN (002) peak width to eliminate the instrumental broadening and to correct BN (002) peak position prior to calculating the average crystallite sizes and interlayer distances. Crystallite size of post-treated powders along the c-axis (*L*c) and the a-axis (*L*a) were calculated from the Scherrer's equation;

$$La,c = (K \times \lambda)/(\beta \times \cos\theta), \quad (1)$$

where *K* is a dimensionless shape factor (0.9 for (002) plane, 1.84 for (100) plane), λ is the wavelength of X-ray beam (Cu Kα), β is the full width half maxima (FWHM) of diffraction peaks at (002) and (100) planes (radian), and θ is Bragg angle (degree) [22,23]. The average interlayer distance for BN along the c-axis (d_{002}) were calculated using Bragg's law;

$$n\lambda = 2d\sin\theta, \quad (2)$$

where λ is the wavelength of X-ray beam, and θ is Bragg angle (degree) [24]. Regular bright-field transmission electron microscopy (TEM), selected area electron diffraction (SAED), High-resolution TEM and high angle annular dark-field scanning

TEM (HAADF-STEM) were employed to study the morphology, crystal structure, and lattice distance of the synthesized particles using a FEI Tecnai G2 F20 Super-Twin FE-TEM operating at 200 kV.

3. Results

3.1 Chemistry and crystallographic structure of the initial BCNO compounds

Table 1 shows the representative chemical compositions of the synthesized BCNO compounds based on the EDS analysis as a function of starting H_3BO_3:$C_3H_6N_6$ molar ratio (hereafter referred to as BA:M ratio). Chemical composition represents the average of 20 different area scan measurements. As the BA:M ratio in the starting composition is increased, nitrogen and carbon contents decrease while boron and oxygen contents increase.

XRD analysis was conducted on the synthesized BCNO compounds to identify their long-range crystallographic structure (Fig. 1). XRD patterns of the synthesized BCNOs show two broad maxima, which span from 20-30° and 40-50° for all the ratios. This indicates that the synthesized BCNOs exhibit no long-range crystallographic structure and are amorphous in nature [2]. It is worth noting that the broad maxima spanning around 20-30° shifts toward lower angles as the BA:M ratio of starting composition is increased.

3.2 Effect of the starting composition and post heating temperature on BN formation

The synthesized BCNOs were subjected to post heating at 1400°C, 1600°C, and 1800°C under flowing Ar atmosphere. Figure 2 shows representative chemical compositions of the powders after heat treatment, of which starting BA:M ratios were 1:1,

3:1, and 6:1, respectively. The values represent the average of 20 different EDS area scans. For 1:1 and 3:1 ratios, post-treated powders contain mainly B and N atoms regardless of heat treatment temperature. Low quantities (< 6 at. %) of C and O were also detected. It should be noted the apparent C count collected by the EDS might be higher than the actual value, as it might collect signals from the carbon tape used on the sample holder. For 6:1 ratio, considerable amounts of O were detected after heat temperatures at 1400°C and 1600°C, suggesting the coexistence of B-N-O. On the other hand, a significant reduction in O content (~ 0.9 at. %) is observed when the post heating temperature is increased to 1800°C.

XRD analysis was applied to analyze the long-range crystallographic order of the post-treated powders. Figure 3 shows the normalized XRD patterns of the BCNOs post-treated at 1400°C. For BA:M= 1:1 and 1.5:1 ratios, two relatively broad peaks around 26.4° and 42.5° were observed, which correspond to (002) and (10) reflection of disordered turbostratic BN (t-BN) [25]. The turbostratic nature of the material can also be confirmed from the absence of the (004) peak at 54.8° [26]. As the BA:M ratio is increased, the two broad peaks become sharper and also the (002) peak shifted toward the higher Bragg angles, suggesting an increase in the crystallite size and a decrease in d-spacing, respectively. For 6:1 ratio, the (10) reflection of BN at around 40-43° splits into two (100) and (101) reflections, indicating an increase in the degree of 3-D structural ordering of BNs formed [18]. For 3:1 and 6:1 ratios, boron oxide (B_2O_3; JCPDS card No. 06-0297) was observed (black dots in Fig. 3). The presence of B_2O_3 suggests that excess oxygen in the starting BCNO reacted with boron and formed B_2O_3. Taken together, these observations

indicate that a higher BA:M ratio in the starting composition resulted in a higher structural ordering of the BN formed.

When the post treatment temperature is increased to 1600°C (Suppl. Fig. 1) and 1800°C (Fig. 4), a similar trend to that of 1400°C was observed. Higher BA:M ratio in the starting composition and higher post treatment temperature results in shift of (002) peak toward the higher angles and a decrease in FWHM (Fig. 4). This suggests shorter d-spacing (d_{002}) and larger crystallite size (*Lc*); in other words, increased structural ordering. The XRD spectra for 1:1 and 1:5 ratios still indicate less-ordered structure without 3-D structural ordering even after the post heating at 1800°C. On the contrary, higher BA:M ratios showed 3-D structural ordering as supported by the emergence of (004) peak at ~ 54.8° and split of (10) peak into (100) and (101) peaks as revealed by XRD [26]. It should be noted that B_2O_3 was not observed for high BA:M ratios. We attribute this to the sublimation of B_2O_3, of which sublimation temperature is around 1500°C [27].

Figure 5 shows representative FE-SEM micrographs of the post-treated powders with different BA:M ratios (2:1, 3:1, and 6:1) in the starting composition and different post heat treatment temperatures (1400°C, 1600°C, and 1800°C). At 1400°C, BN grains were not discernible for 2:1 ratio, and only irregular shape chunks were observed. However, for 3:1 ratio, small grains were discernible and for 6:1 ratio, the size of grains increased. At 1600°C, BN grains were observed for all mixtures, but higher BA:M ratios showed larger grains. With further increase in temperature to 1800°C, larger and relatively round BN flakes were observed. For 6:1 ratio the size of the BN flakes were larger than 1 μm. The FE-SEM observations indicate that increase in BA:M ratio in the starting composition

promotes the formation of BN and its growth, which are in accordance with the foregoing trend observed through X-ray analyses.

4. Discussion

4.1 The assessment of structural ordering of BN powders

The hexagonal form of BN has commonly been classified into three sub-polytypes; turbostratic (t-BN), mesographitic (m-BN) and highly ordered hexagonal (h-BN) phases [2,28]. t-BN and m-BN are intermediate structures that form from BCNO compounds prior to the formation of highly ordered h-BN [2,28]. The stacking layers of these intermediate structures along the c-axis in the hexagonal unit cell are disordered and non-uniform, resulting in shorter coherence lengths and larger interlayer distances along the c-axis [25]. In addition, the crystallite sizes of these intermediate structures are smaller than that of highly ordered h-BN. Thus, t-BN and m-BN are also known as disordered and partially disordered h-BN, respectively.

Despite that there is no common agreement on the classification of these sub-polytypes, some researchers classified them based on the structural ordering, i.e. d-spacing and crystallite sizes. For instance, the criterion suggested by Thomas et al. defines t-BN as $d_{002} > \sim 0.345$ nm and Lc < 2 nm and defines highly ordered h-BN as $d_{002} = 0.333$ nm and Lc > 15nm with m-BN having the intermediate values between t-BN and highly ordered h-BN [2]. Similarly, O'Connor defines t-BN as $d_{002} > 0.356$ nm and Lc < 1.4 nm but with additional consideration for crystallite size along the a-axis, La = 4.6 nm [23]. Highly ordered h-BN is defined as $d_{002} = 0.330$ nm and Lc,a > 15 nm. Furthermore, Saito et al.

defines t-BN as d_{002} > 0.350 nm with *L*c ~ 2 nm and *L*a ~ 10-40 nm and defines highly ordered h-BN as d_{002} < 0.335 nm, and *L*c = 20 nm with *L*a > 40 nm [29].

On the other hand, Kurdyumov et al. suggested that the structural ordering of the layered materials such as graphite and h-BN should be evaluated by the degree of 3-D structural ordering (D_3) along with d-spacing values and crystallite sizes [30,31]. D_3 is defined as the ratio of number of layers oriented regularly with their nearest neighbors to the total number of the layers. Since an imperfection in the layer stacking, i.e. turbostacking faults (TSFs), causes a reduction in the number of layers oriented regularly, D_3 can be defined as follows according to Kurdyumov et al.;

$$D_3 = 1 - \gamma, \tag{3}$$

where γ is the concentration of TSFs and can be calculated from the following equation;

$$\beta_{hkl}(\gamma) = 0.03\ d_{hkl}\ l\ \frac{\gamma}{\sqrt{(1-\gamma)}}\ tg\theta_{hkl}, \tag{4}$$

where $\beta_{hkl}(\gamma)$ is the physical broadening of the *hkl* line caused by TSFs, *d* is the calculated d-spacing value, and θ is the Bragg angle at *hkl* line observed [30–34]. For BN with hexagonal symmetry, the (112) peak can be used to calculate B_{hkl} and the (110) line to correct instrumental broadening [30–34]. (112) and (110) peaks of BN with hexagonal unit cell are at ~ 82.2° and ~ 75.9°, respectively [35]. Based on D_3, highly ordered h-BN can be

defined $D_3 > 0.84$ ($\gamma < \sim 0.16$), whereas completely disordered turbostratic BN is defined as $D_3 = 0$ ($\gamma = 1$) [30].

Table 2 shows the combined and generalized classification on BN sub-polytypes with hexagonal symmetry, based on d-spacing and *L*c values suggested by Thomas et al., *L*a values suggested by O'Connor et al., and D_3 values suggested by Kurdyumov et al..

To assess the degree of structural ordering of BN powders synthesized in this study, we calculated the interlayer distances (d_{002}), crystallite sizes along c and a axes (*L*c and *L*a), and D_3 as shown in Table 3. *L*a/*L*c ratio was included to assess the aspect ratio of the crystallites and the values of a commercially available h-BN powder (Kennametal Grade: BN150) were also included for comparison.

After the post treatment at 1400°C, the powders resulted in $d_{002} \sim 0.356$ nm, and *L*c < 2 nm for 1:1 and 1.5:1 ratios. *L*a could not be calculated due to the emergence of diffusive (10) peak, instead of (100) and (101) peaks. We note here that the calculation of *L*a might be possible by deconvolution of (10) peak into (100) and (101) peaks. However, we could not consider this method since there exist different deconvolution procedures that may result in arbitrary and different values. In addition, D_3 could not be determined as the (112) and (110) peaks of BN were not observed on the XRD patterns (Fig. 3). According to the criteria summarized in Table 2, the powders can be classified as t-BN.

When the BA:M ratio in the starting composition is increased, the observed d-spacing value decreases and crystallite size along the a- and c-axes increases, reaching to the values corresponding to m-BN. Moreover, D_3 can be calculated based on the (112) and (110) peaks, of which values, 0.75 to 0.88, approach the value of commercial h-BN (0.92).

With increase in post-treatment temperature to 1600°C and 1800°C, the structural ordering of BN formed improved, of which D_3 and d_{002} values reached the values of commercial h-BN for BA:M= 6:1 and post-treatment temperature of 1800°C. In addition, still an increase in the BA:M ratio in the starting composition lead to an increase in structural ordering, as supported by larger crystallite sizes along the c- and a-axes, a shorter d-spacing values, and higher D_3 values.

The average crystallite sizes along the a- and c-axes (L_a *and* L_c) were compared to determine the aspect ratio of the BN crystallites at a given conditions (Table 3). All the *La/Lc* ratios show values larger than unity. This indicates that higher growth along a-axis than that along c-axis.

To provide a more detailed comparison on the structural ordering and complement the XRD analyses above, TEM observations were performed on the samples synthesized at 1800°C using 1:1 and 6:1 molar ratios of BA:M. Figure 6 shows the TEM micrographs of the sample synthesized using 1:1 of BA:M. A representative low-magnification bright-field TEM image of sample in Fig. 6a displays a thin flake with irregular morphology. Most of the flakes are few micron in size. SAED pattern of the specimen produced relatively diffusive rings (Fig. 6b, diffraction taken from the marked area in Fig. 6a), suggesting that the sample is not fully crystalline. A representative HR-TEM image (Fig. 6c) reveals local regions exhibiting lattice fringes but in a chaotic fashion. This further indicates that the sample do not possess a highly developed crystallographic structure. Measured lattice spacing of 0.338 nm along the (002) plane, which is consistent with Table 3, further confirms the mesographitic structure of the BN. Elemental analysis also confirmed the BN

nature of the specimen. The particle is mainly composed of B (Fig. 6e), N (Fig. 6f), and a small amount (4 at. %) of O (Fig. 6g).

On the other hand, for the sample of BA:M=6:1, BN with different morphology and crystallographic ordering were observed (Fig. 7). A typical low-magnification TEM image of the sample (Fig. 7a) showed many particles ~ 1 μm in size with relatively rounded morphology. The SAED pattern (Fig. 7b) taken from the area marked in Fig. 7a shows sharp spots, suggesting well-developed crystal structure in the particle. HR-TEM image confirmed such observation at the atomic-scale. The measured lattice distance of ~ 0.12 nm along (110) plane indicates highly ordered crystallographic structure of h-BN (Fig. 7c). It was noticed that fast Fourier transform (FFT) of the HR-TEM image (Fig. 7d) clearly revealed the second set of reflections at 0.127 nm (yellow arrow). Elemental analysis revealed that the particle is mainly composed of B (Fig. 7f), N (Fig. 7g) with a very small amount of O (Fig. 7h) distributed in the outermost layer of the particles. TEM analysis thereby corroborated the XRD observations, i.e., increases in BA:M ratio in the starting composition promotes BN formation and its structural ordering at a given temperature.

4.2 Reaction mechanism of BN formation

As the foregoing results and discussions point out, BN formation and its structural ordering can be promoted at a given temperature when the BA:M ratio in the starting composition increases. Moreover, higher post heating temperature also facilitates BN formation and advances its structural ordering at a given molar ratio. In our previous article, to understand the formation of BN from BCNO, we proposed a reaction mechanism based on thermodynamic considerations [19].

H_3BO_3 and $C_3H_6N_6$ mixture reacts and forms intermediate BCNO compound by evolving gaseous species such as H_2O and NH_3 upon heating to 400°C. With further increase in temperature, CO and N_2 evolve from the BCNO while BN layers form in BCNO matrix. Based on the reactions proposed, we calculated and compared the Gibbs free energies on the formation of BN from H_3BO_3-$C_3H_6N_6$ mixtures with different BA:M ratios, i.e., 2:1 and 6:1 respectively. As the result we found that the temperature dependence of Gibbs free energy (the slope of ΔG_f vs temperature) for BA:M = 6:1 is more negative than that of BA:M = 2:1, which leads to lower theoretical formation temperature of BN for higher BA:M ratios. The above thermodynamic consideration can clearly explain the observation we made in this study, i.e., an increase in BA:M ratio in the starting composition promotes BN formation and advances its structural ordering at relatively lower temperatures.

In addition, one of the key aspects that constitutes the formation and structural ordering of BN is the chemistry of starting BCNO, which can be altered by varying starting BA:M ratio. Higher BA:M ratio in the starting composition yields higher O content in the formed BCNO and it eventually results in B_2O_3 at higher temperatures. For instance, we observed clear peaks of B_2O_3 on the XRD patterns of the 3:1 and 6:1 ratio samples post-treated at 1400°C and 1600°C.

The effect of B_2O_3 on the structural ordering of BN has been studied by several researchers. Thomas et al. showed that B_2O_3 promotes the structural ordering, i.e., from less developed t-BN to highly ordered h-BN due to the enhanced mass transport [2]. In addition, Choi et al. showed that existence of B_2O_3 promotes c-BN formation during high pressure and high temperature process [16]. In another study, Hagio observed the formation

and coexistence of B_2O_3 and t-BN [18]. It was shown that the removal of B_2O_3 diminishes the structural development of the BN formed even though high heat temperature treatment (T ~ 2000°C) was used. Combining the findings in prior works with the current study, it is apparent that B_2O_3 enhances the kinetics of material transfer and layer mobility, thereby promotes the structural ordering of BN.

Taken together, higher BA:M ratio in the starting composition i) thermodynamically promotes the formation of BN by reducing the temperature dependence of Gibbs free energy for BN formation and ii) kinetically promotes the structural ordering of BN by enhancing the diffusion and mass transport of BN layers. The foregoing characterizations and discussion prove that the mechanism suggested in our previous report on the formation of BN and its structural ordering at 400°C ≤ T ≤ 1000°C still takes effect at 1400°C ≤ T ≤ 1800°C, in addition to what we observed at 1200°C and 1 GPa [19,20].

5. Conclusions

We have synthesized amorphous BCNOs at 400°C with various chemistries by varying the H_3BO_3 to $C_3H_6N_6$ molar ratio from 1:1 to 6:1 in the starting composition. The amorphous BCNO compounds subsequently were subjected to post heating between 1400-1800°C. We have systematically studied how the synthesis conditions, i.e., the starting composition of BCNO compound and post heating temperature, affect the formation BN and its structural ordering.

Through FE-SEM, EDS, HR-TEM, SAED and comprehensive XRD analyses, we have shown that an increase in H_3BO_3:$C_3H_6N_6$ molar ratio in the starting composition: i) promotes crystalline BN formation from BCNO at lower heat treatment temperatures, and

ii) increases the structural ordering of the BN formed at a given temperature. We also demonstrated that higher heat treatment temperatures enhances mass transport and crystal growth, thereby promotes structural ordering of BN. The findings can be explained based on the reaction mechanism and resultant thermodynamical calculation on the theoretical temperature of BN formation proposed in our previous paper, which indicates that lower theoretical temperature of BN formation for higher H_3BO_3:$C_3H_6N_6$ ratios.

Taken together, it is possible to control the formation of BN from BCNO, and its structural ordering, particle size and morphology by the judicious design of starting composition and post heating treatments.

Acknowledgments

This research was sponsored by and was accomplished under the Office of Naval Research Grant No: N00014-17-1-2532. Additional support was received from the Defense Advanced Research Projects Agency Grant No: W31P4Q-13-1-0001 and the National Science Foundation I/UCRC Award No.1540027. The authors would like to thank Dr. Atta Ullah Khan for fruitful discussions on X-ray diffraction, Jennifer Weir, Jun Won, and Kaitlin Wang for their assistance in the laboratories. Metin Örnek acknowledges graduate fellowship from the Ministry of National Education, the Republic of Turkey.

References

[1] R.H. Wentorf, Cubic Form of Boron Nitride, J. Chem. Phys. 26 (1957) 956–956.

[2] J. Thomas, N.E. Weston, T.E. O'connor, Turbostratic Boron Nitride, Thermal Transformation to Ordered-layer-lattice Boron Nitride, J. Am. Chem. Soc. 84 (1962) 4619–4622.

[3] K. Madhav Reddy, C. Hwang, M. Ornek, S.L. Miller, W.E. Mayo, A. Burgess, R.A. Haber, K.J. Hemker, Observations of nanocrystalline cubic boron nitride formed with plasma spraying, Acta Mater. 116 (2016) 155–165.

[4] S.S. Batsanov, L.J. Kopaneva, E. V. Lazareva, I.M. Kulikova, R.L. Barinsky, On the Nature of Boron Nitride E-Phase, Propellants, Explos. Pyrotech. 18 (1993) 352–355.

[5] M. Örnek, K.M. Reddy, C. Hwang, V. Domnich, A. Burgess, S. Pratas, J. Calado, K.Y. Xie, S.L. Miller, K.J. Hemker, R.A. Haber, Observations of explosion phase boron nitride formed by emulsion detonation synthesis, Scr. Mater. 145 (2018) 126–130.

[6] C. Ji, V.I. Levitas, H. Zhu, J. Chaudhuri, A. Marathe, Y. Ma, Shear-induced phase transition of nanocrystalline hexagonal boron nitride to wurtzitic structure at room temperature and lower pressure, Proc. Natl. Acad. Sci. 109 (2012) 19108–19112.

[7] M. Örnek, C. Hwang, K.Y. Xie, S. Pratas, J. Calado, A. Burgess, V. Domnich, K.J. Hemker, R.A. Haber, Formation of metastable wurtzite phase boron nitride by emulsion detonation synthesis, J. Am. Ceram. Soc., 101 3276-3281 (2018).

[8] Y. Tian, B. Xu, D. Yu, Y. Ma, Y. Wang, Y. Jiang, W. Hu, C. Tang, Y. Gao, K. Luo, Z. Zhao, L.M. Wang, B. Wen, J. He, Z. Liu, Ultrahard nanotwinned cubic boron nitride, Nature. 493 (2013) 385–388.

[9] C. Hwang, M. Örnek, V. Domnich, W.E. Mayo, S.L. Miller, R.A. Haber, c-BN Seeding Effect on the Phase Transition of a-BN(OC) Compound, in: Ceram. Eng. Sci. Proc., 2015: pp. 83–91.

[10] Y. Meng, H. Mao, P.J. Eng, T.P. Trainor, M. Newville, M.Y. Hu, C. Kao, J. Shu, D. Hausermann, R.J. Hemley, The formation of sp^3 bonding in compressed BN, Nat. Mater. 3 (2004) 111–114.

[11] R. Haubner, M. Wilhelm, R. Weissenbacher, B. Lux, Boron Nitrides — Properties, Synthesis and Applications, in: M. Jansen (Ed.), High Perform. Non-Oxide Ceram. II, Springer Berlin Heidelberg, 2002: pp. 1–45.

[12] O.O. Kurakevych, V.L. Solozhenko, High-pressure design of advanced bn-based materials, Molecules. 21 (2016).

[13] O. Hod, Graphite and hexagonal boron-nitride have the same interlayer distance. Why?, J. Chem. Theory Comput. 8 (2012) 1360–1369.

[14] B. Ertug, Powder Preparation, Properties and Industrial Applications of Hexagonal Boron Nitride, Sinter. Appl. (2013).

[15] A. Lipp, K.A. Schwetz, K. Hunold, Hexagonal Boron Nitride : Fabrication, Properties and Applications, J. Eur. Ceram. Soc. 5 (1989) 3–9.

[16] J. -Y Choi, S.L. Kang, O. Fukunaga, J. -K Park, K.Y. Eun, Effect of B2O3and hBN Crystallinity on cBN Synthesis, J. Am. Ceram. Soc. 76 (1993) 2525–2528.

[17] B.P. Singh, V.L. Solozhenko, G. Will, On the low-pressure synthesis of cubic boron nitride, Diam. Relat. Mater. 4 (1995) 1193–1195.

[18] T. Hagio, K. Nonaka, T. Sato, Microstructural development with crystallization of hexagonal boron nitride, J. Mater. Sci. Lett. 16 (1997) 795–798.

[19] M. Örnek, C. Hwang, K.M. Reddy, V. Domnich, S.L. Miller, E.K. Akdoğan, K.J. Hemker, R.A. Haber, Formation of BN from BCNO and the development of ordered BN structure: I. Synthesis of BCNO with various chemistries and degrees of crystallinity and reaction mechanism on BN formation, Ceram. Int. 44 [13] 14980-14989 (2018).

[20] C. Hwang, M. Örnek, K.M. Reddy, V. Domnich, S.L. Miller, K. Hemker, R.A. Haber, Effect of synthesis conditions of BCNO on the formation and structural ordering of BN at 1200 °C and 1 GPa, Diam. Relat. Mater. 87 (2018) 156–162.

[21] T. Kawasaki, Y. Kuroda, H. Nishikawa, and H. Hara, Hexagonal system boron nitride powder, US Patent (US5854155), 1998.

[22] B.E. Warren, X-ray diffraction in random layer lattices, Phys. Rev. 59 (1941) 693–698.

[23] T.E. O'connor, Process for the production of boron nitride; US Patent (US3241919), 1966.

[24] B.E. Warren, X-ray Diffraction. Courier Corporation, 1969.

[25] S. Alkoy, C. Toy, T. Gönül, A. Tekin, Crystallization behavior and characterization of turbostratic boron nitride, J. Eur. Ceram. Soc. 17 (1997) 1415–1422.

[26] M.G. Balint, M.I. Petrescu, An attempt to identify the presence of polytype stacking faults in hBN powders by means of X-ray diffraction, Diam. Relat. Mater. 18 (2009) 1157–1162.

[27] P. Patnaik, Handbook of Inorganic Chemicals. 2003.

[28] M. Hubáček, M. Ueki, T. Sato, V. Brožek, High-temperature behaviour of hexagonal boron nitride, Thermochim. Acta. 282–283 (1996) 359–367.

[29] H. Saito, M. Ushio, "The formation mechanisms and some properties of boron nitride from ammonium thiocyanate and orthoboric acid -Synthesis of the hexagonal boron nitride (Part 2)," J. Ceram. Assoc. Japan, 77 151-163 (1969).

[30] A. V. Kurdyumov, V.L. Solozhenko, W.B. Zelyavski, Lattice Parameters of Boron Nitride Polymorphous Modifications as a Function of Their Crystal-Structure Perfection, J. Appl. Crystallogr. 28 (1995) 540–545.

[31] A. V Kurdyumov, On packing defects in graphite-like boron nitride, Kristallografiya. 20 (1975) 969–973.

[32] V.F. Britun, A. V. Kurdyumov, Mechanisms of martensitic transformations in boron nitride and conditions of their development, High Press. Res. 17 (2000) 101–111.

[33] V.I. Levitas, Y. Ma, J. Hashemi, M. Holtz, N. Guven, Strain-induced disorder, phase transformations, and transformation-induced plasticity in hexagonal boron nitride under compression and shear in a rotational diamond anvil cell: In situ x-ray diffraction study and modeling, J. Chem. Phys. 125 (2006) 44507.

[34] V.L. Solozhenko, V.Z. Turkevich, G. Will, Synthesis of Boron Nitride by Self-Propagating Reactions at High Pressure, J. Am. Ceram. Soc. 79 (2005) 2798–2800.

[35] R.S. Pease, An X-ray study of boron nitride, Acta Crystallogr. 5 (1952) 356–361.

Tables

Table 1. Representative chemical compositions of starting BCNOs based on EDS analyses.

Starting BA:M Ratio (molar)	**Chemical composition, at.%**			
	Boron	Carbon	Nitrogen	Oxygen
1:1	9.4	31.9	48.8	9.9
3:1	13.8	25.4	40.0	20.8
6:1	22.6	15.3	23.8	38.2

Table 2. The classification of BN sub-polytypes, which have hexagonal unit cells, based on d-spacing, crystallite sizes along the a- and c-axes (*L*a, *L*c), along with the corresponding 3-D structural ordering values.

BN sub-polytypes	**Structural characteristics**			
	d_{002} (nm)	*L*c (nm)	*L*a (nm)	D_3
t-BN	> 0.345[a]	< 2[a]	< 5[b]	0[c]
m-BN	0.345 - 0.333[a]	2-15[a]	5-15[b]	-
h-BN	≤ 0.333[a,b]	> 15[a,b]	> 15[b]	> 0.84[c]

[a]value from Ref. 2
[b]value from Ref. 23
[c]value from Ref. 30

Table 3. Microstructural analyses of BN synthesized in this study from BCNO as a function of starting BA:M ratio, heat treatment temperature, and their classification into corresponding sub-polytypes based on d-spacing and crystallite sizes.

Synthesis Conditions		**Structural Characteristics**					
Post treatment temperature	Molar Ratio	d_{002} (nm)	*L*c (nm)	*L*a (nm)	Corresponding sub-polytypes	*L*a/*L*c	D_3
1400°C	1:1	0.356	1.4	-	t-BN	-	-
	1.5:1	0.356	1.8	-	t-BN	-	-
	2:1	0.336	7.1	10.9	m-BN	1.6	0.75
	3:1	0.335	11.3	25.0	m-BN	2.2	0.82
	6:1	0.334	10.4	26.9	m-BN	2.6	0.88
1600°C	1:1	0.363	1.8	-	t-BN	-	-
	1.5:1	0.365	1.7	-	t-BN	-	-
	2:1	0.337	8.8	19.2	m-BN	2.2	0.79
	3:1	0.335	13.0	33.4	m-BN	2.6	0.83
	6:1	0.334	25.7	53.1	h-BN	2.1	0.91
1800°C	1:1	0.344	2.3	-	m-BN	-	-
	1.5:1	0.345	2.3	-	m-BN	-	-
	2:1	0.336	10.3	26.7	m-BN	2.6	0.79
	3:1	0.335	10.2	36.3	m-BN	3.5	0.79
	6:1	0.333	24.1	67.4	h-BN	2.8	0.92
Commercial h-BN[a]		0.333	31.9	64.1	h-BN	2.01	0.92

[a]Kennametal (Grade: BN150)

Figures

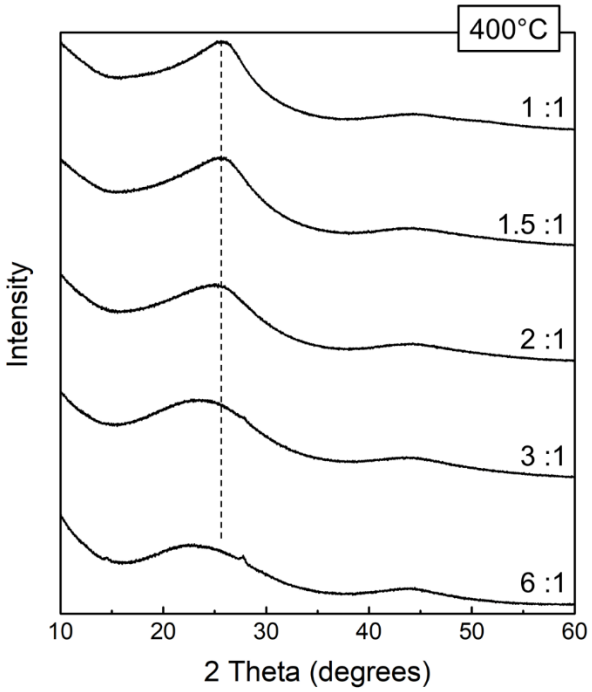

Figure 1. X-ray diffraction patterns of initial BCNOs synthesized at 400°C for H_3BO_3:$C_3N_6H_6$ molar ratios of 1:1, 1.5:1, 2:1, 3:1, and 6:1 show the amorphous nature of the powders.

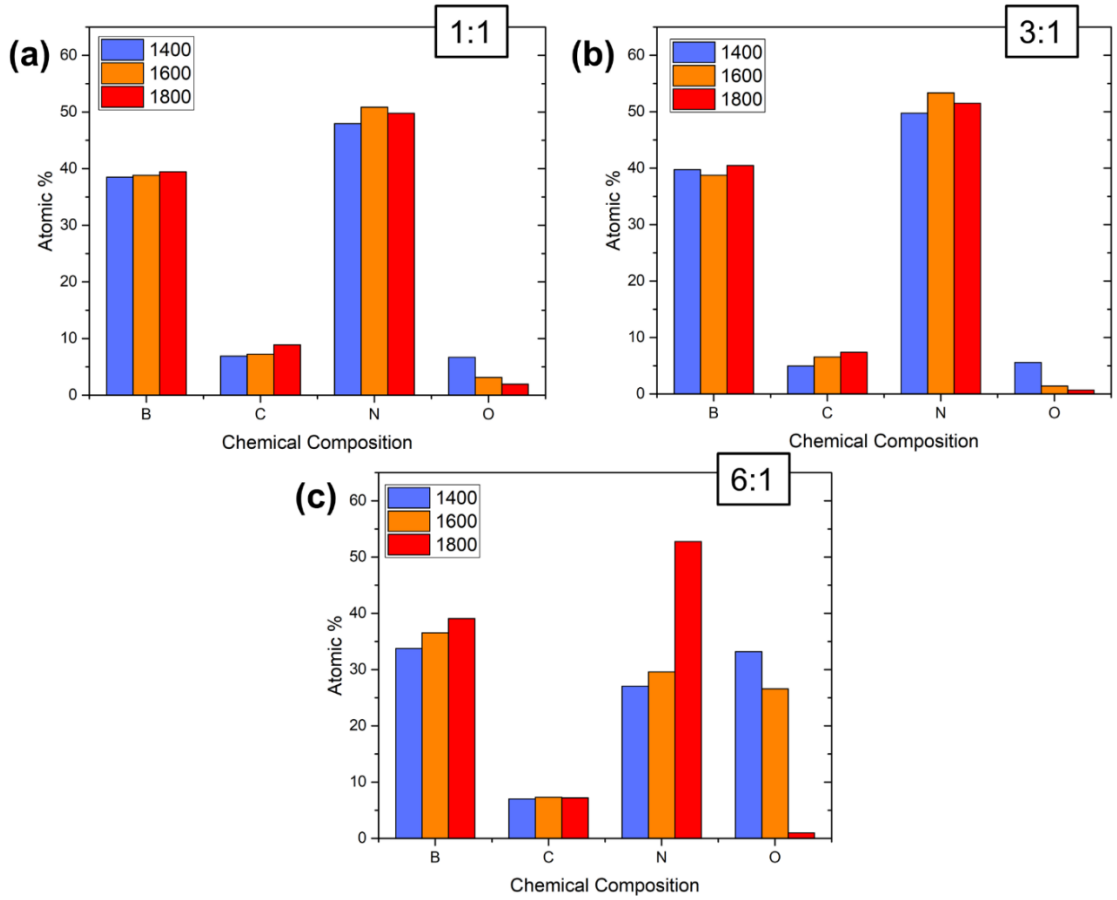

Figure 2. Representative chemical variations in the synthesized powders based on EDS analyses as a function of heat treatment temperature using H_3BO_3:$C_3N_6H_6$ molar ratios of **a)** 1:1 **(b)** 3:1, **(c)** 6:1.

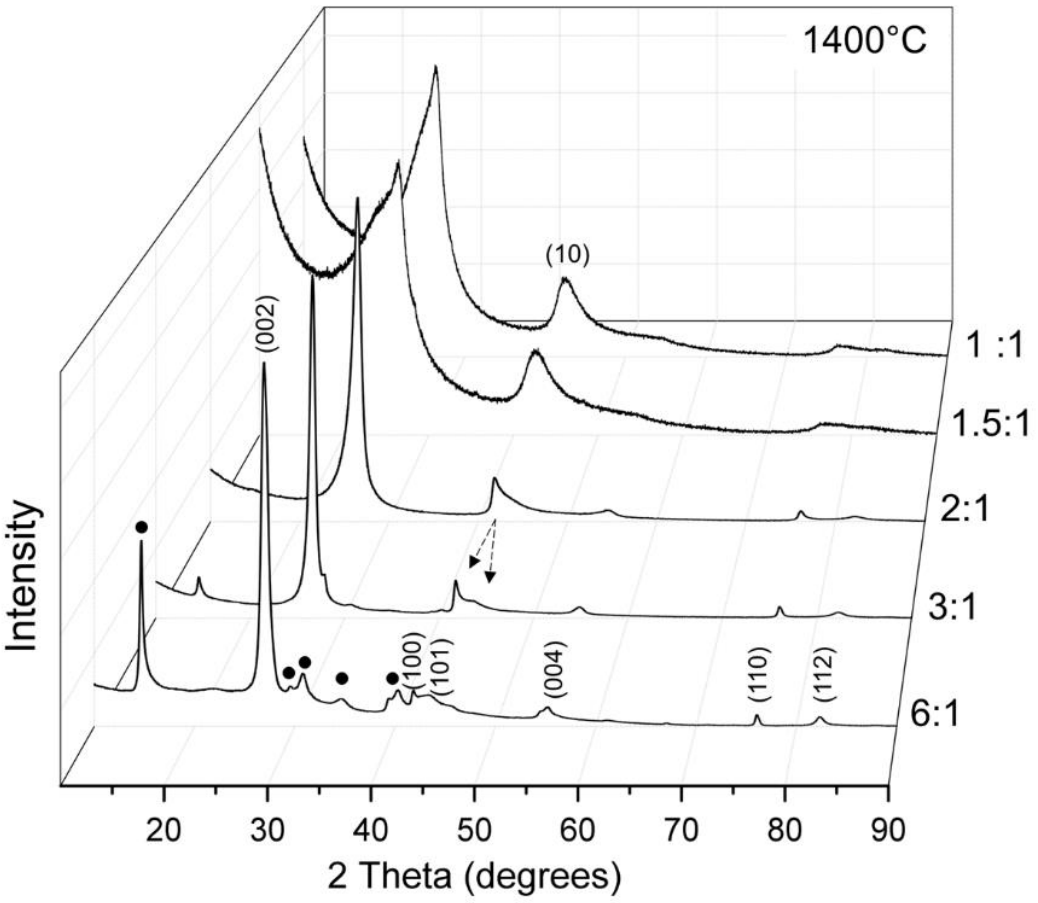

Figure 3. X-ray diffraction patterns showing phase and long-range crystallographic evolution of a-BCNO precursors into crystalline BN and B_2O_3 after the post treatment at 1400°C as a function of boric acid (H_3BO_3)-melamine ($C_3H_6N_6$) molar ratios. B_2O_3 peaks are indexed as ●.

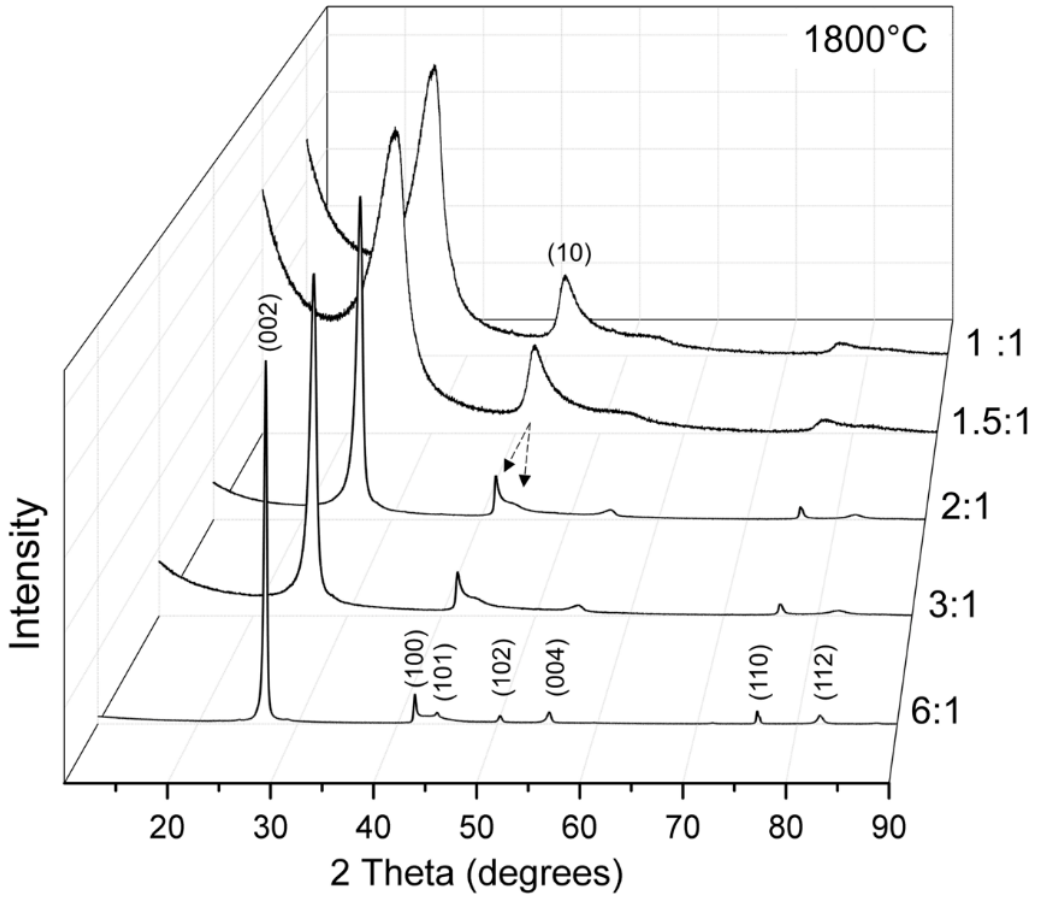

Figure 4. X-ray diffraction patterns showing phase and long-range crystallographic evolution of a-BCNO precursors into crystalline BN after the post treatment at 1800°C as a function of boric acid (H_3BO_3)-melamine ($C_3H_6N_6$) molar ratios. B_2O_3 peaks were not observed in any of the samples.

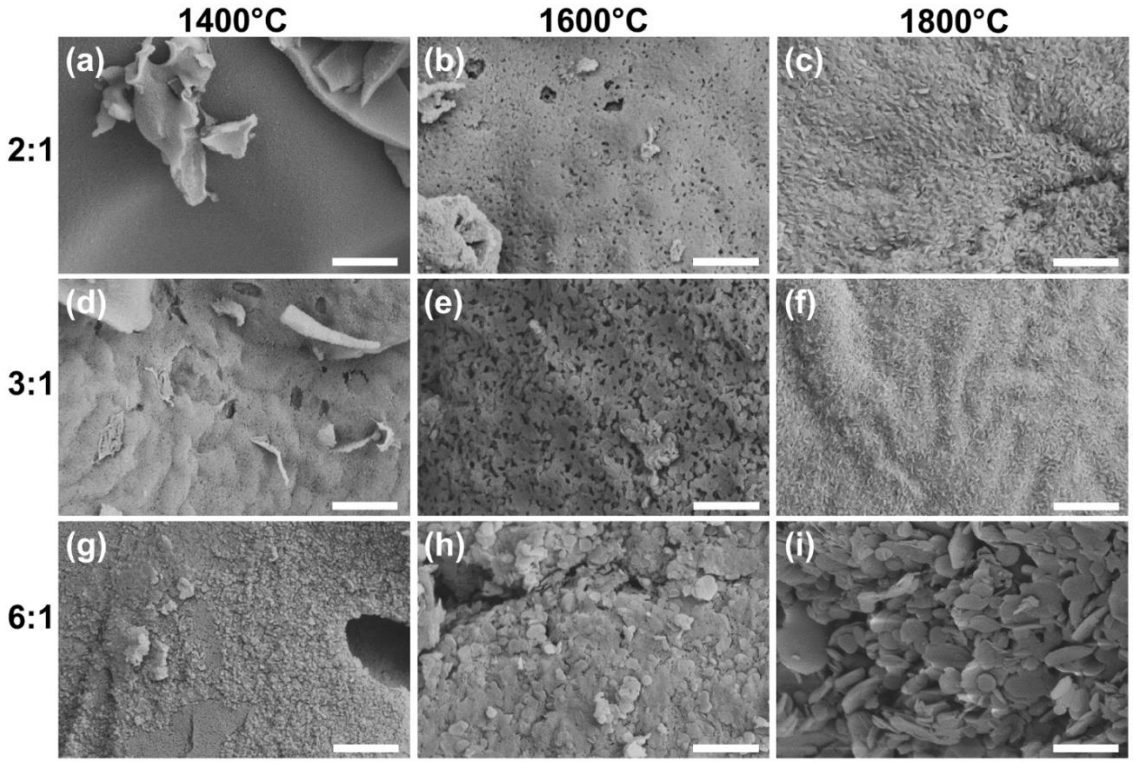

Figure 5. Representative FE-SEM micrographs of synthesized BN powders for BA:M = 2:1 molar ratio at **(a)** 1400°C, **(b)** 1600°C, and **(c)** 1800°C, for BA:M = 3:1 molar ratio at **(d)** 1400°C, **(e)** 1600°C, and **(f)** 1800°C, and for BA:M = 6:1 molar ratio at **(g)** 1400°C, **(h)** 1600°C, and **(i)** 1800°C. Scale bars in micrographs correspond to 1μm.

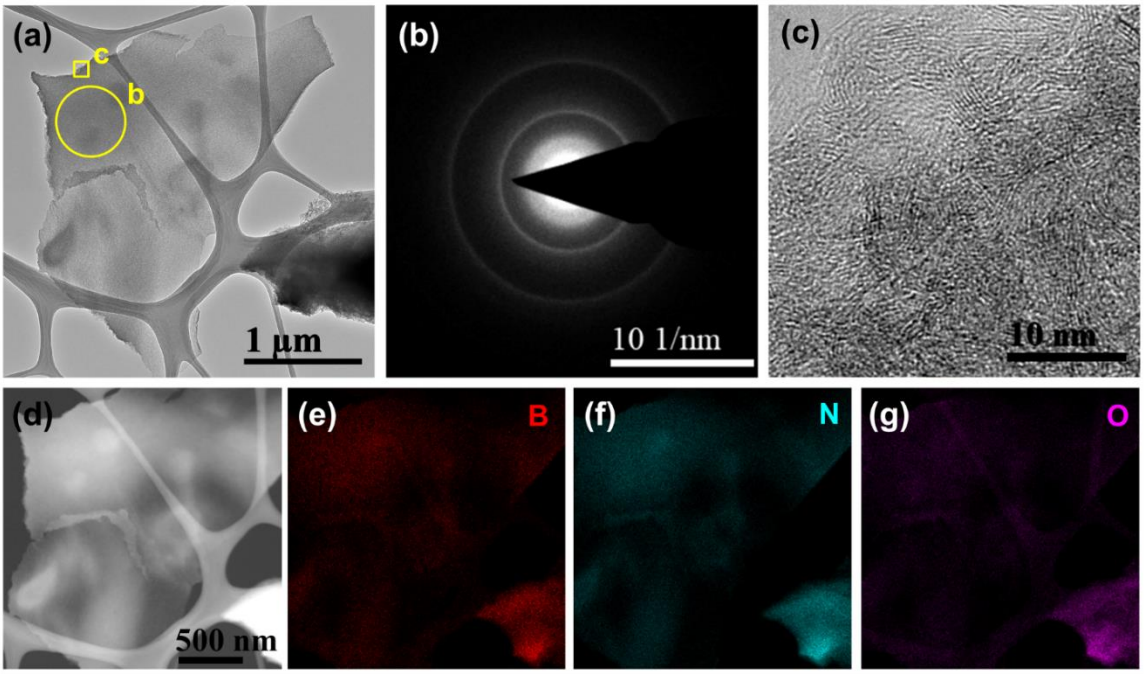

Figure 6. BN powders synthesized using BA:M = 1:1 molar ratio at 1800°C. **(a)** A low-magnification representative TEM image showing irregular and thin BN flake **(b)** a SAED pattern taken from region marked in (a) showing the existence of crystalline phase **(c)** a high-resolution TEM image showing randomly ordered small lattice regions. **(d)** EDX spectrum image taken from the flake shown in (a). Elemental analysis shows that the flake is composed of **(e)** boron, **(f)** nitrogen and **(g)** oxygen.

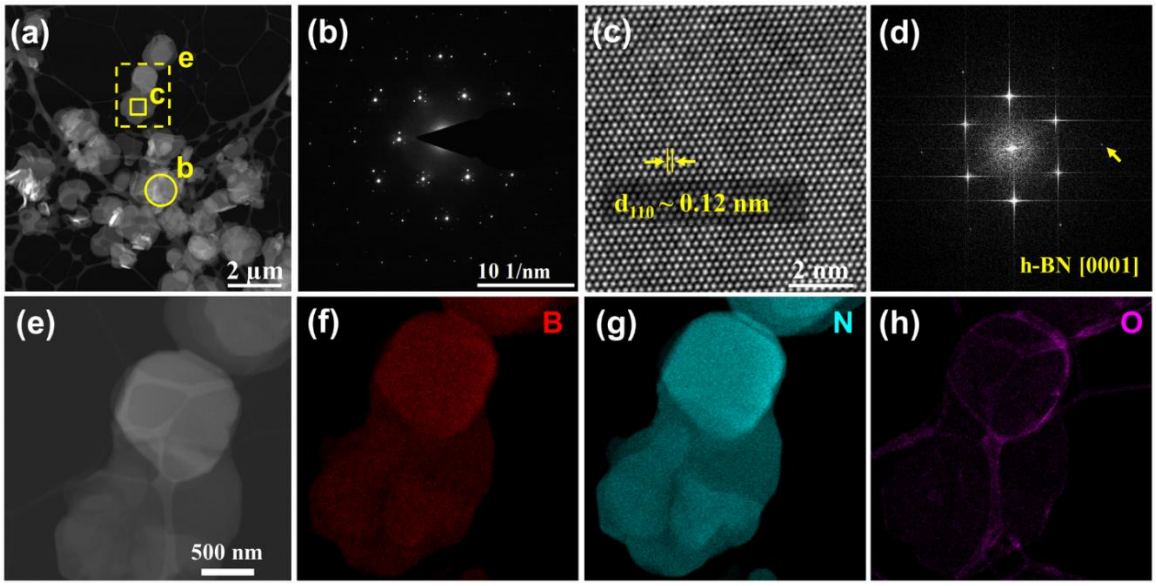

Figure 7. BN powders synthesized using BA:M = 6:1 molar ratio at 1800°C. **(a)** A representative low-magnification TEM image displays BN flakes ~ 1 µm in size **(b)** a SAED pattern taken from region marked in (a) showing well defined diffraction spots indicating high crystallinity **(c)** a HR-TEM image showing perfect crystal with interplanar distance of ~ 0.12 nm along (110) plane. **(d)** FFT of HR-TEM image reveals a second set of reflections as marked by yellow arrow. **(e)** EDS map taken from the flake shown in (a) shows that the flake is composed of mainly **(f)** boron, **(g)** nitrogen and **(h)** a very low amount of oxygen.

Supplementary Figure

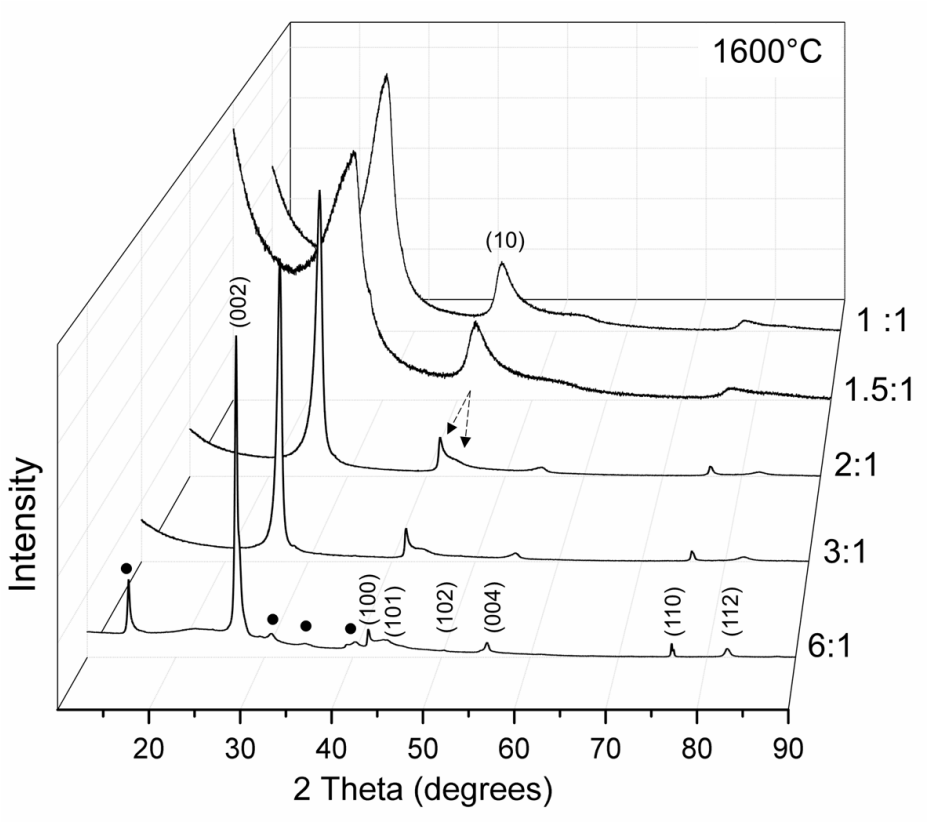

Supplementary Figure 1. X-ray diffraction patterns showing phase and long-range crystallographic evolution of a-BCNO precursors into crystalline BN, and B_2O_3 after the post heat treatment at 1600°C as a function of boric acid (H_3BO_3)-melamine ($C_3H_6N_6$) molar ratios. B_2O_3 peaks are indexed as ●.

Chapter 5.

Observations of Nanocrystalline Cubic Boron Nitride Formed with Plasma Spraying

K Madhav Reddy[a], Chawon Hwang[b], Metin Örnek, Steven L. Miller[c], William E. Mayo[c], Alan Burgess[d], Richard A. Haber[b], Kevin J Hemker[a*]

[a]*Department of Mechanical Engineering, Johns Hopkins University, Baltimore, MD 21218, USA*

[b]*Department of Materials Science and Engineering, Rutgers, The State University of New Jersey, Piscataway, NJ 08854, USA*

[c]*H&M Analytical Services, Inc. 35 Hutchinson Rd, Allentown, NJ 08501, USA.*

[d]*SprayWerx Technologies Inc, 486 Fairway Drive, North Vancouer, British Columbia, Canada V7G 1L5.*

*Corresponding author E-mail: hemker@jhu.edu

Abstract

Cubic boron nitride (c-BN) has a superior hardness and strength as compared to other oxide and non-oxide ceramics that are commonly used as abrasives and in cutting tool applications. To date, c-BN powders are produced under high pressures, usually greater than 10 GPa, and the expense associated with this has limited its use in a wide range of engineering applications. Here we report on the synthesis of nanocrystalline c-BN from metastable precursors without high external pressures using novel plasma spray processing techniques. Transmission electron microscopy and EELS measurements indicate that the initial metastable precursor particles are amorphous and comprised of boron, carbon, nitrogen and oxygen with weak interatomic bonding that may easily undergo phase transition during plasma spraying. Postmortem X-ray diffraction and TEM analysis of deposited particles revealed the formation of crystalline phases of BN. Further, high-resolution TEM observations demonstrated that c-BN phase can be induced during the plasma spray process with the addition of appropriate catalysts. These observations point to a novel pathway for facilitating the transition from a low-density (2.2g/cc) amorphous state to the high-density (3.5 g/cc) cubic BN phase.

Keywords: Metastable Precursors, Plasma Spray, Transmission Electron Microscopy, Nanocrystalline, Boron Nitride

1. Introduction

Boron Nitride (BN) exists in several polymorphic forms such as amorphous BN (a-BN), hexagonal BN (h-BN), turbostratic BN (t-BN), rhombohedral BN (r-BN), monoclinic BN (m-BN), orthorhombic BN (o-BN), wurtzite BN (w-BN) and cubic BN (c-BN) phases [1-3]. At ambient pressure, h-BN exists in a stable crystalline structure that can be transformed to low density (~2.2 g/cc) metastable phases namely t-BN, m-BN and r-BN at relatively low pressures of less than 2 GPa. By contrast, transition to higher density (~3.5 g/cc) w-BN, o-BN and c-BN phases develops only at high temperatures and high pressures above 10 GPa and these phases have a rigid atomic packing structure [4-6]. Among them, c-BN is known to be the hardest, with a hardness only next to diamond, and it has found application in the fields of protective coatings and hard facing applications [7,8]. Importantly, c-BN possesses high oxidation resistance and low chemically reactivity, and it is perhaps best known for cutting ferrous material and carbide forming hard substances where diamond fails completely [9,10]. However, currently produced c-BN is synthesized from the initial graphitic h-BN precursor with a high temperature and high pressure (HTHP) process and has grain sizes that range from hundreds of nanometers to tens of micrometers [2,4,8,11]. Reducing the temperatures and pressures needed to synthesize c-BN would both economize the production of c-BN and allow for better microstructural control.

Previous efforts to minimize the threshold pressure for the transformation of h-BN to c-BN have employed a catalytic processing methodology [12-18]. The common catalyst-solvent materials that are used for the synthesis of c-BN are Li, Al, Mg, Ca, Li_3N, LiF, Mg_3N_2, Ca_3N_2, $Ca_3B_2N_4$ and $Mg_3B_2N_4$ [13-15]. The catalyst-solvent method utilizes the

eutectic reaction between BN and the catalyst to accelerate crystallization, which occurs at a much faster rate in the eutectic solution, allowing for a reduction of pressures to ~6 GPa for the c-BN phase formation [16]. Further, alloy catalyst addition, such as Mg-Al, Fe-Al, Cu-Sn, Mg-Sn, Al-Co, Al-Mn, Al-Cr, and Al-Ni, reduced the pressures to ~5 GPa, suggesting that the presence of low melting temperature phases enhances the phase transformation of h-BN into c-BN [17-18].

Alternatively, metastable a-BN has been used as an initial precursor, which is found to reduce the activation energy barrier for the nucleation and growth due to low structural ordering, and allows the a-BN to be readily converted to c-BN at pressures higher than 6 GPa without the addition of catalysts [19-21]. Singh *et al* investigated using a magnesium boron nitride solvent catalyst in the presence of a-BN and were able to reduce the threshold pressure of crystallization for c-BN to 2.5 GPa [22,23]. To date, c-BN has not been synthesized below 2 GPa with conventional processing methods [23].

The plasma spray process has proven to be a powerful technique to synthesize a variety of metal and ceramic nanocrystalline powders [24, 25]. In contrast to conventional processing methods, plasma spraying utilizes the high temperature plasma stream in which injected material powders are rapidly softened and sometime melted while being accelerated towards a substrate [26,27]. During this process, high velocity impact on the substrate may induce desirable structural transformations [28]. However, this process has not been well explored for synthesizing high pressure stable phases, or to develop an understanding of the phase transitions in ceramic materials [29,30].

Here we report of the synthesis of nanocrystalline c-BN without applying external pressure. The nanocrystalline c-BN is prepared by a novel plasma spray technique

involving initial metastable amorphous BNCO (a-BNCO) with boric acid (H_3BO_3) and beta boron (β-B) catalysts. The phase evolution of nanocrystalline c-BN is demonstrated using X-ray diffraction and high-resolution transmission electron microscopy (HRTEM) characterization.

2. Experimental Details

2.1 Synthesis of BNCO precursor

An initial precursor of an a-BNCO compound was synthesized by heating a mixture of boric acid (H_3BO_3, Borax, Optibor®) and melamine ($C_3H_6N_6$, DSM, MelaminebyDSM^{TM}) in 3:1 mole ratio at 200 °C in air for 2 h and 400 °C in N_2 gas atmosphere (2 L/min) for 3 h. To prepare powders having good flowability suitable for plasma spray processing, first a slurry was prepared and then spray dried based on the process reported by V. K. Pujarie et al. US Patent 6645612 B2, 2003) [31]. In brief, a-BNCO powders were added in surfactant (alkoxy silane, Dow Corning, Z-6040)-H_2O solution and after mixing (ball milling for 1 h using ZrO_2 balls and HDPE plastic jar) a binder-H_2O solution (3 wt% PEG 400 in DI H_2O) was added to the dispersion and then post ball-milling was conducted for 600 seconds. The solid content of slurry was 30 wt% and the amounts of surfactant and binder-H_2O solution were designed to be 5 wt% of solid content and 9 wt% of the initial dispersion, respectively. Spray drying of slurry thus prepared was carried out with a spray drier (BÜCHI, B-290) at conditions of 200 °C inlet temperature and 600 L/h air flow rate. Two compositions of powders were prepared for plasma spray process: i) a-BCNO+H_3BO_3 mixture (a-BCNO: H_3BO_3=75:25 wt %) and ii)

a-BNCO+H_3BO_3+B (a-Boron, ABCR GmbH & CO. KG, Grade 1-A) mixture (a-BNCO:H_3BO_3:B=60:20:20 wt%).

2.2 Processing of BN using a novel plasma spray technique

Plasma spraying was carried out with a DC Axial type gun (SprayWerx Technologies Inc., Axial III) at the National Research Council Canada. The main operating conditions including plasma gas chemistry, applied current and power, stand-off-distance, and gas flow rate are summarized in Table 1. The measured temperature and particle velocity during the plasma spray are summarized in Table 2 and were conducted using an Accuraspray system produced by Tecnar Automation, St-Bruno, QC. Powders were plasma-sprayed onto a water-cooled aluminum chill plate and then scraped off plate using a steel scrapper.

2.3 Characterization

All the samples prepared in this study, were characterized by x-ray diffraction (XRD), scanning electron microscopy (SEM), and transmission electron microscopy (TEM). The crystal structure and average crystallite size were evaluated using XRD. SEM studies were done using a field emission SEM (ZEISS, SIGMA) to obtain the surface morphology of pre-and post-processed samples. The pre- and post processed powders was dispersed in distilled water and then allowed to settle on carbon coated copper grids for investigation by transmission electron microscopy (Philips FEI CM-300) equipped with a Gatan detector 200 electron energy loss spectroscopy (EELS) detector. The bright field TEM images were used to study the grain size and morphology, while selected area electron diffraction (SAED) was used to study the crystal structure and lattice spacing. The chemical composition and bonding was established by electron energy loss spectroscopy

(EELS) of both pre- and post-process powder samples. The fine grain size obtained by TEM was estimated using image processing and analysis (UTHSCSA Image Tool). Image simulations were performed by using the Win HREM (HREM Research Inc.). For these multisilice simulations, a structural model of the cubic BN unit cell (a=b=c=3.615 A^o; $\alpha=\beta=\gamma=90^o$) was given in an input file [32]. The imaging conditions used in simulation and experiments were as follows: the incident electron beam energy was 300 keV, the spherical aberration coefficient (Cs) was 1.2 mm, the defocus spread of the primary beam was 10 nm, the beam convergence was 0.3 nm^{-1}, thickness was 5 nm and defocus value was +10 nm.

3. Results

3.1 Characterization of a-BNCO synthesized precursor

Figure 1 shows the synthesized powders obtained from the initial precursors of H_3BO_3 and $C_3H_6N_6$ by heat treatment at a final temperature of 400^{o}C for 3 h in the presence of a pure N_2 atmosphere. The XRD pattern of synthesized powders (Fig. 1a) exhibits broad peaks indicating the amorphous phase. SEM images display irregular shaped agglomerate particles of as-synthesized powders in the range of few hundred nm to 40 μm as shown in Fig 1b. Low magnification TEM images (e.g. Fig.1c) show thin sheets of agglomerated irregular particle that produce a selected area diffraction pattern (insert) indicative of an amorphous sample. Representative high resolution TEM images (e.g. Fig. 1d) demonstrate that the localized region does not form a periodic atomic lattice, further indicating that the synthesized powders are completely amorphous. An EELS spectrum taken for a single particle (Fig. 1e) shows the K-edges of boron, carbon, nitrogen and oxygen indicating the

presence of these elements in the starting chemical synthesized powders. The chemical bonding of each element can be deduced from the fine structure of the K-edges and as noted in Fig. 1e sigma (σ) and pi (π) bonds [33] were associated with B at 191.6 and 198.7 eV, C at 285.0 and 296.0 eV, N at 398.0 and 407.0 eV, and O at 531.0 and 538.0 eV respectively. The presence of significant π bonding in an amorphous material is indicative of weak interatomic bonding with SP^2 bonded clusters [34, 35]. Quantative analysis of the peaks in the EELS spectra allow for local composition measurements and the measured relative B, C, N compositions are reported in Fig. 1f, oxygen is less 5% atomic content. The results indicate a large composition variation with less than 25 atomic % of boron.

3.2 TEM characterization of H_3BO_3 and β-B catalysts

In order to increase the boron content in the synthesized BNCO precursor, we have used two catalysts H_3BO_3 and beta boron (β-B). TEM images of H_3BO_3 revealed a thin fibrous network (e.g. Fig. 2a) and a higher magnification view (inset) showed a layered structure. EELS spectra taken from the thin layered region displayed B-K and O-K near edge elements both exhibiting π and σ bonding at 191.6 eV, 198.7 eV, and 538. 0 eV, 547. 5 eV peak positions indicating weak bonding between layers that do not have long range three-dimensional order as shown in Fig. 2b [36]. A representative TEM image of beta boron (β-B) (Fig. 2c) shows the amorphous structure in the fine size particles, and the corresponding EELS spectra confirms the structure to be dominated by a single edge for elemental boron (B-K) [33] (Fig. 2(d)).

3.3 Illustration of pre- and post-plasma spray deposition processes of BNCO materials

To increase the flowability of a-BNCO particles with their catalysts during the plasma spraying process, a sprayed dried slurry method was adopted. A typical SEM image of the BNCO powders (Fig. 3a) shows an agglomerated spherical morphology with diameters ranging from 2 μm to 40 μm. The sprayed drying was done for a-BNCO with a H_3BO_3 catalyst and for a-BNCO with both H_3BO_3 and β-B catalysts, and both were fed at similar plasma spray conditions to see the effect of these catalysts on the metastable a-BNCO precursor. The schematic in Fig. 3b illustrates the novel plasma spray process that was used to synthesize crystalline BN phases. The precursor powders were fed into a plasma spray gun, where the powders were heated to high temperatures in a N_2 atmosphere. The measured temperature and velocity during the plasma spray were ~4200 K and 515 m/s (Table 2). The residence time during plasma deposition was 50 μs. These ionized powder particles were deposited on the water-cooled aluminum substrate through a carrier gas. The federate of powder particles during plasma spray was 5 g/min. The final conversion efficiency is about 5-10 wt.% based on the amount of particles scrapped off from the cooling substrate. The deposited powder materials on substrate were collected and used for post processing investigation. Fig. 3c SEM image of deposited material appears like flattened pancakes with irregular morphology agglomerates of BNCO that are 5-20 μm in size, which is different from the pre-deposited spherical microstructure (Fig. 3a) suggesting that a structural transition may have taken during the plasma spray process.

Figure 4 zoom in SEM image of plasma spray BNCO particle clearly shows the signature of melted zone as shown with an arrow (white color). An elemental dispersive

spectroscopy (EDS) analysis (Fig. 4 (b-e)) taken from the scanned area (Fig .4a yellow color box) revealed rich in boron, nitrogen and oxygen elements and deficiency in carbon region in melted region indicating the possible formation of BN and B_2O_3 phases in post processed plasma spraying.

3.4 Influence of H_3BO_3 catalyst on plasma spraying of a-BNCO

Figure 5 summarizes the characterization of the powder that was produced by plasma spraying BNCO with the H_3BO_3 catalyst precursor. An XRD pattern (Fig. 5a) of the sprayed product reveals the presence of t-BN, B_2O_3 and unreacted H_3BO_3. Low magnification TEM images show a thin irregular morphology of particles (Fig. 5b), and the SAED pattern taken from the region in Fig. 5(b) is quite sharp and has well-defined circular rings (Inset Fig. 5c) as compared to the diffused electron diffraction pattern obtained from the as-synthesized a-BNCO precursor (see in Fig. 1c), indicating the existence of crystalline phases. The peak positions extracted using circular average method match those of t-BN and c-BN (Fig. 5c). The observed intensity peaks are associated with t-BN reflections for basal and prismatic planes, as well as c-BN planes reflections (Fig. 5c). A higher magnification TEM image of Fig. 5(b) can be found in Fig. 5d, and it shows evidence of the stacking ordering of t-BN and the fine crystalline growth of c-BN in an amorphous BNCO material. The EELS spectrum taken from this region shows strong B-K and N-K edges at 191.6-198.7 eV and 398.0-423.5 eV and a small intensity of C-K edge and O-K edge can be found (Fig. 5e). Quantitative estimates of the amounts of each element from BNCO particles were obtained from the size of the B-K, N-K and C-K peaks and the results (Fig. 5f) point to equal amounts of B and N and a C composition of less than 20

atomic % indicating the definitive chemical changes during plasma spraying (see Fig. 1f).

3.5 Influence of H_3BO_3 and β-B catalysts on plasma spraying of a-BNCO

Figure 6 summarizes the characterization of the material produced by plasma spraying of the a-BNCO precursor with the H_3BO_3 and the β-B catalyst. XRD patterns (Fig. 6a) evidenced crystalline peaks of β-B, t-BN, c-BN and unreacted H_3BO_3 indicating significant structural changes associated with the addition of the catalysts. The peak broadening in the XRD peaks suggests that the average size of the crystalline c-BN is about 8 nm. The Quantitative analysis from the XRD profile (Fig. 6a) shows the 5 % weight fraction of c-BN phase as estimated from refinement technique. A low magnification TEM image displays the irregular BNCO particles and within each particle evidence of grains with a spherical morphology can be seen (Fig. 6b). The SAED ring pattern from this region (Fig. 6c) confirms the polycrystalline nature of the particle and the measured lattice parameters indicate significant amounts of the c-BN phase along with t-BN and β-B phases. Increasing the magnification of the TEM image in Fig. 6b shows a wide range of fine grain sizes within the BNCO material, see Fig. 6d. The calculated fraction of c-BN grains from TEM images ranging from 2.5 to 8 % in a-BNCO particles measured using image analysis consistent with XRD measurement.

3.6 TEM characterization of formed nanocrystalline c-BN with plasma spraying

Figure 7 shows direct TEM observations of fine c-BN grains that were synthesized by plasma spraying a-BNCO in the presence of H_3BO_3 and β-B. The grain sizes estimated from TEM images within the BNCO particles ranged from 1 to 20 nm with an average of 6± 3 nm. Fig 7b shows a high-resolution TEM image taken from the region in Fig. 6d and provides direct evidence of a grain size of about 5 nm with the cubic crystal structure and

lattice spacing (d_{hkl}=0.21 nm) of c-BN. A high magnification image (Fig. 7c) reveals a perfect lattice image that is consistent with the structure model image simulation of c-BN along with the [101] direction. The EELS spectra from this region displayed only σ bonding at 196.5 eV for the B-K edge and 420.5 eV for the N-K edge. The presence of only σ bonding is further evidence of the c-BN phase and is a characteristic of SP^3 bonded materials [33-34]. Fig. 8a, a low magnification TEM image on carbon coated films, shows that the nanocrystalline c-BN grains can be well separate from other low-density phases of BNCO and t-BN obtained after ultrasonicating for 1200 seconds. High resolution TEM images (Fig. 8b) confirm that the fine spherical grains have lattice spacing of about 0.21 nm, as estimated using line intensity profiles (Inset Fig. 8b), and compare well with c-BN oriented along a <110> zone axis.

Figure 9 provides a comparison of threshold pressures for the formation of c-BN using different initial crystalline and amorphous precursors with their catalysts [1,4,12-23, 37]. The graphical plot clearly illustrates that the introduction of amorphous starting material seems a promising route to achieve c-BN at relatively low pressures as compared to high crystallinity in h-BN. In our work, we have observed formation of nanocrystalline c-BN at relatively low pressures as made possible by the incorporation of metastable precursors into plasma spray processing.

4. Discussion

The microstructural observations of nanocrystalline c-BN formation can be rationalized by considering the influence of four key parameters: the initial precursor, the

catalysts, the chemical reactions and the rapid deposition that occur during the plasma spray process.

The effect of using an amorphous BNCO precursor on the formation of c-BN during the plasma spray process was evaluated in this study and was found to significantly reduce the high pressures required for the phase transformation. The precursor that was synthesized from $C_3H_6N_6$ and H_3BO_3 had an amorphous structure containing boron, carbon, nitrogen and a small amount of oxygen indicating the form is BNCO with no microscopically detectable ordered structure as shown in Fig. 1. Also, the BNCO precursor was found to have weak chemical bonding between the atoms, which is the result of Pi bonds that may easily melt and reduce the activation energy barrier for the formation of c-BN during the plasma spray process (Fig. 1e). Lorenz *et al.* in-situ high pressure-high temperature XRD observations demonstrated that a-BN leads to a considerable reduction of the temperature and pressure (1200^{o}C and 7GPa) need to transform a-BN to c-BN [38]. By comparison, the ordered t-BN precursor to c-BN formation proceeds through an intermediate h-BN at relatively a higher temperature and pressure (1450^{o}C and 8 GPa) and is accompanied by a lower rate conversion from h-BN to c-BN [19, 38]. These references coupled with our observations suggests that using metastable precursors with a high number of structural imperfections facilitated the phase transition to c-BN by reducing required processing pressures and temperatures to those accessible by plasma spray processing.

The addition of H_3BO_3 and β-B catalysts to the metastable BNCO precursor also played an important role in obtaining stoichiometric BN phases and enhancing c-BN formation. On average the initial a-BNCO precursor was found to have approximately 15

at. % boron compared to ~40 at. % of each carbon and nitrogen (Fig. 1f). A key finding in the current study is the fact that we can increase the boron content by adding H_3BO_3 and β-B catalysts to the precursor powders (Fig. 5e). We found that plasma spraying a-BNCO particles with only the H_3BO_3 catalyst induced a phase transition, which formed a stoichiometric t-BN and a small fraction of c-BN phase (Fig. 5 a, c). Further, addition of both H_3BO_3 and β-B to a-BNCO during plasma spraying resulted in a significant yield of nanocrystalline c-BN (Fig. 6 and 7). We speculate that the catalysts both increase the boron content and promote softening and melting of the a-BNCO particles in a manner similar to that reported in the belt chamber experiments of Lorenz et al. [39]. Lorenz et al. attributed the rapid nucleation of c-BN in h-BN (with a Mg_3N_2 catalyst at ~ 6GPa and temperatures above 1650^{o}C) to the melting the h-BN and the formation of c-BN upon solidification [39]. Their results indicate that the application of appropriate high temperatures and pressures in the presence of a catalyst can lead to extremely fast formation of very small c-BN grains in a molten state. In this light, our results suggest that adding H_3BO_3 and β-B to a-BNCO enhanced melting and nucleation of c-BN phase during the high temperature plasma spray process.

The chemical reactions of a-BNCO particles with catalysts during the plasma spray process can be estimated from the BN phases and compositions measured in postmortem XRD and TEM observations. As we have confirmed from the TEM characterization, the addition of H_3BO_3 and β-B to a-BNCO powders leads to the formation of stoichiometric t-BN and c-BN nanograins without the presence of carbon and oxygen, as shown in Fig. 7 and Fig. 8. The microstructural analysis suggests that the BNCO material is melted during plasma spraying and that the local chemical composition changes to BN phases before

deposition on a cooled substrate (Fig. 2). The average atomic percentages measured by EELS of the precursor, a-BNCO, was 15% boron, 40% carbon, 40% nitrogen, and 5% oxygen. These atomic percentages can be taken as the effective stoichiometry of the a-BNCO particles, thus the starting precursor was effectively $B_3C_8N_8O_1$. The chemical reactions that occur during vapor phase reduction can be estimated using the starting compositions of the precursor and catalysts, the relative amount of each, and the gases that are present and the resultant equation is similar to what Yoon et al. [40] and Choi et al. [41] previously suggested.

$$\begin{aligned} 3(B_3C_8N_8O_1)_s + \ 4\,H_3BO_{3_{(s)}} + 24\,B_{(s)} + N_{2(g)} + H_{2(g)} + 8O_{2(g)} \\ \rightarrow 18\,BN_{(s)} + \ B_3C_8N_8O_{1(s)} + B_2O_{3(s)} + 2\,H_3BO_{3(s)} \\ + 12\,B_{(s)} + \ 4\,H_2O_{(g)} + 3CO_{2(g)} + 13CO_{(g)} \end{aligned} \qquad (1)$$

XRD and TEM observations of the plasma sprayed products point to the presence of t-BN and c-BN in addition to unreacted $B_3C_8N_8O_1$, H_3BO_3 and B initial precursor and catalysts. Choi *et al.* reported that a-BN with B_2O_3 liquid easily crystallizes and transforms to c-BN around 4 GPa [41]. Based on our experimental observations, we argue that the BNCO precursors melted during the plasma spray process and decomposed producing various gases and resulting in a structural transformation into stoichiometric BN.

Local impact pressures associated with deposition may have played a role in the formation of both t-BN and c-BN. The impact pressure on BNCO materials was estimated by assuming the shock wave is generated when the melt particles impact on the cooled substrate [44-46]. In the present case, the instantaneous Hugoniot pressure P_H upon impact

on the substrate is calculated from the Rankine Hugoniot equation [47]. For a simple shock wave in a material at rest;

$$P_H = \rho_o U_s U_p \quad (2)$$

where ρ_o the density; particle velocity (U_p); U_s is the shock velocity.

The shock velocity [48] can be written

$$U_s = \mathrm{a} + \mathrm{bU_p} \quad (3)$$

a = Sound velocity; b is Gaussian parameters can be expressed as

$$b = 0.5 + \left(\frac{3\alpha k}{2}\right)\rho_o C_v \quad (4)$$

where α is thermal expansion coefficient, k is the bulk modulus; C_v is specific heat at constant volume.

The estimated pressure range is between 1.4 to 3.1 GPa which is significantly lower than the pressures that have reported for the formation of c-BN [1,4,12-23,37]. When velocity of the impacting particle is 515 m/s, density is ~2 g/cc and velocity of the sound in isotropic materials is between 1400 to 3000 m/s [26, 49]. The local impact pressure may have assisted in the formation of c-BN but it is too low to be the critical cause of this transformation. Moreover, dissipation of the total energy as heat, work hardening, or phase transformations would further lower the impact pressure and its influence on the formation of c-BN. Taken as a whole, our result suggest that the formation of c-BN occurs because of an interplay between multiple factors, including but not limited to the use of an amorphous precursor, the role of the two catalysts as well as the temperature and impact pressure associated with the plasma spray process.

5. Summary and Conclusions

In this work we have systemically studied BN phase evolution associated with plasma spraying and found that incorporating metastable catalysts with an amorphous BNCO precursor significantly lowered the threshold pressure for the formation of nano-crystalline c-BN. The experimental evidence in support of this finding was qualitatively and quantitatively demonstrated with x-ray diffraction and TEM characterization. The main results are summarized as follows

(a) TEM observations and EELS quantative analysis of the initial precursor showed primarily an amorphous BNCO that possessed significantly less boron (~20 atomic %) as compared to carbon and nitrogen. The addition of H_3BO_3 and B catalysts to the metastable a-BNCO precursor enhanced the boron content and also showed an effect on the formation of c-BN during plasma spraying.

(b) Plasma spraying a metastable a-BNCO precursor with a H_3BO_3 catalyst resulted in crystalline BN phases, mainly t-BN with small trace amounts of c-BN phases. The TEM-EELS quantitive composition analysis revealed the stoichiometric BN in a localized BNCO material.

(c) TEM observations of a plasma sprayed metastable a-BNCO precursor with H_3BO_3 and β-B catalysts revealed significant nanocrystalline c-BN formation with an average grain size of 6± 3 nm. High resolution TEM images show the lattice spacing of about ~0.21 nm which compares well with simulated spacing's of the c-BN phase. The EELS spectra of the fine grain size in BNCO material predominately displays only the σ bonding for both B-K and N-K edge, which also confirms that these grains are c-BN.

(d) Analysis of BNCO particles in the plasma sprayed materials point to the decomposition of hydrates and carbides in the presence of a N_2 atmosphere, which suggests melting and vaporization that would assist in the formation of the t-BN phase and the nucleation of small crystallites of c-BN.

(e) Addition of β-B with the a-BNCO and H_3BO_3 was found to enhance the kinetics of c-BN formation as compared to other polymorphic BN phases.

Acknowledgments

This research was supported by the Defense Advanced Research Projects Agency (DARPA; Extended Solids) and was accomplished under grant W31P4Q-13-1-001.

References

[1] R. Haubner, M. Wilhelm, R. Weissenbacher, B. Lux, Boron nitrides-properties, synthesis and applications, structure and bonding, Springer-Verlag Berlin Heidelberg 102 (2002), 1-45.

[2] R. H. Wentorf Jr, Synthesis of the cubic form of boron nitride, J. Chem. Phys. 34 (1961) 809-812.

[3] R. T. Paine, C. K. Narula. Synthetic routes of boron nitride, Chem. Rev. 90 (1990) 73-91.

[4] F. P. Bundy, R. H. Wentrof, JR. Direct Transformation of Hexagonal Boron Nitride to Denser Forms, J. Chem. Phys. 38 (1963) 1144-1149.

[5] L. Xu, J. Zhan, J. Hu, Y. Bando, X. Yuan, T. Sekiguchi, M. Mitome, D. Golberg, High yield synthesis of rhombohedral boron nitride triangular nanoplates, Adv. Mater. 19 (2007) 2141-2144.

[6] J. Y. Huang, H. Yasuda, H. Mori. HRTEM and EELS studies on the amorphization of hexagonal boron nitride induced by ball milling, J. Am. Ceram. Soc. 83 (2000) 403-409.

[7] R. H. Wentorf, R. C. DeVries, F. P. Bundy, Sintered superhard materials, Science 208 (1980) 873–880.

[8] G. Liu, Z. Kou, X. Yan, L. Lei, F. Peng, Q. Wang, K. Wang, L. Li, Y. Li, Y. Wang, Y. Bi, Y. Leng, D. He, Submicron cubic boron nitride as hard as diamond, Appl. Phys. Lett. 106 (2015) 121901.

[9] S. Veprek, The search for novel superhard materials, J. Vaccum Sci. Tech. 17 (1999) 2401-2420.

[10] J. Angserd, F. Liu, H. O. Andéren, Nanostructure of a cubic BN cutting tool material, Int. J. Refract. Metals Hard Mater. 49 (2015) 283-287.

[11] O. Fukunaga. Science and technology in the recent development of boron nitride materials, J. Phys.: Condens. Matter 14 (2002) 10979-10982.

[12] S. Nakano, O. Fukunaga, New scope of high pressure-high temperature synthesis of cubic boron nitride, Diam. Relat. Mater. 2 (1993) 1409-1413.

[13] M. Kagamida, H. Kanda, M. Akaishi, A. Nukui, T. Osawa, S. Yamaoka, Crystal growth of cubic boron nitride Li_3BN_2 solvent under high temperature and pressure, J. Cryst. Growth. 94 (1989) 261-269.

[14] O. Fukanaga, S. Takeuchi, Nucleation of cubic boron nitride in the non-metallic and metallic solvents, J Phys: Conf. Ser. 215 (2010) 012138.

[15] M. M. Bindal, S. K. Singhal, B. P. Singh, R. K. Nayar, R. Chopra, A. Dhar, Synthesis of cubic boron nitride using magnesium as the catalyst. J. Cryst. Growth 112 (1991) 386-401.

[16] L. Vel, G. Demazeau, J. Etourneau, Cubic boron nitride: Synthesis, physicochemical properties and applications, Mater. Sci. Engg B 10 (1991) 149-164.

[17] H. Saito and M. Ushio, Yogyo-Kyokaishi, 77 (1969) 151

[18] T. Kobayashi, K. Susa, S. Taniguchi, New catalysts for the high-pressure synthesis of cubic BN, Mater. Res. Bull, 10 (1975) 1231-1235.

[19] H Lorenz, I. Orgzall, Influence of the initial crystallinity on the high pressure-high temperature phase transition in boron nitride, Acta Mater. 52 (2004) 1909-1916.

[20] H. Sumiya, T. Iseki, A. Onodera, High pressure synthesis of cubic boron nitride from amorphous state, Mat. Res. Bull. 18 (1983) 1203-1207.

[21] S. K. Singhal, J. K. Park, Synthesis of cubic boron nitride from amorphous boron nitride containing oxide impurity using Mg-Al alloy catalyst solvent, J. Cryst. Growth 260 (2004) 217-222.

[22] B. P. Singh, G. Nover, G. Will, High pressure phase transformations of cubic boron nitride from amorphous boron nitride using magnesium boron nitride as the catalyst, J. Cryst. Growth 152 (1995) 143-149.

[23] B. P. Singh, V. L. Solozhenko, G. Will, On the low-pressure synthesis of cubic boron nitride, Diam. Relat Mater. 4 (1995) 1193-1195.

[24] J. Karthikeyan, C. C. Berndt, J. Tikkanen, S. Reddy, H. Herman, Plasma sprayed synthesis of nanomaterials powders and deposits, Mater. Sci. Engg A 238 (1997) 275-286.

[25] D. Goberman, Y. H. Sohn, L. Shaw, E. Jordan, M. Gell, Microstructure development of Al_2O_3-13 wt. % TiO_2 plasma sprayed derived from nanocrystalline powders, Acta Mater. 50 (2002) 1141-1152.

[26] P. Fauchais, Understanding plasma Spraying, J. Phys. D: Appl. Phys. 37 (2004) 86-108.

[27] A. Vardelle, C. Moreau, N. J. Themelis, C. Chazelas, A perspective on plasma spray technology, Plasma Chem. Plasma Process. 35 (2015) 491-509.

[28] S. Sampath and H. Herman, Rapid solidification and microstructure development during plasma spray deposition, J. Therm. Spray Techn. 5 (1996) 445-456.

[29] X. Zhou, V. Shukla, W. R. Cannon, B. H. Kear, Metastable phase formation in plasma sprayed ZrO_2 (Y_2O_3)-Al_2O_3, J. Am. Ceram. Soc. 86 (2003) 1415-1420.

[30] P. V. Ananthapadmanabhan, T. K. Thiyagarajan, K. P. Sree Kumar, N. Venkatramani. Formation of nano-sized alumina by in flight oxidation of aluminum powder in a thermal plasma reactor, Scripta Mater. 50 (2004) 143-147.

[31] V. K. Pujari, W. T. Collins, J. J. Kutsch, High solids hBN slurry, hBN paste, spherical hBN powder, and methods of making and using them, US 6645612 B2 (2003).

[32] V. L. Solozhenko, V. V. Chernyshev, G. V. Fetisov, V. B. Rybakov, I. A. Petrusha, Structure analysis of the cubic boron nitride crystals, J. Phys. Chem. Solids 51 (1990) 1011-1012.

[33] C. C. Ahn, O. L. Krivanek, EELS atlas: a reference collection of electron energy loss spectra covering all stable elements. Warrendale, Pa: Gatan, Inc., (1983)

[34] Y. Meng, H. K .Mao, P. J. Eng, T. P. Trainor, M. Newville, M. Y. Hu, C. Kao, J. Shu, D. Hausermann, R. J. Hemley, The formation of SP^3 bonding in compressed BN. Nature Mater. 3 (2004) 111-114.

[35] Z. W. Sieh, K. Cherrey, N. G. Chopra, X. Blase, Y. Miyamoto, A. Rubio, M. L. Cohen, S. G. Louie, A. Zettl, R. Gronsky, Synthesis of BxCyNz nanotubules, Phys. Rev B 51 (1995) 11229.

[36] Y. Li, R. S. Ruoff, R. P. H. Chang Boron acid nanotubes, nanotips, nanorods, microtubes and microtips, Chem. Mater. 15 (2003) 3276-3285.

[37] T. E. Mosuang, T. E. Lowther, Influence of defects on the hBN to cBN transformation, Phys Rev. B 66 (2002) 014112

[38] H. Lorenz, I. Orgzall, Insitu observation of the crystallization of amorphous nitride at high pressures and temperatures, Scripta Mater. 52 (2005) 537-540.

[39] H. Lorenz, B. Lorenz, U. kühne, C. Hohlfeld, The kinetics of cubic boron nitride formation in the system BN-Mg_3N_2, J. Mater. Sci. 23, 3254-3257 (1988).

[40] S. J. Yoon, A. Jha, Vapour phase reduction and the synthesis of boron-based ceramic phases, J. Mater. Sci. 30 (1995) 607-614.

[41] J. Y. Choi, S. J. Kang, O. Fukunaga, J. K. Park, K. Y. Eun, Effect of B_2O_3 and hBN crystallinity on cBN synthesis, J. Am. Ceram. Soc. 76 (1993) 2525-2528.

[42] A. V. Kurdyumov, V. F. Britun, I. A. Petrusha. Structural mechanisms of rhombohedral BN transformations into diamond like phases, Diam. Relat. Mater. 5 (1996) 1229-1235.

[43] V. F. Britun, A. V. Kurdyumov, Mechanisms of martensitic transformations in boron nitride and conditions of their development, High Press. Res. 17 (2000) 101–111.

[44] R. Goswami, S. Sampath, H. Herman. Shock synthesis of nanocrystalline Si by thermal sparying, J. Mater. Res. 14 (1999) 3489-3492.

[45] R. Goswami, H. Herman, S. Sampath, J. B. Parise. Diamond synthesis by high velocity thermal spray. The laboratory analogue of a meteorite impact, J. Mater. Res. 15 (2000) 25-28.

[46] R. Goswami, H. Herman, S. Sampath, J. Parise, Y. Zhu, D. Welch, Shock induced transformation in hexagonal boron nitride by high velocity thermal spray, J. Am. Ceram. Soc. 85 (2002) 2437-2443.

[47] W. J. Nellis, Shock compression in ultrapressure research, Scripta Metall. 22 (1988) 121-125.

[48] J. A. Zukas, T. Nicholas, H. F. Swift, L. B. Greszczuk, D. R. Curran, Impact Dynamics Johns Wiley and Sons, NY, 1982.

[49] G. V. Samsonov, Handbook of the physicochemical properties of the elements. Springer Science & Business Media, 2012.

Tables

Table 1. Plasma spraying parameters for a-BNCO+H_3BO_3 and a-BCNO+H_3BO_3+B mixtures

Parameters	**a-BNCO+H_3BO_3**	**a-BNCO+H_3BO_3+B**
Plasma gas chemistry	100% N_2	90% N_2-10% H_2
Nozzle size of gun (inch)	½	½
Current (A)	100	100
Power (kW)	59	66
Stand-off-distance (mm)	75	75
Total gas flow rate (slpm)	200	200
Carrier gas/flow rate (slpm)	Ar/15	Ar/15

Table 2. Temperature (T) and velocity (V) measurement during plasma spray powders of a-BNCO+H_3BO_3 and a-BNCO+H_3BO_3+B.

Run	TGF (slpm)	N_2 (%)	H_2 (%)	Ar (%)	Power (kW)	T_{50}	V_{50}	T_{75}	V_{75}	T_{100}	V_{100}
Distance (mm)	200					50	50	75	75	100	100
1-1	200	10	0	90	27	3400	300	2850	278	ND	ND
1-2	200	10	10	80	40	3870	400	3340	340	ND	ND
1-3	200	100	0	0	59	4125	442	4241	438	4870	401
1-4	200	90	10	0	66	3861	552	4230	515	4470	400

Figures

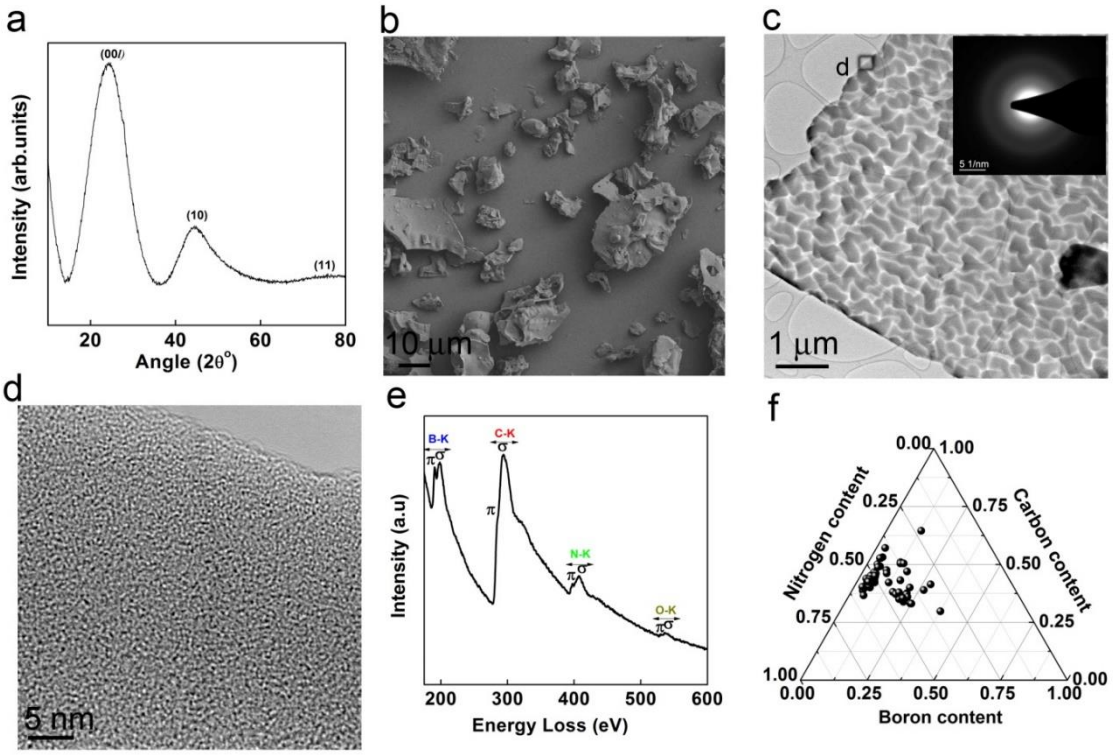

Figure 1. Phase analysis and structural characterization of the heat-treated Melamine and boric acid precursor powders. (a) X-ray diffraction (XRD) shows significant peaks broadening suggestive of an amorphous phase. (b) A typical SEM image of precursor powders displaying a non-uniform surface morphology. (c) TEM bright-field (BF) and SAED pattern of the as-deposited material with a halo ring pattern consistent with the presence of an amorphous phase. (d) High-resolution TEM image confirming a completely amorphous structure. (e) EELS spectra of the as-deposited material identifying the presence of π and σ bonds associated with the K edges for boron (B), carbon (C), nitrogen (N) and oxygen (O). (f) EELS-based measurements of atomic composition of the BNCO deposition, taken at a number of different regions and showing large compositional variations.

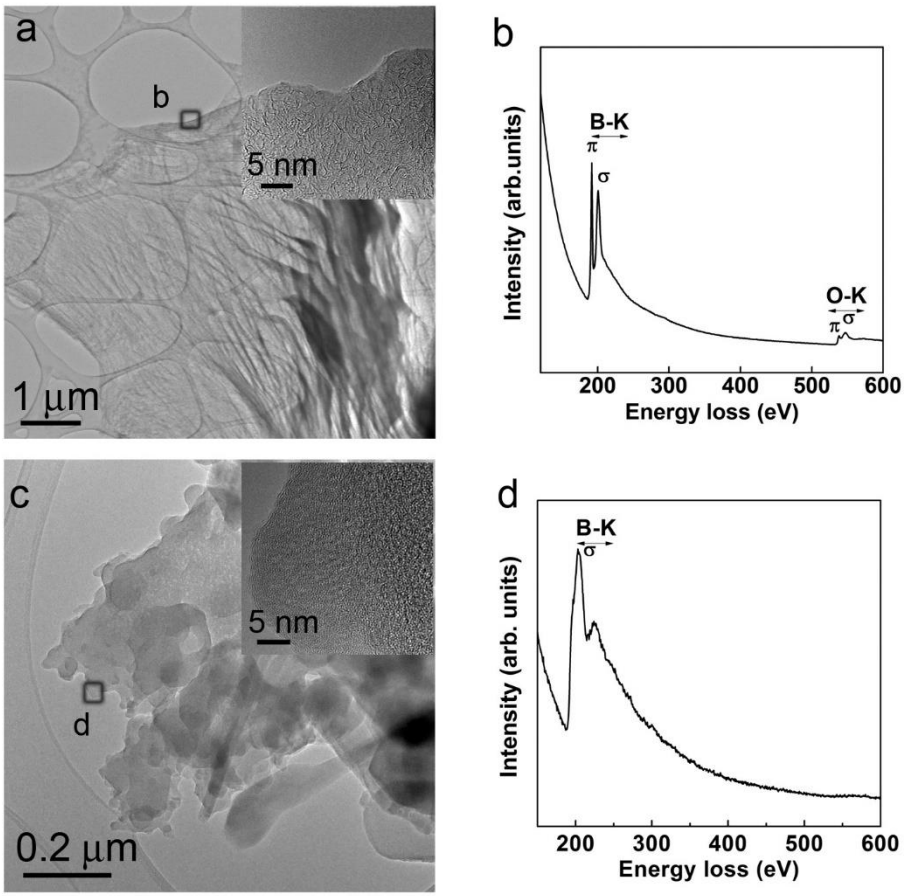

Figure 2. Microstrucure of H_3BO_3 and β-B catalyst. (a) TEM image of H_3BO_3 shows the fibrous network structure (Inset zoom in image). (b) EELS spectra taken from the same region shows π and σ bonding in both B-K and O-K elements. (b) TEM image of β-B shows the amorphous structure. (d) EELS spectra shows only B-K elements with σ chemical bonding.

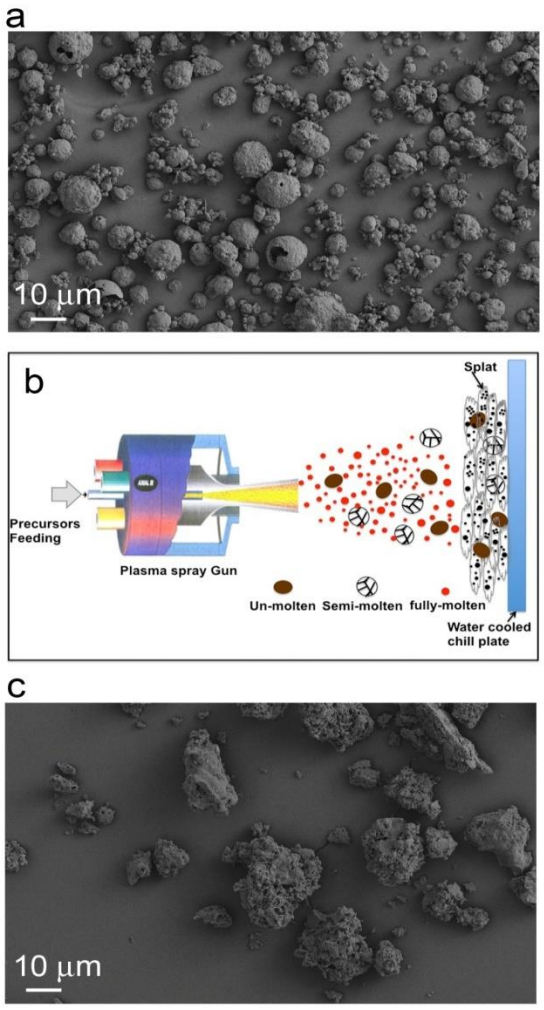

Figure 3. (a) A representative SEM image of pre-processed plasma spray BNCO material showing the spherical morphology with a particle size range from few hundred nm to 40 µm (b) A schematic description of the plasma spray process employed to and achieved final powders product. The heat-treated precursor powders are injected into a high temperature plasma flame, where they are rapidly accelerated to a high velocity and locally melted, the molten particles are deposited on the substrate and rapidly cooled to form splats. (c) The collected post-processed plasma sprayed BNCO material is in irregular morphology.

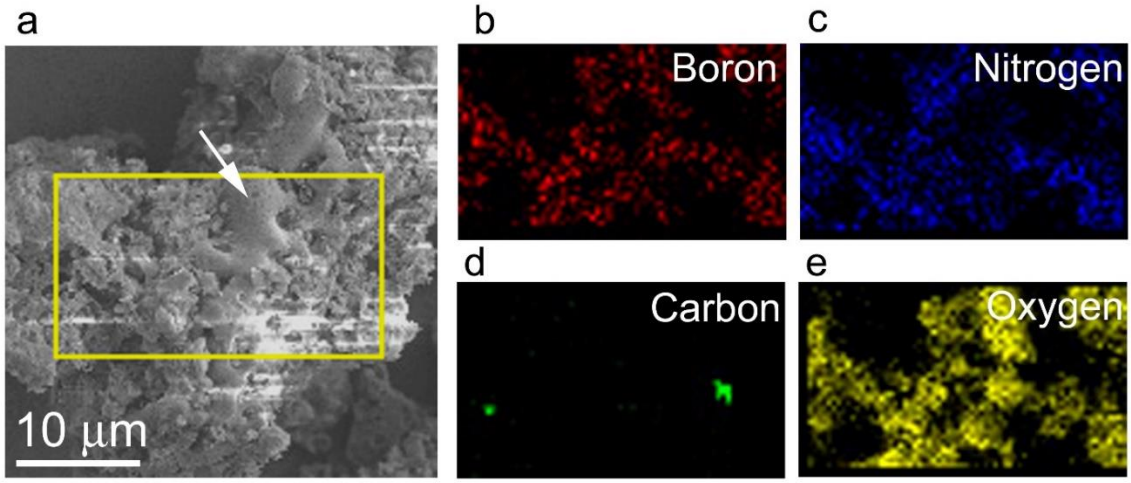

Figure 4. (a) Typical zoom-in SEM image of post-processed plasma sprayed BNCO material shows the signature of melt zone (white arrow). EDS maps (b-e) reveals melt zone are rich in B-N and B-O indicating the possible formation of boron nitride and boron oxide phases.

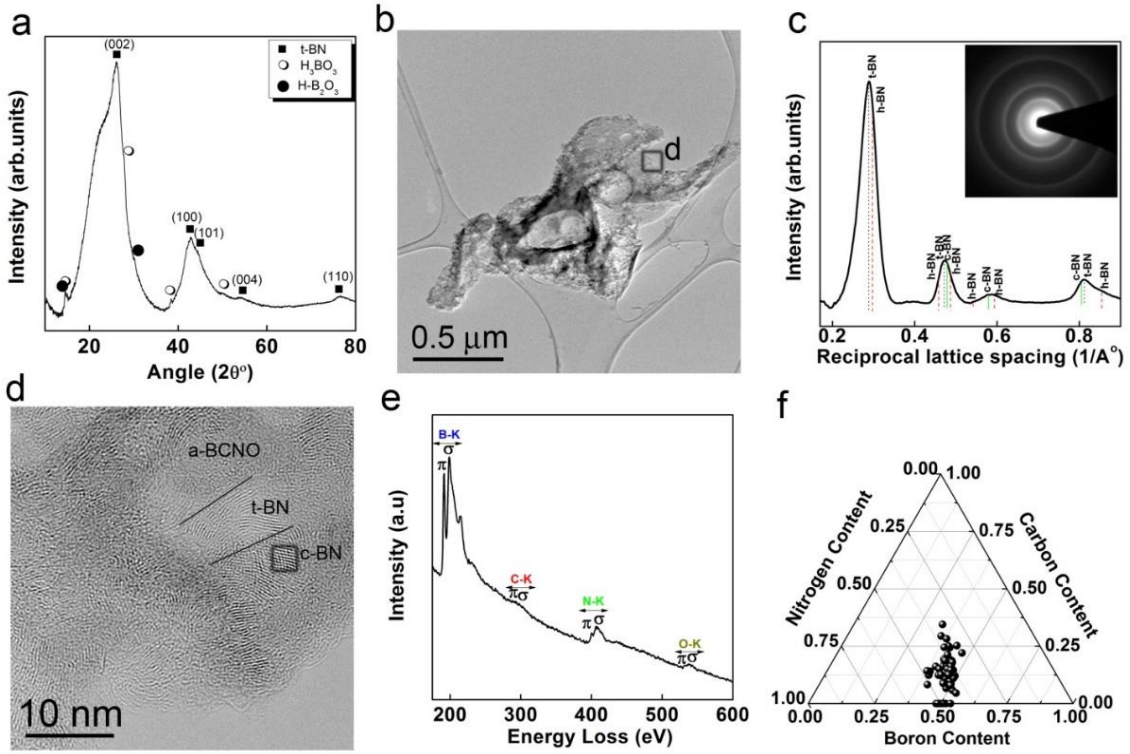

Figure 5. Plasma sprayed a-BNCO with the H_3BO_3 additive (a) XRD patterns evidence the presence of turbostratic BN (t-BN) and a small amount of unreacted H_3BO_3. (b) A low-magnification TEM image showing thin irregular BNCO powder particles. (c) A SAED diffraction pattern taken from this region indicating the existence of crystalline phases, the extracted profile intensity of the SAED reveals the presence of t-BN with a small fraction of cubic BN (c-BN), but no h-BN phase. (d) High-resolution TEM image confirming the presence of t-BN and c-BN grains embedded in BNCO particles. (e) An EELS spectra taken from the region in (d) and evidencing π and σ bonds associated with the B-K edge and N-K edge. The π and σ bonds associated with the C-K edge and O-K edge is significantly reduced as compared pre-processed a-BNCO particles (f) Quantitative assessment of the edges revealed equal compositions of B and N and a reduction in carbon content to less than 20 atomic % wt.

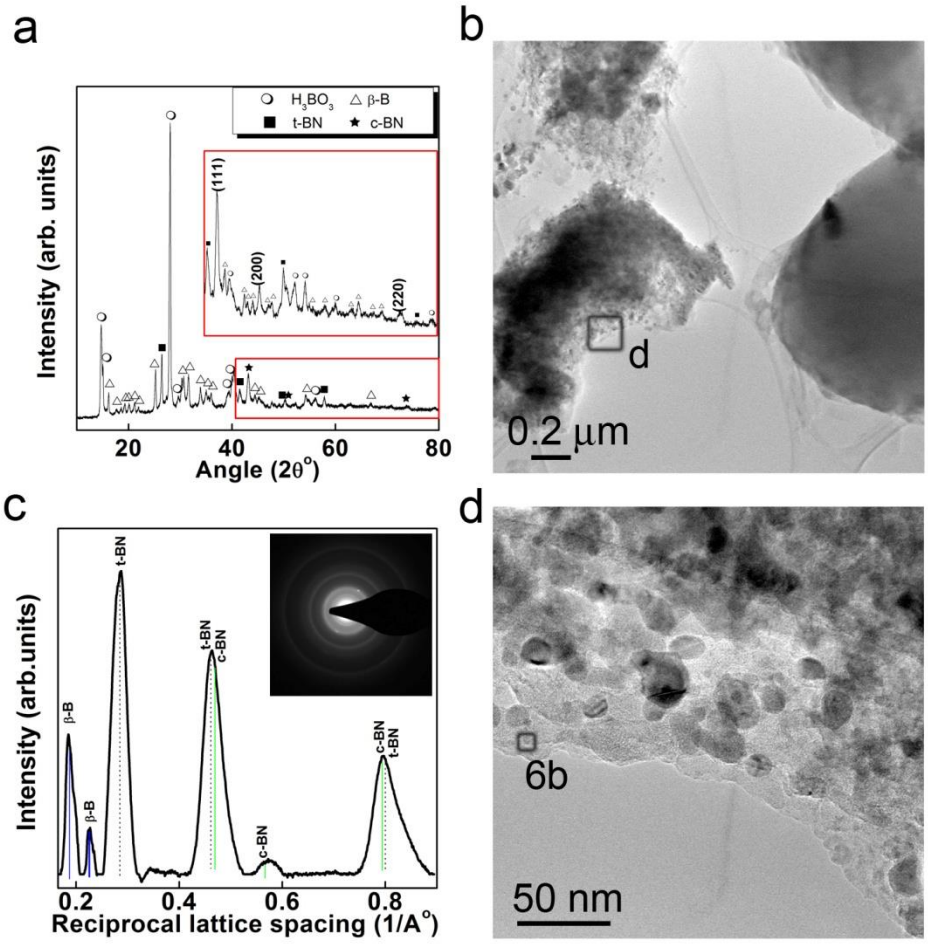

Figure 6. Plasma sprayed a-BNCO with H_3BO_3 and B additives. (a) XRD analysis showing the presence of t-BN and c-BN in addition to unreacted H_3BO_3 and B catalysts. (b) A low-magnification TEM images showing the presence of high-density fine crystallites within the BNCO deposited material. (c) A SAED pattern taken from the as-deposited materials and showing relatively sharp diffraction rings of uniform intensity, suggesting the presence of grains with random orientation. (a) Zoom-in TEM image reveals that the as-deposited BNCO material is composed of many nano-crystals.

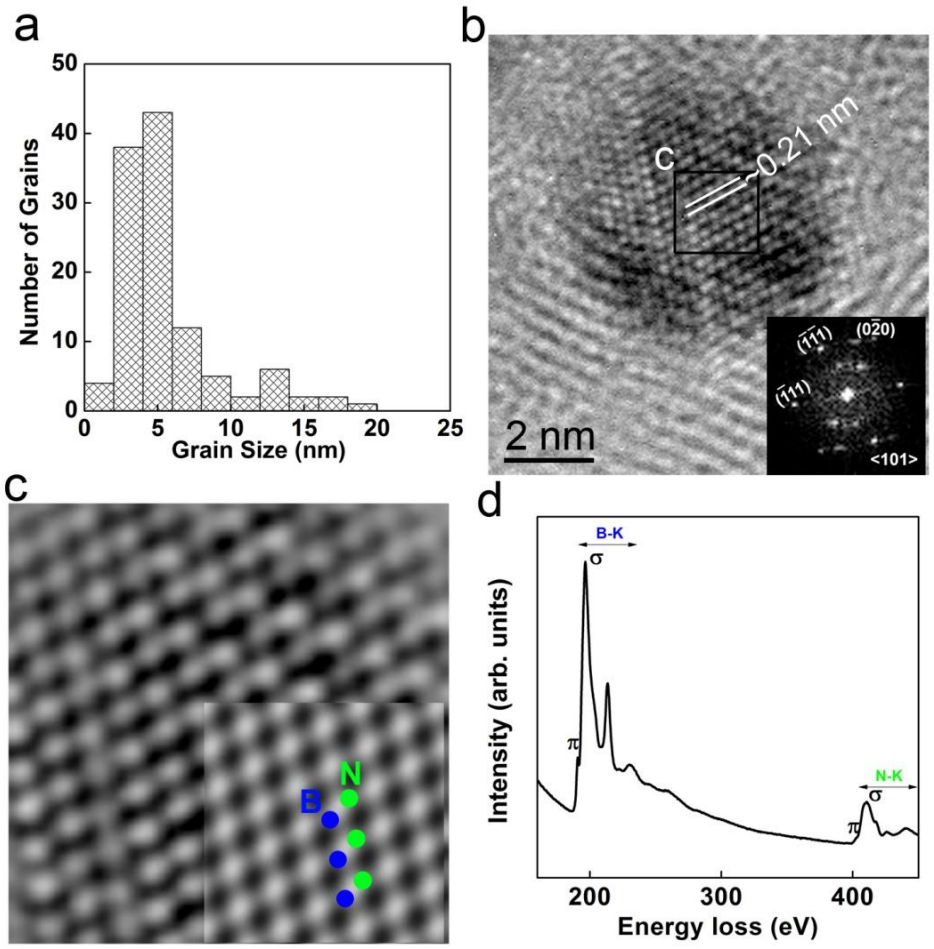

Figure 7. Experimental and simulated images of c-BN. (a) Grain size estimated from the plasma sprayed BNCO particles shows in the range of ~2 to 20 nm (Figure 5b and d). (b) A typical high-resolution TEM image taken along <110> orientation (as indicated by the FFT in the insert) and showing a nanograin within a-BNCO particles a lattice spacing of 0.21 nm, which is indicative of cubic BN. (c) A higher magnification experimental image is compared with an image simulation (insert) that was produced using the crystal structure for c-BN, a thickness of 4 nm, and a defocus of +10 nm showing consistent with lattice space. The atomic position of boron and nitrogen are shown in the inset image (d) The EELS spectra of this nanoparticle reveals only σ-bonding for the B-K edge and the N-K edge and confirms the presence of the c-BN phase.

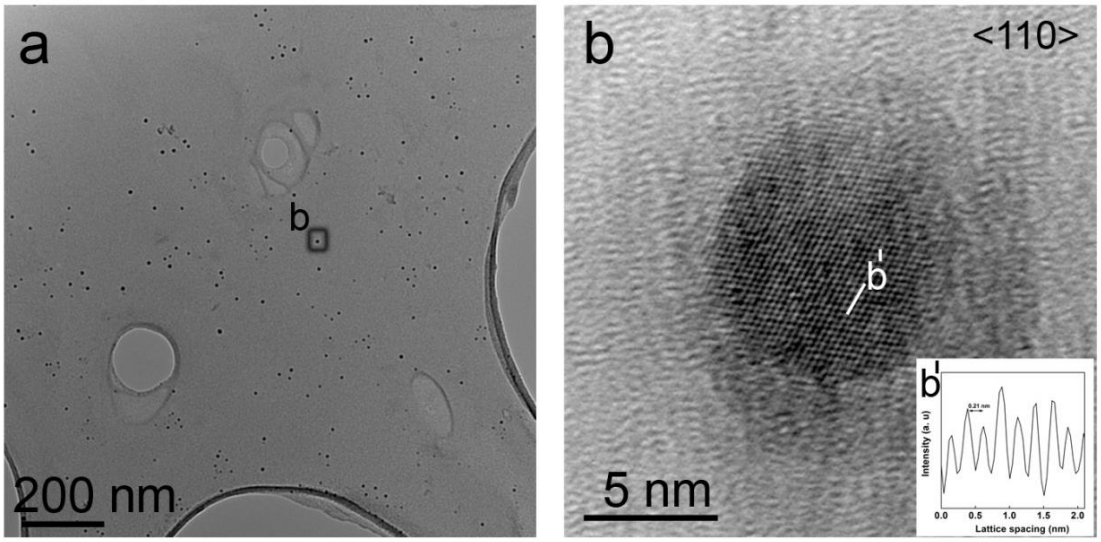

Figure 8. c-BN fine nanostructured microstructure. (a) TEM image shows the well separate c-BN fine grains from the plasma spray BNCO materials. (b) Zoom in Fourier filtered TEM image of fine grain size reveals the c-BN oriented along <110> zone axis. (b^1) inset displays the line intensity profile estimated lattice spacing of 0.21 nm.

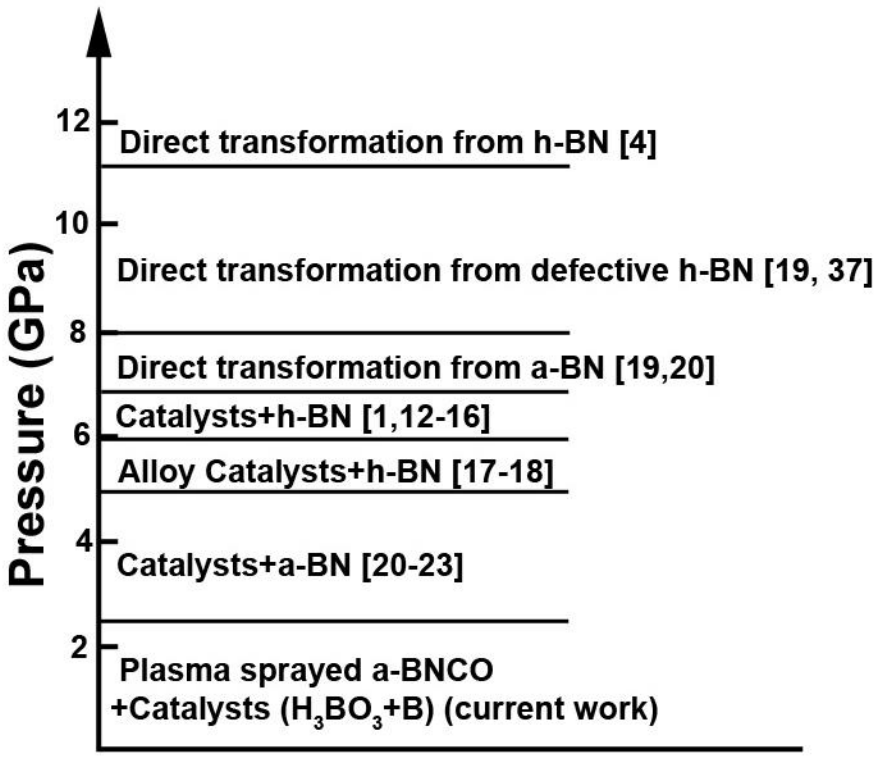

Figure 9. Graphical representation of published threshold pressure approaches for the formation cubic BN from the different precursors with their catalysts [1,4, 12-23, 37]. The present work shows relatively low pressure synthesis of c-BN with appropriate catalyst in a plasma sprayed process.

Chapter 6.

Observations of explosion phase boron nitride formed by emulsion detonation synthesis

Metin Örnek[1], K. Madhav Reddy[2+], Chawon Hwang[1], Vladislav Domnich[1], Alan Burgess[3], Silvio Pratas[4], Joao Calado[4], Kelvin Y. Xie[2], Steven L. Miller[5], Kevin J. Hemker[2], Richard A. Haber[1*]

[1] *Department of Materials Science and Engineering, Rutgers, The State University of New Jersey, Piscataway, NJ 08854, USA*

[2] *Department of Mechanical Engineering, Johns Hopkins University, Baltimore, MD 21218, USA*

[3] *SprayWerks Technologies Inc., North Vancouver, British Columbia V7G 1L5, Canada*

[4] *Innovnano, Materiais Avançados SA, Antanhol 3040-570, Portugal*

[5] *H&M Analytical Services Inc., Allentown, NJ 08501, USA*

*Corresponding author e-mail: rich.haber@rutgers.edu, and address: 607 Taylor Road, Piscataway, NJ 08854, USA (Tel: +1(848)445-5924)

[+]Author present address: *State Key Laboratory of Metal Matrix Composites, Shanghai Jiao Tong University, Shanghai 200240, China*

Abstract

Emulsion detonation synthesis (EDS) is a recently developed process to synthesize nano-sized ceramics based on detonation of two water-in-oil emulsions. The process produces high pressure and temperature along with fast cooling, thus providing ideal environment for metastable phase formation. Here we applied the process for the first time on hexagonal boron nitride (h-BN). Characterization studies demonstrated the formation of metastable explosion BN phase (e-BN) with grain sizes of 10-20 nanometers embedded in h-BN matrix. These findings support the potential use of EDS a novel and promising pathway for the synthesis of e-BN and other metastable BN phases.

Keywords: Explosion Phase Boron Nitride, Emulsion Detonation Synthesis, Metastable Ceramic, High Pressure-High Temperature Synthesis.

1. Introduction

Emulsion detonation synthesis (EDS) is a recently developed process for the synthesis of nanometer-sized ceramic materials based on the detonation of two water-in-oil emulsions [1, 2]. The process can produce high pressures up to 10 GPa and high temperatures up to 2000°C along with a cooling rate as fast as 10^9 K/s. Thus, it can provide an ideal environment for nanometer- sized material to form. For example, the process has successfully synthesized nanostructured cubic zirconia (ZrO_2), alumina (Al_2O_3), titanium dioxide (TiO_2), spinel ($MgAl_2O_4$), aluminum nitride (AlN), magnetite (Fe_3O_4) and aluminum doped zinc oxide (AZO) ceramics [1-3]. In addition to the synthesis of nanometer-sized materials, we hypothesized the process could also provide an ideal environment for high pressure phases or metastable phases to form considering the high pressure, high temperature, and fast cooling rate produced by the process. Here we applied the process, for the first time, on boron nitride system.

Boron nitride (BN) has many polymorphs such as cubic, wurtzite, hexagonal, rhombohedral, turbostratic, tetragonal, explosion and amorphous phases [4-7]. Among these, cubic BN (c-BN), wurzite BN (w-BN) and explosion BN (e-BN) can be synthesized through high pressure-high temperature (HPHT) process. e-BN is one of the intermediate phases of BN with a metastable nature, which forms during the transformation process from the low-density phases, such as turbostratic (t-BN) and hexagonal (h-BN), to high density phases, such as w-BN and c-BN [8]. It exhibits attractive properties such as high-energy band gap and potentially high bulk modulus. Further, the hardness of e-BN has been reported to be an order of magnitude higher than that of h-BN [9].

2. Experimental Procedures

In this work, we report the observation of the formation of nanoscale metastable e-BN phase formed by applying the EDS process on h-BN. We prepared an emulsion of two related phases: internal (aqueous) and external (insoluble). The internal phase contains h-BN (Grade BN150, Kennametal, UK) with a particle size of $D_{(90)}$ = 14 μm mixed in mineral oil. Adding h-BN as a component for internal phase improves the particle distribution along the emulsion structure [10]. The external phase contains fuels that are miscible within hydrocarbons and their derivatives such as paraffinic waxes. The external phase provides consistency to the emulsion during the detonation [10]. Internal/external phases were designed based on the formulations calculated using THOR program [3]. Both phases were emulsified by mixing in a stainless-steel container with a static mixer. The emulsion thus formed was poured into a cylindrical polymethyl methacrylate (PMMA) tube 70 mm in diameter and 210 mm in length: shockwaves require a tube length longer than 2-5 times its diameter to stabilize at a speed over 4000 m/s[10]. Both ends of the tube were closed with lids of the same material. Another emulsion called the initiator was inserted in the tube, which contained ammonium nitrate, water, and mineral oil with an emulsifying agent. The tube was placed into a reaction chamber and detonation was ignited by electrical detonator inserted into the initiator emulsion. After detonation, particles were collected from the sample collector attached to the reaction chamber.

Interaction of detonation with the particles starts at the detonation front called the Von Neumann (VN) spike, where the maximum pressure is provided by shockwave. VN spike is followed by the reaction zone, where the chemical decomposition reaction occurs and ends in the Chapman, Jouguet (C, J) point in the case of ideal detonation [11]. As the

detonation front runs through the solid loading (h-BN) along with the reaction zone formed, high rate momentum and heat are transferred to the particles. As byproducts of the reaction, various gases (such as CO, CO_2, H_2O, NH_3 and N_2) form and expand, providing rapid cooling to the reaction product(s) [12].

Detonation velocity was also calculated using the THOR program, which uses numerical methods. Spherical morphology was taken into account rather than flake or platelet to avoid further complexity. Pressure at (C, J) point was calculated according to the following equation.

$$P(C,J) \approx \rho\,(Us)^2/4\ , \qquad (1)$$

where ρ is the emulsion density (g/cm^3), and *Us* is the detonation velocity (m/s). Table 1 shows compositions, densities of emulsions, calculated detonation velocity and pressure values.

Initial h-BN powder and Emulsion Detonation Synthesized (EDS-ed) particles were analyzed using particle size analyzer, XRD, FTIR, and HRTEM coupled with energy-dispersive X-ray spectroscopy (EDX). Particle size distribution was analyzed using laser diffraction particle size analyzer (Malvern Mastersizer 3000, United Kingdom). Phase identification and crystalline structure were analyzed using X-ray diffractometer (PANalytical, Netherlands) X'Pert Diffractometer: 45kV and 40 mA with Cu Kα (λ=1.540598 Å) radiation at a scanning rate of 0.04°/min. Bonding characteristics were analyzed using FTIR spectrometer (Mattson Instruments Galaxy 5000 Series, Wisconsin). Morphology, crystal structure, and lattice spacing were analyzed using TEM microscope (Philips FEI CM-300, Netherlands) with incident electron beam energy of 300 keV. The elemental analysis was done using EDX detector (Oxford, United Kingdom).

3. Results

Fig. 1 (a) shows the XRD patterns of EDS-ed particles compared to the initial h-BN. EDS-ed particles showed additional peaks that match either e-BN or ZrO_2 apart from the peaks of h-BN: the presence of ZrO_2 is caused by contamination from the detonation chamber. The peaks around 35.6°, 56.6° and 63.3° (in 2θ) correspond to reflections of (311), (333) and (440) planes of e-BN, respectively [13, 14]. The peak around 30.4° corresponds to (220) plane of e-BN and/or (101) plane of ZrO_2 [13-15]. And the peak around 43.5° corresponds to reflections of (400) plane of e-BN and/or (101) plane of ZrO_2 [15].

Fig. 1 (b) shows comparison of characteristic (strongest) peak of h-BN at 26.7° before and after the EDS process, which corresponds to (002) plane and provides an indication of change in structural ordering [16]. EDS-ed h-BN showed slight peak shift from 26.734° to 26.746°, which corresponds to decrease in interlayer distance from 0.332 nm to 0.330 nm. It also showed peak broadening, increase in full width at half maxima from 0.253° to 0.338°, indicating that either crystallite size or 3-dimensional structural ordering of h-BN decreased after EDS process.

FTIR spectroscopy was employed in order to investigate possible changes in the atomic bonding characteristics of the powders before and after the EDS process. Fig. 2 shows FTIR spectra of initial h-BN and EDS-ed particles compared to the reference spectra of nanosized c-BN (H&M Analytical Inc., New Jersey) and e-BN (as originally reported by Batsanov *et al.*) [17]. The starting h-BN (Fig. 2a) consists of only sp^2 bonding and shows two characteristic absorption bands at 800 cm^{-1} and 1367 cm^{-1}, which are attributed to B-N-B bending and B-N stretching vibrations, respectively [18]. Nano-sized c-BN (Fig. 2c)

predominantly consists of sp^3 bonding and shows a broad absorption band centered around 1100 cm^{-1}, consistent with the typical c-BN absorption spectra reported in literature [19]. For e-BN, there exist significant discrepancies in literature with regard to absorption peak positions assigned to this phase. A number of narrow peaks in the range of 800-1200 cm^{-1}, as shown in Fig. 2d, have not been observed in the follow-up FTIR studies of e-BN by other groups [20, 21]. Instead, the characteristic broad band of h-BN 1367 cm^{-1} was deconvoluted into several peaks in these latter studies, with an attempt to assign the resulting peaks at ~1550 cm^{-1} and ~1250 cm^{-1} to the vibrational modes of e-BN [20, 21]. We note here that this treatment of the absorption spectra as reported in references [20, 21] is highly debatable, as alternative peak deconvolution procedures are also possible. In our observations (Fig. 2b), EDS-ed particles show absorption features very similar to h-BN, which is in fact consistent with our XRD analysis, showing that the EDS'ed material is predominantly h-BN. One additional spectral feature of the EDS'ed material was the rather narrow and weak peak at 1135 cm^{-1} (Fig. 2b). The position of this band correlates with the characteristic features of sp^3 bonded BN (cf. Fig. 2c). The observation of this peak in the EDS'ed material may suggest that some small amount of sp^3 bonded BN has formed during the process. Observation of the absorption features of sp^3 bonded BN may also be related to the e-BN phase, as the latter is known to contain both sp^2 and sp^3 bonding [21].

To corroborate the XRD and FTIR results and identify a direct evidence for the formation of e-BN phase we further employed TEM analysis coupled with EDX (Fig. 3 and 4). EDS-ed particles showed the typical thin and irregular sheets of h-BN containing nano-sized grains (Fig. 3a). The EDX spectrum (Fig. 3b), taken from the marked area in Fig. 3a, identified the presence of boron and nitrogen elements; peaks of Cu arise from the

supporting Cu-grid used. Selected area electron diffraction (SAED) pattern (Fig. 4a) taken from the fine particles of Fig.3a, identified the presence of crystalline phases. Intensity profile extracted from the SAED pattern (Fig. 4b) confirmed coexistence of e-BN phase along with h-BN phase [13, 14, 20]. Fig. 4 (c) and (d) show direct observations of e-BN phase in h-BN matrix, which has an approximate grain size of 10-20 nm. Fig. 4 (c) shows an e-BN grain projected along <111> orientation and lattice spacing values of 0.48 nm and 0.24 nm along the (222) and (111) planes, which are consistent with the values theoretically calculated and experimentally observed for e-BN [13]. The matrix showed the lattice spacing of 0.219 nm of h-BN. Fig. 4 (d) shows e-BN grain projected along <211> and lattice spacing values of 0.48 nm and 0.295 nm, which match the values of e-BN phase.

4. Discussion and Conclusions

As shown above we observed the formation of e-BN phase, but not the high-pressure/closely packed phases (c-BN or w-BN). The absence of high-pressure phases can be explained based on the fact that formation of high-pressure phase from h-BN requires pressures typically in excess of 7 GPa, which is higher than the pressure calculated for the process conditions in this study, that is 5 GPa (see Table 1) [22]. The synthesis conditions and the nature of e-BN phase have been reported in literature. Batsanov *et al.* first reported e-BN phase by conducting a shock compression experiment using t-BN (so-called not-fully developed or disordered h-BN) as a starting material; however, the mechanism behind the e-BN formation was not discussed [17]. Later Akashi *et al.* carried out a multiple-shock compression study using well-crystallized h-BN and showed that h-BN transforms to t-BN and w-BN by a first shock. Thereafter, the newly formed t-BN transforms into e-BN by a

second shock [23]. Nameki *et al.* further investigated e-BN formation from t- BN precursor under shock-compression and showed that e-BN forms only if the cooling rate is high enough, otherwise e-BN transforms to t-BN due to high residual temperature [13].

Taking into consideration the above and the principle of EDS process, we speculate e-BN phase forms as follows during the process. Due to pressure and temperature generated by detonation, h-BN particles experience structural disordering. Depending on the peak pressure and temperature that is reached, local areas of the particles further experiences a transformation to metastable e-BN phase. Then, depending on the cooling rate provided by the out gases, metastable e-BN phase stabilizes in case that fast cooling is provided.

The local and limited formation of e-BN phase are closely related to three parameters: (i) pressure fluctuations and hot spot formation, (ii) particle size, and (iii) cooling rate. As the shock wave propagates during the detonation, the pressure that particles experience fluctuates and creates hot spots [24]. The regions that experience both the structural disordering and hot spot may only transforms to metastable e-BN. Other regions would only show structural disordering. In addition, particle size larger than reaction zone results in limited or no reaction according to detonation theory [24]. The $D_{(90)}$ particle size of h-BN used in this study was around 14 μm; whereas the length of the reaction zones typically varies from a few microns to a few hundred microns in the case of liquid explosives [25-27]. Thus, the region of particles, which does not experience high pressure required for e-BN formation, naturally would maintain the hexagonal structure, leading to only local and limited formation of e-BN phase in h-BN matrix. Moreover, cooling rate is another crucial parameter that determines the degree of phase transformation

as it effects the retention of resultant phase(s) during the process. Higher cooling rate yields more formation of the metastable phase(s) [13, 28]. In our case, it is highly possible that part of the initially formed metastable e-BN phase transformed back to stable h-BN phase during cooling, where the particles do not experience a sufficiently high cooling rate. We suggest that by using finer h-BN particles along with an increased cooling rate the formation of e-BN phase and its retention would improve. Related works are underway and will be the subject of a separate paper.

In summary, we applied EDS process, for the first time, on h-BN to evaluate its feasibility for the synthesis of metastable e-BN phase. We observed local formation of metastable e-BN phase in h-BN. Possible mechanism and key parameters for the formation of e-BN during the process were discussed to provide insight on further improvement in the formation and retention of e-BN phase. These findings demonstrate that EDS process has potential to synthesize metastable e-BN phase.

Acknowledgments

This research was sponsored by and was accomplished under the Office of Naval Research Grant No: N00014-17-1-2532. Additional supports were received from the Defense Advanced Research Projects Grant No: W31P4Q-13-1-0001, and the National Science Foundation I/UCRC Award No.1540027. The views and conclusions contained in this document are those of the authors and should not be interpreted as representing the official policies, either expressed or implied, of the Defense Advanced Research Projects Agency, the National Science Foundation or the U.S. Government. The U.S. Government is authorized to reproduce and distribute reprints for Government purposes notwithstanding

any copyright notation herein. The authors would like to thank Kynckolas Sutherland and Austin James Cruz for their valuable assistance in the laboratory. Metin Örnek acknowledges support from the Ministry of Education, the Republic of Turkey.

References

[1] S.M.P. Da Silva, J.M.C. Da Silva, Continuous process for nanomaterial synthesis from simultaneous emulsification and detonation of an emulsion, US Patent 8,557,215 (2013).

[2] J.M.C. Da Silva, E.M.D.S. Antunes, Nanometric-sized ceramic materials, process for their synthesis and uses thereof, US Patent Application Publication, 2013/0251623 (2013).

[3] N. Neves, A. Lagoa, J. Calado, A.B. do Rego, E. Fortunato, R. Martins, I. Ferreira, Journal of the European Ceramic Society 34(10) (2014) 2325-2338.

[4] K.M. Reddy, C. Hwang, M. Ornek, S.L. Miller, W.E. Mayo, A. Burgess, R.A. Haber, K.J. Hemker, Acta Materialia 116 (2016) 155-165.

[5] S. Batsanov, L. Kopaneva, E. Lazareva, I. Kulikova, R. Barinsky, Propellants, explosives, pyrotechnics 18(6) (1993) 352-355.

[6] M.G. Balint, M.I. Petrescu, Diamond and Related Materials 18(9) (2009) 1157-1162.

[7] R. Haubner, M. Wilhelm, R. Weissenbacher, B. Lux, in: M. Jansen (Ed.), High Performance Non-Oxide Ceramics II, Springer Berlin Heidelberg (2002), pp. 1-45.

[8] S.S. Batsanov, Diamond and Related Materials 20(5-6) (2011) 660-664.

[9] V.V. Pokropivny, A.S. Smolyar, A.V. Pokropivny, Physics of the Solid State 49(3) (2007) 591-598.

[10] E.M.D.S. Antunes, J.M.C. Da Silva, A.L.C. Lagoa, Process for nanomaterial synthesis from the preparation and detonation of an emulsion, products and emulsions thereof, US Patent Application Publication, 2013/0224488 (2013).

[11] W. Fickett, W.C. Davis, Detonation: theory and experiment, Courier Corporation (2012).

[12] P.W. Cooper, Explosives engineering, Vch Pub (1996).

[13] H. Nameki, T. Sekine, T. Kobayashi, V. Fat'yanov, T. Sato, S. Tashiro, Journal of Materials Science Letters 15(17) (1996) 1492-1494.

[14] T. Akashi, H.-R. Pak, A.B. Sawaoka, J Mater Sci 21(11) (1986) 4060-4066.

[15] B. Bondars, G. Heidemane, J. Grabis, K. Laschke, H. Boysen, J. Schneider, F. Frey, J Mater Sci 30(6) (1995) 1621-1625.

[16] J. Thomas, N.E. Weston, T. O'connor, Journal of the American Chemical Society 84(24) (1962) 4619-4622.

[17] S. Batsanov, G. Blokhina, A. Deribas, Journal of Structural Chemistry 6(2) (1965) 209-213.

[18] R. Geick, C.H. Perry, G. Rupprecht, Physical Review 146(2) (1966) 543-547.

[19] O. Kutsay, C. Yan, Y.M. Chong, Q. Ye, I. Bello, W.J. Zhang, J.A. Zapien, Z.F. Zhou, Y.K. Li, V. Garashchenko, A.G. Gontar, N.V. Novikov, S.T. Lee, Diamond and Related Materials 19(7-9) (2010) 968-971.

[20] J. Wang, Y. Gu, Z. Li, W. Wang, Z. Fu, Crystal Growth & Design 13(2) (2013) 599-605.

[21] A. Olszyna, J. Konwerska-Hrabowska, M. Lisicki, Diamond and Related Materials 6(5-7) (1997) 617-620.

[22] V.F. Britun, A.V. Kurdyumov, High Pressure Research 17(2) (2000) 101-111.

[23] T. Akashi, A. Sawaoka, S. Saito, M. Araki, Japanese Journal of Applied Physics 15(5) (1976) 891.

[24] R.C. Ripley, F. Zhang, F.S. Lien, Proceedings of the Royal Society A: Mathematical, Physical and Engineering Sciences 468(2142) (2012) 1564-1590.

[25] R. Engelke, J.B. Bdzil, The Physics of Fluids 26(5) (1983) 1210-1221.

[26] S.A. Sheffield, R.P. Engelke, R.R. Alcon, R.L. Gustavsen, D.L. Robbins, D.B. Stahl, H.L. Stacy, M. Whitehead, Particle velocity measurements of the reaction zone in nitromethane, Los Alamos National Laboratory, 2002.

[27] B. Dobratz, P. Crawford, UCRL-52997, Lawrence Livermore National Laboratory, CA (1985).

[28] A. Aleksenskii, M. Baidakova, A.Y. Vul, V.Y. Davydov, Y.A. Pevtsova, Physics of the Solid State 39(6) (1997) 1007-1015.

Tables

Table 1. The composition and density of prepared emulsions and corresponding calculated values of detonation velocity and pressure obtained from EDS process.

h-BN % wt in emulsion	Oil % wt in emulsion	Emulsion Density (g/cm^{-3})	Calculated Detonation Velocity (m/s)	Calculated Pressure P(C,J)
10	15	1.1	4300	5 GPa

Figures

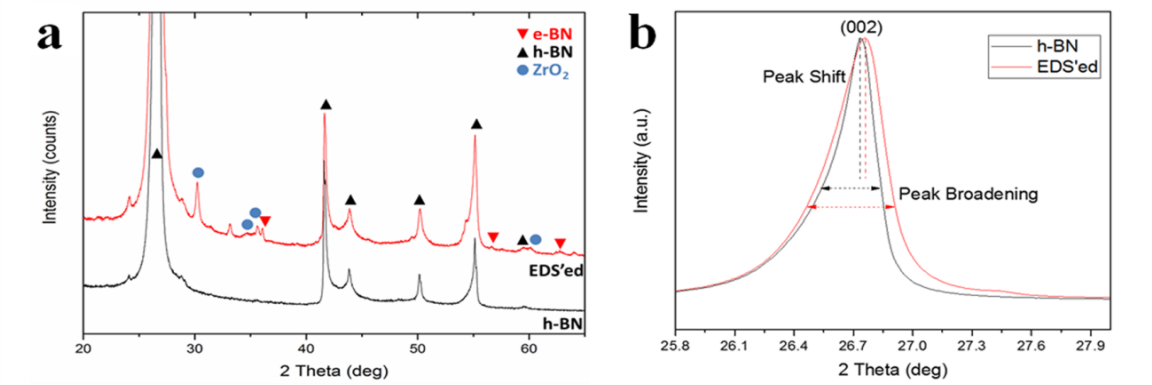

Figure 1. XRD analysis of powders before and after EDS. **(a)** (311), (333) and (440) peaks of e-BN phase revealed at 2θ≈ 35.6°, 56.6° and 63.3°, respectively. h-BN, e-BN and ZrO_2 peaks are indexed as ▲, ▼and ●, respectively. **(b)** Normalized XRD pattern shows broadening at 2θ≈ 26.6° of h-BN (002) compared to starting BN powders, which is indicative of decrease in either 3-dimensional structural ordering or crystallite size.

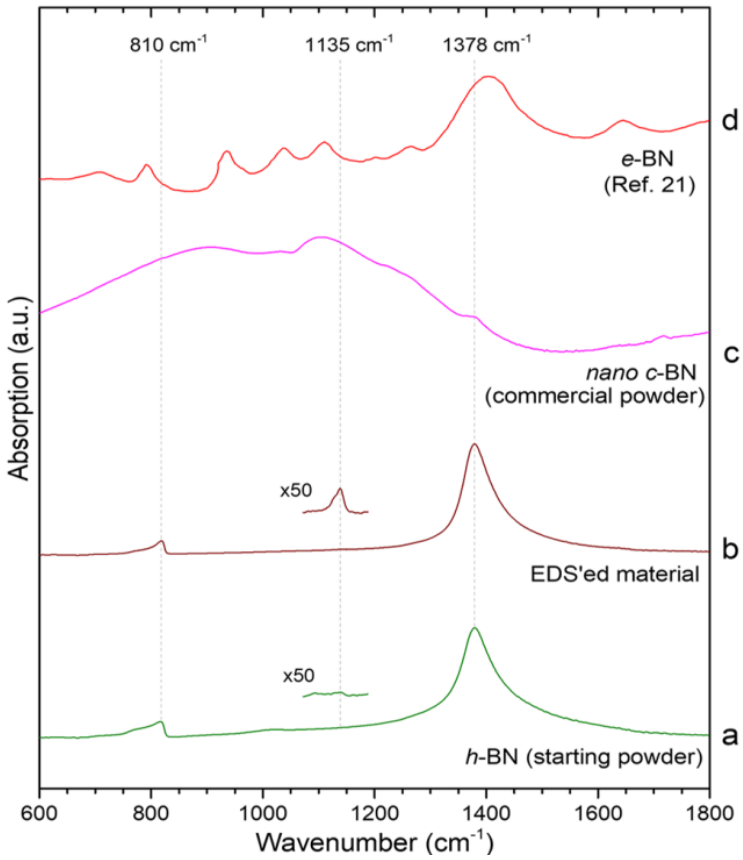

Figure 2. FTIR spectra of the powders **(a)** before and **(b)** after the EDS process. Starting h-BN powders exhibit two relatively narrow bands at 810 cm^{-1} and 1378 cm^{-1} that are attributed to h-BN vibrational modes. EDS'ed powders revealed additional narrow band at 1135 cm^{-1} as shown in the magnified inset spectrum, possibly indicating sp^3 bonding. FTIR spectra of **(c)** commercial nanosized c-BN and **(d)** e-BN (Ref. 21) are included for comparison. The spectrum of t-BN is identical to that of h-BN.

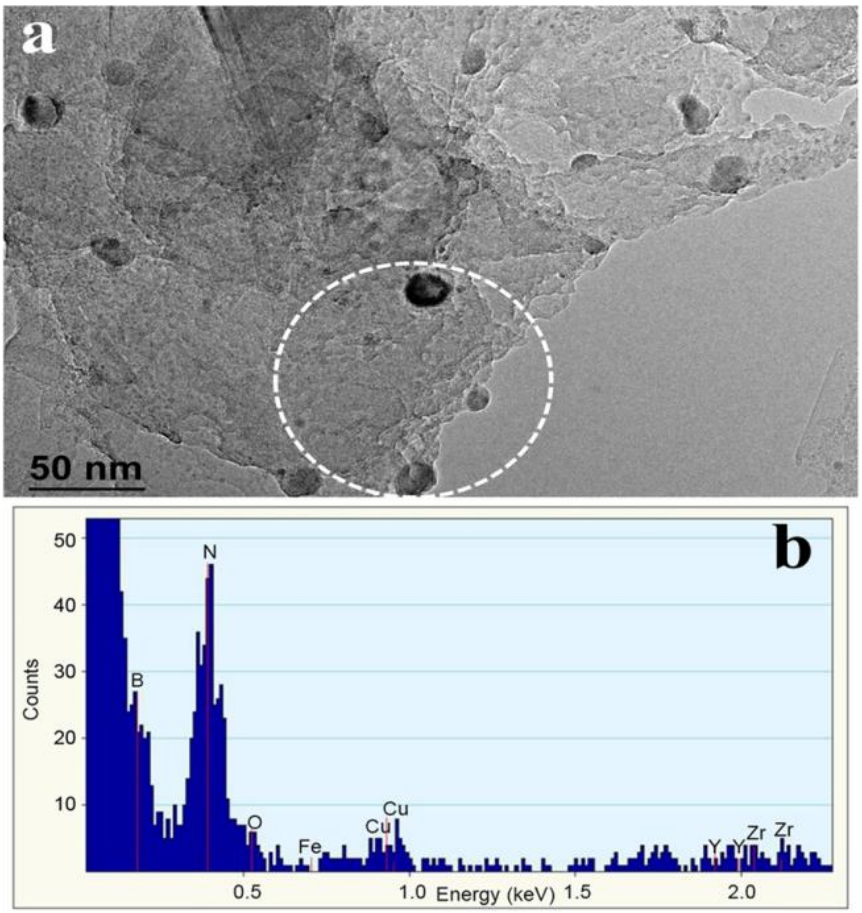

Figure 3. Microstructure and elemental analysis of EDS'ed powder: **(a)** Low magnification TEM image shows the sheet-like morphology. **(b)** EDX spectra taken from the corresponding area (dotted circle) in (a) shows that powder EDS'ed powder mainly contains B and N elements.

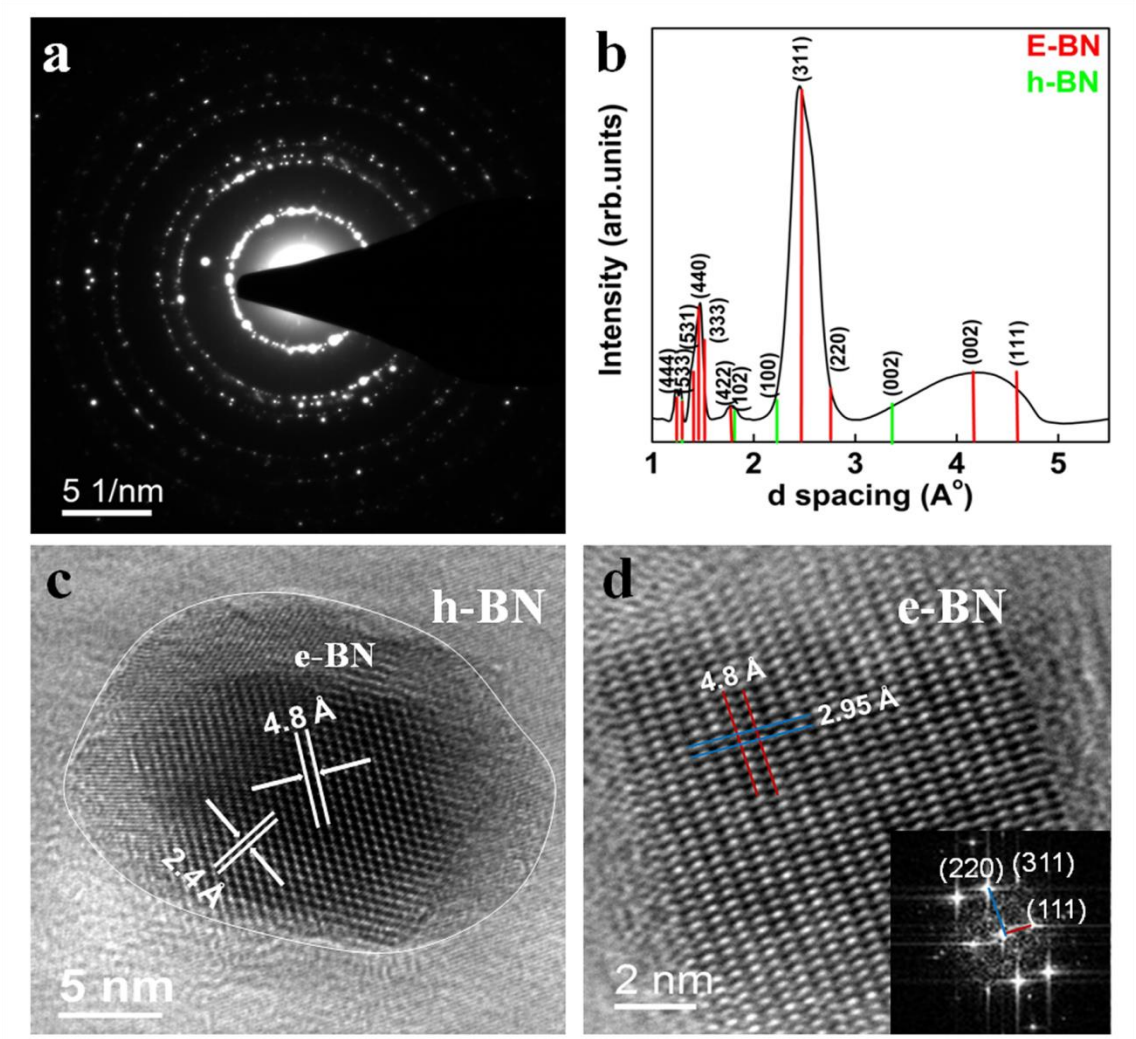

Figure 4. (a) SAED pattern taken from the region of Fig. 3 indicating the existence of crystalline phases, **(b)** the extracted profile intensity vs. d spacing values of the SAED reveals the presence of e-BN and h-BN. **(c)** HRTEM image taken along <111> orientation shows lattice spacing values of 0.48 nm and 0.24 nm along the (222) and (111) planes. **(d)** A zoom in HRTEM image taken along ⟨211⟩ orientation and corresponding FFT inset image also confirms the e-BN phase, with lattice spacing of 0.480 nm of (111) plane and 0.295 nm of (220) plane.

Chapter 7.

Formation of metastable wurtzite phase boron nitride by emulsion detonation synthesis

Metin Örnek[1], Chawon Hwang[1], Kelvin Y. Xie[2], Silvio Pratas[3], João Calado[3], Alan Burgess[4], Vladislav Domnich[1], Kevin J. Hemker[2], Richard A. Haber[1,*]

[1] *Department of Materials Science and Engineering, Rutgers, The State University of New Jersey, Piscataway, NJ 08854, USA*

[2] *Department of Mechanical Engineering, Johns Hopkins University, Baltimore, MD 21218, USA*

[3] *Innovnano, Materiais Avançados SA, Antanhol 3040-570, Portugal*

[4] *SprayWerks Technologies Inc., North Vancouver, British Columbia V7G 1L5, Canada*

*Corresponding author e-mail: rich.haber@rutgers.edu and address: 607 Taylor Road, Piscataway, NJ 08854, USA. Tel: +1 (848) 445-5924

Abstract

Emulsion detonation synthesis (EDS) is a newly developed process to synthesize nano-sized ceramic powders based on the detonation of two water-in-oil emulsions. The process provides high pressure and temperature along with rapid quenching. In this work, we report the formation of wurtzite phase BN (w-BN) for the first time by EDS process, using hexagonal BN (h-BN) as the precursor. Characterization studies demonstrated the formation of w-BN with sizes varying from nanometer to micrometer scale either embedded in or grown from h-BN matrix. These findings provide a new avenue to synthesize metastable and superhard BN phases.

Keywords: Wurtzite phase boron nitride; Hexagonal phase boron nitride; Emulsion detonation synthesis; Transmission electron microscopy (TEM); Electron energy loss spectroscopy (EELS).

1. Introduction

Emulsion detonation synthesis (EDS) is a newly developed industrially scaled process to synthesize nanometer-sized ceramic powders based on the detonation of two water-in-oil emulsions.[1-3] The process can produce high pressures up to 10 GPa and high temperatures up to 2000°C along with a fast cooling rate of 10^9 K/s, which provides a favorable environment for nanometer-sized material to form.[1-4] When compared to conventional detonation synthesis that uses military explosives, although it can not reach the same pressure and temperature levels, EDS method has an enormous flexibility in terms of taylor-made synthesis approaches, since it allows among other aspects: i) homogenous dispersion of starting precursors, thus ensuring an effective shock transmission between the detonation wave and starting precursors and ii) control of the detonation atmosphere by controlling the composition of emulsion, e.g. introducing nitrogen-rich compounds and/or oil emulsions, to prevent oxidation during the reaction.[1-3] Prior work showed that nanostructured cubic zirconia (ZrO_2), alumina (Al_2O_3), titanium dioxide (TiO_2), spinel ($MgAl_2O_4$), aluminum nitride (AlN), magnetite (Fe_3O_4), and aluminum doped zinc oxide (AZO) ceramics can be successfully synthesized by this process.[1-4]

Recently, we demonstrated that this novel technique could also be employed to B-N systems.[5] Boron nitride is a widely used ceramic material with many known polymorphs such as high-density phases (e.g; cubic and wurtzite (metastable) structures), and low-density phases (e.g. hexagonal, rhombohedral, turbostratic, explosion, and amorphous structures).[6-10] Among these, cubic BN (c-BN), wurzite BN (w-BN), and explosion BN (e-BN) can be synthesized through high pressure-high temperature (HPHT) process e.g. dynamic shock or static high-pressure methods.[11-13] In particular, cubic and wurtzite

crystals are dense and close-packed, exhibiting unique properties such as high hardness (due to diamond-like covalent sp^3 hybridized bonds), high thermal conductivity, high wear resistance, and higher chemical resistivity against ferrous alloys.[8,14,15] These attractive properties make the high-density phases of BN superior to diamond, as diamond deteriorates when used to machine ferrous metals or their alloys.[8,16-18]

In our previous work, we have suggested that EDS could be a potential route to synthesize metastable or high-density BN phases due to the HPHT and the rapid quenching environment the process provides.[5] We demonstrated the formation of metastable e-BN grains, 10-20 nm in size, embedded in an h-BN matrix, for the first time by applying the process on h-BN at 5 GPa.[5] This finding encouraged us to further explore the application of EDS process on B-N system with the aim to synthesize other metastable or high-density BN phases.

In this work, we succeeded in raising the pressure generated during the process from 5 GPa to 7 GPa by increasing the emulsion density and we observed the formation of metastable w-BN for the first time through EDS process.

2. Experimental Details

Detonation velocity and pressure were calculated based on experimental parameters using the THOR program (see Table 1), which uses numerical equations to assess the reaction environment of the detonation/reaction system.[4] Details of calculations and the experiments, and reaction mechanisms involved in the process are shown and discussed in our earlier work.[5] Phase structure was identified by X-ray diffractometer (XRD; PANalytical X'Pert, Netherlands): 45kV and 40 mA with Cu Kα (λ=1.540598 Å)

radiation at a scanning rate of 0.04°min^{-1}. Chemical bonding characteristics were determined using a Fourier transform infrared spectrometer (FTIR; Mattson Instruments Galaxy 5000 Series, Wisconsin). Particle morphology and crystal structure were studied using transmission electron microscopy (TEM; Philips FEI CM-300, Netherlands) with incident electron beam energy of 300 keV. The bonding structures of various BN phases were identified using scanning transmission electron microcopy (STEM) coupled with electron energy loss spectrometer (EELS) that is equipped on a TEM (JEOL 2100F, Japan).

3. Results

XRD pattern of EDS'ed particles is shown in Fig. 1a. The spectral range of interest is centered on between (2θ) ~ 40-65°, where the corresponding major peaks of w-BN and h-BN are mainly located. The peaks around 41.60°, 43.85°, 50.16°, 55.10°, and 59.50° (in 2θ) match the reflections of (100), (101), (102), (004), and (103) planes of h-BN, respectively.[19,20] Further, the peaks around 40.80°, 42.75°, 46.30°, and 60.55° (in 2θ) match the reflections of (100), (002), (101), and (102) planes of w-BN.[21] As such, XRD analysis suggested the presence of hexagonal and wurtzite phases of BN, with h-BN as the dominant phase.

FTIR spectroscopy was employed to see the change in atomic bonding characteristics of the material before and after EDS process. Fig. 1b shows FTIR spectra of starting h-BN (Kennametal, UK) and EDS'ed particles along with reference materials: commercial w-BN and c-BN (UK Abrasives, USA). The initial h-BN only consists of sp^2 bonding and showed two typical absorption bands at 816 cm^{-1} and 1378 cm^{-1}, which are attributed to B-N-B bending and B-N stretching vibrations, respectively.[22] Sp^3 bonded

commercial c-BN showed a broad absorption band from around 800 and 1200 cm^{-1} with a narrow peak around 1090 cm^{-1}. w-BN also consists of sp^3 bonding and showed a narrow peak around 1090 cm^{-1} with an accompanying lower intensity peak at 1250 cm^{-1}. EDS'ed particles mainly showed similar features to h-BN, but also showed a broader absorption band around 1000-1150 cm^{-1} with a narrow peak at 1090 cm^{-1}, which matches the absorption bands of both w-BN and c-BN. This observation indicates the existence of sp^3 bonding in the EDS'ed material, supporting the prior XRD analysis results that showed the coexistence of w-BN with h-BN as shown in Fig. 1a.

To support our observations and obtain direct evidence for the formation of w-BN, we employed TEM analysis coupled with energy dispersive X-ray (EDX) spectroscopy and electron energy-loss spectroscopy (EELS). Fig. 2a shows the representative microscope image of EDS'ed powder, which has irregular shape with wrinkling and shows phase contrast within the sheet. EDX spectroscopy mapping detected only B and N, indicating the sheet is BN. Analysis of selected area electron diffraction (SAED) of the entire sheet confirmed the coexistence of h-BN and w-BN (see Fig. 2b). To obtain information on the phase contrast within the sheet, EELS spectra were taken from two areas with different contrasts (marked as 1, and 2 in Fig. 2a). EELS spectra taken from area 1 displayed B-K and N-K edges exhibiting both π (189-195 eV for B, 395-401 eV for N) and σ (195-220 eV for B, 401-447 eV for N) bonding signatures (Fig. 2c).[23] EELS spectra taken from area 2 displayed B-K and N-K edges exhibiting only σ bonding signatures (Fig. 2d).[24,25] The presence of both π and σ bonding indicates the typical interlayer and intralayer bonding consisting of sp^2 bonds, which corresponds to h-BN, and the presence of only σ bonding indicates that the bonding consists of sp^3 bonds only, which corresponds to w-

BN.[8,24,25] Therefore, these results indicate that EDS'ed particles consist of sp^3 bonded w-BN embedded in sp^2 bonded h-BN.

Since π-bonding signature is present in h-BN but not in w-BN, this provides a means to map the size and distribution of w-BN. Fig. 3 shows TEM images and EELS mapping results on an EDS'ed particle. EELS mapping based on the energy range from B-K edge (189-220 eV) showed relatively uniform intensity on the map (Fig. 3c). However, when only the π bonding signal of boron is selected (189-195 eV), the most apparent feature is the low signal intensity regions marked by white arrows in Fig. 3d. These regions still consist of boron without the π bonding signal, indicating they are w-BN grains embedded in an h-BN sheet. The size of the w-BN particles is about 50 to 250 nm. Similar observations were made in the N-K edge maps (Figs. 3e and 3f), where the regions marked by white arrows in Fig. 3f are also free of π bonding signal of nitrogen.

Figure 4 shows another EDS'ed particle analyzed using STEM-EELS mapping technique. In this case, a large portion of the h-BN sheet transformed to a w-BN grain ~ 1 micron in size. Fig. 4c and 4e show total counts of B and N respectively. Figure 4d and 4f show a lack of the π-bond counts of B and N on the right part of the sheet, indicating about half of the h-BN sheet in the region of interest transformed to w-BN. We note that in both high angle annular dark-field (HAADF) micrographs (Figs 3b and 4b), several small bright particles are present, with their higher brightness suggesting a higher atomic number. Indeed, EDX spectroscopy revealed that these particles are rich in heavier elements (e.g. Zr, Cr, Fe, etc.), which are contaminants resulting from the EDS process and should not be confused with the BN grains.

4. Discussion

Taken together, we observed the formation of w-BN; showing either (i) grain-like morphology that is embedded in an h-BN matrix or (ii) sheet-like morphology grown from h-BN sheets. Prior studies demonstrated the transformation of h-BN to w-BN by employing static high-pressure methods, dynamic shock compression, detonation synthesis, or pulsed mechanical treatment (planetary milling).[8,12,13,21,25-34] However, the pressure required/generated for the transformation from solely h-BN to w-BN varied between as low as 6.7 GPa in static high-pressure methods, 12 GPa or higher in dynamic shock compression methods, and 20-25 GPa in detonation synthesis method.[8,32,33] In this study, the pressure (7 GPa) generated to obtain w-BN is close to the lowest pressure reported in static high-pressure methods.

Limited formation of w-BN phase in this work is assumed to be closely related to certain parameters: (i) Pressure fluctuation and hot spot formation: While the shock wave propagates during the detonation, the pressure that particles experience fluctuates and creates hot spots.[35] The regions that experience both the structural disordering and the hot spot formation might transform to w-BN while other regions would only show structural disordering. (ii) Particle size of the starting h-BN: Particle size larger than the reaction zone results in limited or no reaction according to detonation theory.[35] In liquid explosive systems, length of the reaction zones typically varies from a few microns to a few hundred microns.[35-38] Considering the $D_{(90)}$ particle size of h-BN used in this study, which is around 14 μm, the region of particles which does not experience high pressure due to the limited reaction zone would naturally maintain the hexagonal structure. (iii) Cooling rate: It has been shown by previous research that cooling rate is another important aspect for

detonation systems. Higher cooling rate yields higher yield and higher retention of the formed metastable phase(s).[25,39] In our case, it is highly possible that part of the formed metastable w-BN transformed back to h-BN through the excess heat in the system. Slow cooling rate therefore results in less efficient retaining of w-BN phase formed during the reaction. Considering the parameters and mechanisms discussed above, we suggest that increasing pressure and cooling rate by changing the emulsion/explosive chemistry, and decreasing the particle size of the starting powder would result in a higher w-BN yield, and possibly the formation of c-BN as well. The study related to these suggestions is underway and will be the subject of a separate paper.

5. Conclusions

In summary, we applied EDS process on h-BN at 7 GPa to evaluate its applicability to synthesize metastable or high-density phases of BN. We made direct observation on the formation of metastable high-density w-BN phase either embedded in or grown from h-BN matrix. Possible mechanism and parameters for the formation of w-BN during the process were discussed to provide insight on further improvement in the formation of w-BN. These findings demonstrate that EDS process has potential to synthesize metastable and high-density phases of BN ceramics.

Acknowledgments

This research was sponsored by and was accomplished under the Office of Naval Research Grant No: N00014-17-1-2532. Additional support was received from the Defense Advanced Research Projects Grant No: W31P4Q-13-1-0001, and the National Science

Foundation I/UCRC Award No.1540027. The authors would like to thank Avie Shah and Kaitlin Wang for their valuable assistance in the laboratory. Metin Örnek acknowledges scholarship from the Ministry of National Education, the Republic of Turkey.

References

1. Da Silva JMC, Antunes EMDS. Nanometric-sized ceramic materials, process for their synthesis and uses thereof. US Patent 8,557,215; 2013.

2. Da Silva SM, Da Silva JMC. Continuous process for nanomaterial synthesis from simultaneous emulsification and detonation of an emulsion. US Patent 9,327,257; 2016.

3. Antunes EMDS, Da Silva JMC, Lagoa AL. Process for nanomaterial synthesis from the preparation and detonation of an emulsion, products and emulsions thereof. US Patent 9,115,001; 2015.

4. Neves N, Lagoa A, Calado J, Do Rego AB, Fortunato E, Martins R, et al. Al-doped ZnO nanostructured powders by emulsion detonation synthesis–Improving materials for high quality sputtering targets manufacturing. J. Eur. Ceram. Soc. 2014;34(10):2325-38.

5. Örnek M, Reddy KM, Hwang C, Domnich V, Burgess A, Pratas S, et al. Observations of explosion phase boron nitride formed by emulsion detonation synthesis. Scr. Mater. 2018;145:126-30.

6. Wentorf RH. Cubic Form of Boron Nitride. J. Chem. Phys. 1957;26(4):956.

7. Hamilton EJM, Dolan SE, Mann CM, Colijn HO, McDonald CA, Shore SG. Preparation of Amorphous Boron Nitride and Its Conversion to a Turbostratic, Tubular Form. Science. 1993;260(5108):659-61.

8. Ji C, Levitas VI, Zhu H, Chaudhuri J, Marathe A, Ma Y. Shear-induced phase transition of nanocrystalline hexagonal boron nitride to wurtzitic structure at room temperature and lower pressure. Proc. Natl. Acad. Sci. U. S. A. 2012;109(47):19108-12.

9. Liu J, Vohra YK, Tarvin JT, Vagarali SS. Cubic-to-rhombohedral transformation in boron nitride induced by laser heating: In situ Raman-spectroscopy studies. Phys. Rev. B. 1995;51(13):8591-4.

10. Batsanov SS, Blokhina G, Deribas A. The effects of explosions on materials. J. Struct. Chem. 1965;6(2):209-13.

11. Batsanov SS. Features of phase transformations in boron nitride. Diamond Relat. Mater. 2011;20(5-6):660-4.

12. Akashi T, Sawaoka A, Saito S, Araki M. Structural changes of boron nitride caused by multiple shock-compressions. Jpn. J. Appl. Phys. 1976;15(5):891.

13. Bundy F, Wentorf Jr R. Direct transformation of hexagonal boron nitride to denser forms. J. Chem. Phys. 1963;38(5):1144-9.

14. Vel L, Demazeau G, Etourneau J. Cubic boron nitride: synthesis, physicochemical properties and applications. Mater. Sci. Eng. B. 1991;10(2):149-64.

15. Reddy KM, Hwang C, Örnek M, Miller SL, Mayo WE, Burgess A, et al. Observations of nanocrystalline cubic boron nitride formed with plasma spraying. Acta Mater. 2016;116:155-65.

16. Bobrovnitchii G, Filgueira M. Study of quenched steels machining with a polycrystalline Hexanite-R cutting tool. J. Mater. Process. Technol. 2005;170(1):254-8.

17. Tian Y, Xu B, Yu D, Ma Y, Wang Y, Jiang Y, et al. Ultrahard nanotwinned cubic boron nitride. Nature. 2013;493(7432):385-8.

18. Vepřek S. The search for novel, superhard materials. J. Vac. Sci. Technol. A. 1999;17(5):2401-20.

19. Thomas J, Weston NE, O'Connor TE. Turbostratic1 Boron Nitride, Thermal Transformation to Ordered-layer-lattice Boron Nitride. J. Am. Chem. Soc. 1962;84(24):4619-22.

20. Alkoy S, Toy C, Gönül T, Tekin A. Crystallization behavior and characterization of turbostratic boron nitride. J. Eur. Ceram. Soc. 1997;17(12):1415-22.

21. Sōma T, Sawaoka A, Saito S. Characterization of wurtzite type boron nitride synthesized by shock compression. Mater. Res. Bull. 1974;9(6):755-62.

22. Geick R, Perry CH, Rupprecht G. Normal Modes in Hexagonal Boron Nitride. Phys. Rev. 1966;146(2):543-7.

23. Ahn CC, Krivanek OL. EELS Atlas: A Reference Collection of Electron Energy Loss Spectra Covering All Stable Elements: Gatan; 1983.

24. Schmid HK. Phase identification in carbon and BN systems by EELS. Microsc., Microanal., Microstruct. 1995;6(1):99-111.

25. Meng Y, Mao HK, Eng PJ, Trainor TP, Newville M, Hu MY, et al. The formation of sp3 bonding in compressed BN. Nat. Mater. 2004;3(2):111-4.

26. Nameki H, Sekine T, Kobayashi T, Fat'yanov V, Sato T, Tashiro S. Rapid quench formation of E-BN from shocked turbostratic BN precursors. J. Mater. Sci. Lett.. 1996;15(17):1492-4.

27. Coleburn N, Forbes J. Irreversible transformation of hexagonal boron nitride by shock compression. J. Chem. Phys. 1968;48(2):555-9.

28. Corrigan F, Bundy F. Direct transitions among the allotropic forms of boron nitride at high pressures and temperatures. J. Chem. Phys. 1975;63(9):3812-20.

29. Solozhenko V, Elf F. On the threshold pressure of the hBN-to-wBN phase transformation at room temperature. J. Superhard Mater. 1998;20:62-3.

30. Britun VF, Kurdyumov AV, Borimchuk NI, Yarosh VV, Danilenko AI. Formation of diamond-like BN phases under shock compression of graphite-like BN with different degree of structural ordering. Diamond Relat. Mater. 2007;16(2):267-76.

31. Levitas VI, Ma Y, Hashemi J, Holtz M, Guven N. Strain-induced disorder, phase transformations, and transformation-induced plasticity in hexagonal boron nitride under compression and shear in a rotational diamond anvil cell: In situ x-ray diffraction study and modeling. J. Chem. Phys. 2006;125(4):044507.

32. Adadurov GA, Aliev ZG, Atovmyan LO, Bavina TV, Borod'Ko YG, Breusov ON, et al. Formation of a Wurtzite-like Modification of Boron Nitride in Shock Compression. In Soviet Phys. Doklady. 1967; (12):173.

33. Gavrilkin SM, Batsanov SS, Gordopolov YA, Smirnov AS. Effective detonation synthesis of cubic boron nitride. Propellants Explos. Pyrotech. 2009;34(6):469-71.

34. Batsanov SS, Gavrilkin SM, Bezduganov S, Romanov P. Reversible phase transformation in boron nitride under pulsed mechanical action. Inorg. Mater. 2008;44(11):1199.

35. Ripley RC, Zhang F, Lien FS. Acceleration and heating of metal particles in condensed matter detonation. Proc. R. Soc. London, Ser. A. 2012;468(2142):1564-90.

36. Engelke R, Bdzil JB. A study of the steady-state reaction-zone structure of a homogeneous and a heterogeneous explosive. Phys. Fluids. 1983;26(5):1210-21.

37. Sheffield SA, Engelke RP, Alcon RR, Gustavsen RL, Robbins DL, Stahl DB, et al. Particle velocity measurements of the reaction zone in nitromethane. Los Alamos National Laboratory, 2002.

38. Dobratz B, Crawford P. LLN L Explosives Handbook. UCRL-52997, Lawrence Livermore National Laboratory, CA. 1985.

39. Aleksenskii A, Baidakova M, Vul AY, Davydov VY, Pevtsova YA. Diamond-graphite phase transition in ultradisperse-diamond clusters. Phys. Solid State. 1997;39(6):1007-15.

Tables

Table 1. The physical and chemical properties of the prepared emulsions and corresponding values of calculated detonation rate and pressure for EDS process.

h-BN % wt in emulsion	Oil % wt in emulsion	Emulsion Density (g/cm^{-3})	Calculated Detonation Velocity (m/s)	Calculated Pressure P(C,J)
10	15	1.18	4900	7 GPa

Figures

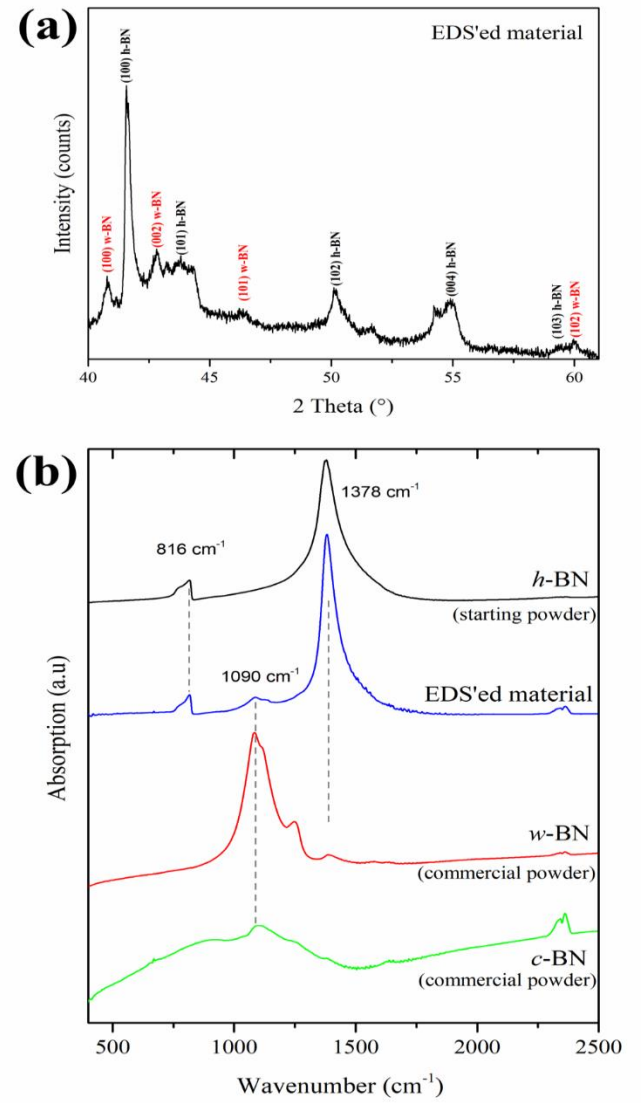

Figure 1. XRD and FTIR spectra of EDS'ed particles (**a)** (100), (002), (101), and (102) peaks of w-BN phase revealed at $2\theta \approx 40.80°$, 42.75°, 46.30°, and 60.55° respectively. **(b)** EDS'ed particles revealed a narrow band at 1090 cm^{-1}, which match the absorbance bands of commercial wurtzite and cubic BNs, indicating sp^3 bonding.

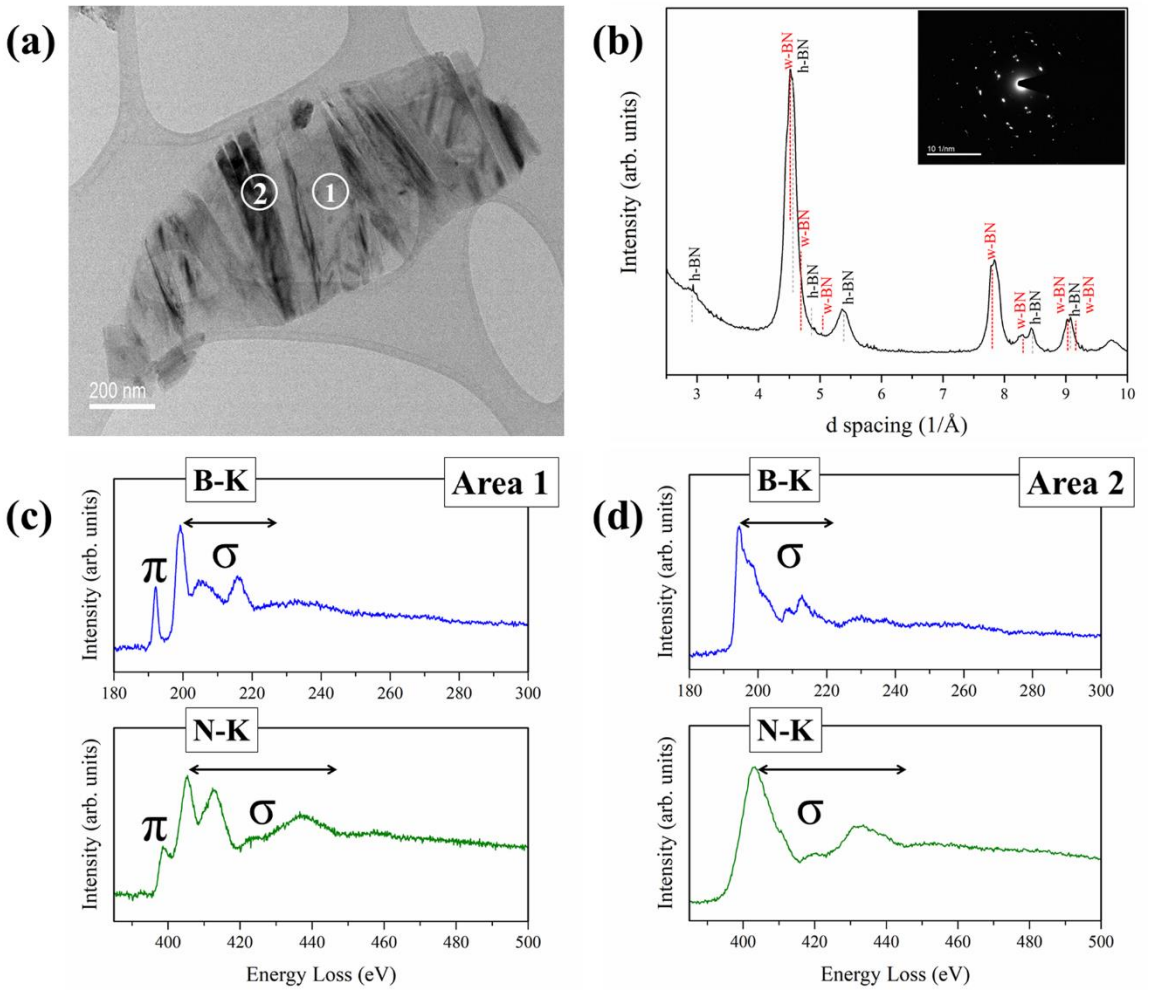

Figure 2. TEM and EELS analysis of the EDS'ed particles **(a)** Bright field image of the particle shows irregular morphology with absorption and diffraction contrast **(b)** SAED taken from entire grain with corresponding d-spacing analysis indicates two sets of diffraction pattern: wurtzite and hexagonal phases. EELS spectra **(c)** taken from Area 1 on (a) displayed π and σ bonding for boron and nitrogen, indicating the typical interlayer and intralayer bonding characteristics of sp^2 bonded h-BN. **(d)** Area 2 displayed only σ bonding for boron and (d) nitrogen, indicating sp^3 bonding.

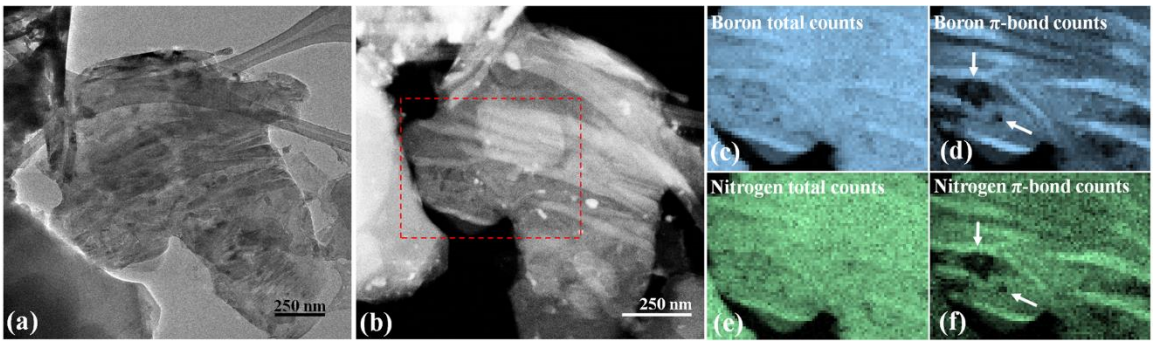

Figure 3. TEM and STEM/EELS map analysis of the EDS'ed particles. **(a)** Bright field and **(b)** high annular dark-field (HAADF) micrographs display different contrast**.** Chemical mapping using the energy range from B-K edge (189-220 eV) showed relatively uniform intensity in **(c)** total boron count, however low intensity signal is observed in π count **(d)**. A similar observation was made in the N-K edge map as shown in **(e)** total nitrogen counts vs. **(f)** only π count, indicating the sp^3 bonded region is embedded in sp^2 matrix.

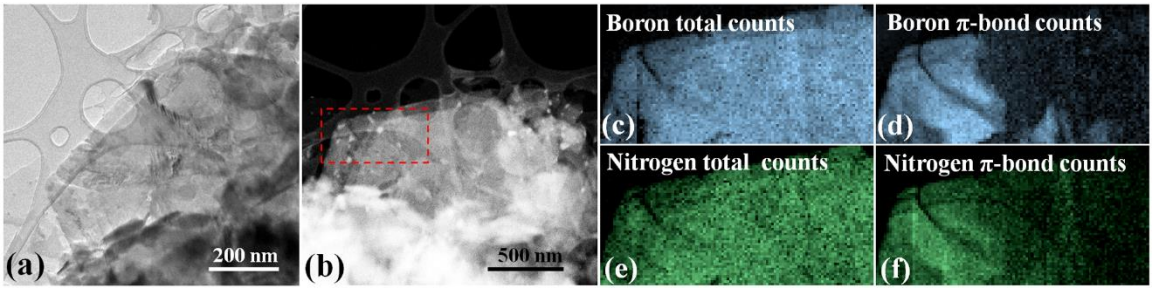

Figure 4. TEM and STEM/EELS map analysis of the particle with sheet morphology. **(a)** Bright field and **(b)** high annular dark-field (HAADF) micrographs display different contrast**.** Chemical mapping using the energy range from B-K edge (189-220 eV) showed relatively uniform intensity in **(c)** total boron count. **(d)** Low intensity signal was observed in π count only **(d)**. A similar observation was made in the N-K edge maps as shown in **(e)** total nitrogen counts and **(f)** only π count, indicating half of the h-BN sheet in the region of interest has transformed to w-BN.

Chapter 8.

Conclusions

This thesis has three main focuses. The first is to synthesize amorphous BCNO compounds and investigate how the synthesis conditions (such as H_3BO_3:$C_3N_6H_6$ molar ratio in the starting composition and heat treatment temperature) impact the formation, chemistry, and degree of crystallinity of the synthesized BCNO. The second focus is to investigate the formation and structural ordering of BN from BCNO by subjecting BCNO compounds to high temperature and high temperature-high pressure treatments under equilibrium (conventional heat-pressure treatments) and non-equilibrium conditions (ultra-fast heating and cooling with and without applying external pressures). The third and last focus is to synthesize metastable phases of BN under non-equilibrium conditions.

BCNO compounds with various chemistries and degrees of crystallinity were prepared by systematically varying the H_3BO_3 to $C_3H_6N_6$ ratio in the starting composition and the synthesis temperature. The prepared BCNOs were then subjected to post treatments such as high temperature and high temperature-high pressure treatments under various conditions. Results obtained through extensive characterization studies suggest that:

a) Heating the H_3BO_3 and $C_3H_6N_6$ mixture yields amorphous BCNO as intermediate compounds at low temperature regimes (< ~ 800°C), and long range crystallographic order of BN layers are formed at > ~ 800°C as H_3BO_3 content increases in the starting composition.

b) Increasing the H_3BO_3 to $C_3H_6N_6$ ratio promotes BN formation from BCNO matrix at lower temperatures and advances its structural ordering at certain temperatures

since the theoretical temperature for BN formation decreases with the increase in H_3BO_3:$C_3H_6N_6$ molar ratio according to thermodynamical calculations based on the proposed reactions.

c) Increase in synthesis temperature promotes crystalline BN formation from BCNO compound and advances its structural ordering since the reactions are endothermic.

d) Crystalline BN grains form directly from BCNO matrix based on direct TEM observation and EELS analysis.

e) Loading pressure of 1 GPa and heating temperature of 1200°C results in a more compressed layered structure of the resultant BN from BCNO.

f) Plasma spraying amorphous BNCO compound results in crystalline BN phases: mainly t-BN with small amounts of c-BN phases. The TEM-EELS quantitative elemental analysis suggests stoichiometric BN formation in localized regions of the BNCO matrix.

g) Plasma spraying amorphous BNCO compound with additional H_3BO_3 and boron, which behave as catalysts, significantly enhanced the formation of nanocrystalline c-BN.

h) Emulsion detonation synthesis process was applied for the first time on h-BN at 5 GPa and local formation of metastable e-BN phase in h-BN was observed.

i) With increase in process pressure to 7 GPa, formation of metastable high-density w-BN phase that is either embedded in or grown from h-BN matrix was observed.

j) Possible mechanism and parameters for the formation of e- BN and w-BN during the EDS process were discussed to provide insight on further improvement in the formation of metastable and/or high-density phases. Higher process pressures, cooling rate, and

particle size of starting powder are suggested to be the key factors that would affect the yield of the resultant BN phases.

Chapter 9.

Future Work

Comprehensive studies were conducted on i) the synthesis of BCNO compounds with varying chemistry and degree of crystallinity and ii) the investigation of the formation and structural ordering of BN phases from BCNO compounds under various conditions such as conventional high temperature and pressure-temperature treatments and ultra-fast heating-cooling.

Based on the results obtained and shared in this thesis, there are some areas that could be explored further. Subjecting BCNO compounds either only to high pressure using diamond anvil cell or to higher pressure (5-10 GPa) and high temperature (1200-2000°C) using belt type apparatus could be tried. These studies would complete all possible experimental conditions in terms of conventional pressure and temperature treatments, and would thereby advance the understanding of the formation of high density and super hard BN and/or other possible super hard phases in B-C-N-O system.

The results obtained through emulsion detonation synthesis method suggest that it could be a promising technique to form not only metastable phases of BN, but also super hard c-BN. Some improvements/adjustments on the experimental conditions such as particle size of the starting powder, the pressure generated by the reaction, and cooling rate can be further explored to enhance the formation of metastable or high-density phases and the retention of resultant phases.